Evaluation and Application of an Algorithm for the Time-Varying Identification of Ankle Stiffness

Tanya Starret Visser

Department of Biomedical Engineering

McGill University, Montreal

August, 2009

A thesis submitted to McGill University

in partial fulfillment of the requirements of the degree of

Master of Engineering

ABSTRACT

Dynamic joint stiffness is an important property involved in the control of posture and movement. It can be separated into two components: intrinsic stiffness, due to the properties of the joint, muscles, and tissues, and reflex stiffness, due to reflex mediated changes in muscle activation. Most motor activities involve time-varying conditions but studies have primarily focused on joint stiffness under static conditions. This thesis evaluated the performance of a parallel-cascade algorithm designed to identify time-varying intrinsic and reflex stiffness. A simulation study showed that the algorithm could identify rapidly changing system dynamics, and that the gain of the parallel pathways, the signal-to-noise ratio, and the number of realizations used impacted the quality of the identification. With a carefully designed experiment, the algorithm produced good results using real data, and showed that results from postural studies cannot predict time-varying stiffness modulation patterns.

RÉSUMÉ

La raideur dynamique est une propriété importante de la posture et du mouvement. Elle se divise en deux constituants: la raideur intrinsèque, provenant des propriétés de l'articulation, des muscles, et des tissues, et la raideur réflexive, provenant de l'activation musculaire enchainée par les réflexes ostéo-tendineux. La majorité des activités moteurs se font sous conditions temporelles changeantes. Par contre, la plupart des études se sont attardées sur la raideur dynamique sous conditions statiques. Cette thèse évalue la performance d'un algorithme 'parallèle-cascade' pour l'identification de raideur intrinsèque et réflexive changeant dans le temps. Sous études simulées, nous avons démontré que l'algorithme peut identifier des dynamiques changeant rapidement. Ces simulations démontrent que le gain relatif des constituants, le rapport signal/bruit, et le nombre de réalisations dans l'ensemble de données influencent la qualité de l'identification. Avec une procédure expérimentale soigneusement établie, l'algorithme produit de bons résultats utilisant de vraies données. Les expérimentations ont démontré que les études stationnaires ne peuvent pas prédire la raideur changeant dans le temps.

ACKNOWLEDGEMENTS

I'd first like to thank my supervisor, Dr. Robert Kearney, for all his advice and support. Dr. Kearney guided me through all stages of this thesis research, and helped me see the small victories in the process of solving a seemingly insurmountable problem.

I'd like to thank my lab colleague, Daniel, for always being willing to take the time to work through problems with me, and for providing advice whenever I needed it. Thanks to Ross Wagner for sharing his computer and workshop expertise. Thanks to Alejandro and Shruti for their friendship and for providing distraction, as required. Also, I'd like to thank Lina Vuch and Pina Sorrini for their kindness and willingness to answer all my questions.

Special thanks to my husband for all the moral support and encouragement he provided, and for being willing to help out in any way.

The Natural Sciences and Engineering Research Council of Canada (NSERC) and the Canadian Institutes for Health Research (CIHR) provided the funding that made this research possible.

CONTRIBUTION OF AUTHORS

Mackenzie Baker developed the time-varying, parallel-cascade (TVPC) algorithm (described in Chapter 3) as part of her master's thesis. Heidi Giesbrecht made improvements to the algorithm. I further modified the implementation of the algorithm by improving the reflex identification procedure, by changing the way data was filtered before decimation, and by increasing the sampling frequency at which data was analyzed. My lab colleague, Daniel Ludvig, provided help and suggestions throughout the process.

I developed a more realistic simulation scheme (used in Chapters 3 and 4) to test the performance of the TVPC algorithm, with input from Daniel. I developed the experimental protocol used in Chapter 5, with the guidance of Dr. Robert Kearney and Daniel Ludvig. I performed the experiments described in Chapter 5. Dr. Ross Wagner troubleshot any technical problems that occurred, both with the experimental setup and the analysis software. Finally, my supervisor, Dr. Kearney provided substantial feedback in the preparation of this thesis manuscript.

TABLE OF CONTENTS

LIST OF FIGURES

LIST OF TABLES

1. Introduction

Getting out of bed, dressing, and teeth brushing are all things that can be done half asleep and yet, each of these tasks involves complex interactions between muscles, connective tissue and bone, all controlled by neurological command signals. This neuromuscular system is what makes human movement possible. The brain plans the movement and sends command signals, via the spinal cord and peripheral nerves, to the muscles. These central commands are complemented by feedback signals from the muscle's sensory receptors, which provide information about muscle tension and stretch. The result is the smooth execution of a desired movement.

The manner in which the neuromuscular system generates smooth, coordinated movements is still poorly understood. A thorough study of the neuromuscular system will provide a better understanding of normal motor function, which will consequently help us understand how neurological diseases affect it. A proper model of motor control will allow clinicians to objectively assess the progression of a disease and the effectiveness of rehabilitation programs. Furthermore, in the field of robotics and prosthetics, an understanding of the control schemes used by the body will allow designers to make limb prosthetics or robots with more natural and smooth movement patterns. [1]

1.1. Dynamic Joint Stiffness and movement

How a limb will respond to an external perturbation, or the type and strength of muscle contraction required to generate a desired movement is determined by a property known as dynamic joint stiffness [2]. Dynamic joint stiffness is defined as the relation between joint position and the torque acting about it [3]. It can be separated into two components [1]:

1. Intrinsic stiffness: due to the mechanical properties of the joint, visco-elastic tissues and active muscle.
2. Reflex stiffness: due to the increased muscle activation in response to a stretch.

The exact role of joint stiffness, and in particular reflex stiffness, in movement is still under debate. To gain a proper understanding of joint stiffness it is important to distinguish

between its two components. Intrinsic and reflex torque cannot be recorded separately; therefore, our lab developed a parallel-cascade system identification algorithm to concurrently identifying intrinsic and reflex ankle stiffness from a single recording of input position and output torque [4]. Intrinsic and reflex stiffness are modeled as parallel pathways that contribute additively to the total output torque. Intrinsic stiffness is modeled as a linear dynamic system relating position to torque. Whereas, reflex stiffness relates joint velocity to torque through a delayed non-linear system, consisting of a static non-linearity followed by a linear low-pass filter. This model has been used to study the properties of ankle stiffness under various stationary conditions in both normal and spinal cord injured subjects [5-8]. These studies documented how each stiffness component changed as the operating point (position/torque) was modified. Their results cannot be used to predict joint stiffness behavior during movement because studies have shown that for matched background activation levels, the reflex response changes depending on the movement being executed [9, 10].

The study of dynamic joint stiffness during movement is a complex problem. Time-invariant system identification techniques cannot be used because they rely on the assumption that the system remains the same throughout the period of time used to identify it. This is not the case during movement, where the changing position and torque cause the stiffness parameters to change over the course of the task. Special identification techniques are required to tackle this problem. Ideally a full ankle stiffness model would be developed, which characterizes all the non-linear behavior of this complex physiological system. Unfortunately, this is not yet possible. As an intermediate step, ankle stiffness can be treated as a time-varying system, where changes in system dynamics, which are in actuality due to the non-linear properties of the system, are treated as functions of time. This allows for ankle stiffness to be characterized during specific tasks in which the operating point changes, without a global model. The stiffness modulation pattern identified for a particular task cannot be used to predict the pattern during another task, but will provide insight into the role of reflexes for that particular situation.

Our lab developed ensemble-based identification techniques to identify rapidly, time-varying linear [11] and non-linear [12] systems. Multiple realizations of the same time-

varying behavior are collected to generate ensembles of input-output data. The ensemble technique identifies the time-varying system by performing the identification across the ensemble instead of in time. This approach is based on the assumption that the system dynamics are identical at each time across the ensemble. These algorithms were integrated into the existing parallel-cascade algorithm to identify time-varying intrinsic and reflex stiffness dynamics [13].

The goal of this thesis was to use the time-varying, parallel-cascade (TVPC) algorithm to study the behavior of intrinsic and reflex stiffness during a non-postural task. A previous student, Heidi Giesbrecht, struggled to get good experimental results. Consequently, it was necessary to investigate the performance limits and optimal operating conditions of the TVPC algorithm. The first goal of this thesis was to assess the algorithm's ability to track rapid changes in joint dynamics, such as step changes in reflex gain. The second goal was to evaluate the performance of the TVPC algorithm as the signal-to-noise ratio decreased and to identify other factors influencing the algorithm's performance, such as the number of realizations in the data ensembles and the relative contribution of the intrinsic and reflex pathways to the total output torque. The final goal of this thesis was to apply the TVPC algorithm experimentally to identify time-varying intrinsic and reflex stiffness during a simple time-varying task. The first two goals were achieved by creating a realistic simulation of ankle stiffness and varying the system parameters to investigate the properties of the TVPC algorithm. Using the knowledge gained through the simulation study, an experiment was carefully designed to meet the final goal.

1.2. THESIS OUTLINE

This thesis is composed of six chapters. Following this introduction is a background chapter. The background chapter covers relevant anatomy and physiology, and includes a review of past studies of dynamic joint stiffness under both postural and time-varying conditions. Chapter 3 gives an overview of time-invariant and time-varying system identification techniques, including the parallel-cascade algorithm, and briefly discusses improvements that the author made to the implementation of the TVPC algorithm. Chapter 4 describes the results of a simulation study evaluating the performance limits of the

TVPC algorithm. It specifically examines the algorithm's ability to track rapid TV system dynamics, and evaluates its performance under various conditions. Chapter 5 presents the results of an experimental study, which used the TVPC algorithm to examine the properties of intrinsic and reflex stiffness during an isometric contraction/relaxation task involving low level contractions. The chapter also includes a detailed experimental methods section. Chapter 6 summarizes key findings and provides suggestions for future work.

2. BACKGROUND

This chapter presents information required to understand the background and rationale for the work described in this thesis. Since the focus of this thesis is ankle stiffness, the stretch reflex, the anatomy and physiology of the ankle, muscles, and related components of the nervous system are explained. The mechanics of the stretch reflex are explained in detail, including the sensory receptors and the reflex pathway. This is followed by a review of past studies of dynamic joint stiffness, and in particular reflex dynamics under both static and time-varying conditions.

2.1. ANKLE ANATOMY

The ankle, also known as the talocrural joint, is a complex joint composed of many tendons, ligaments, bones, and muscles that make movement possible. The tibia, fibula, and talus are the bones that make up the talocrural joint (see Figure 2-1). The tibia is the shinbone; at the proximal end, it forms one half of the knee joint, and at the distal end it interacts with the talus and fibula to form the ankle joint. The fibula is parallel and lateral to the tibia; the two bones are connected along their length by an interosseous membrane; at the proximal end of the fibula, the head articulates with the inferior surface of the lateral condyle of the tibia, and at the distal end, the lateral malleolus of the fibula articulates with the talus, and forms the distal tibiofibular joint. The talus is the most superior bone in the foot; it articulates with the tibia and fibula to form the ankle joint; it also articulates with the calcaneus, the heel bone, to form the subtalar joint.

The foot undergoes 2 main motions (see Figure 2-2): dorsiflexion and plantarflexion (movement of the foot towards and away from the shin, respectively), and inversion and eversion (movement of the soles of the feet towards and away from each other, respectively). Dorsiflexion and plantarflexion occur at the talocrural joint, while inversion and eversion are made possible by movement in the intertarsal joints (primarily the subtalar joint). Focus will be on dorsiflexion and plantarflexion because these motions have been extensively studied and are most relevant to this thesis research.

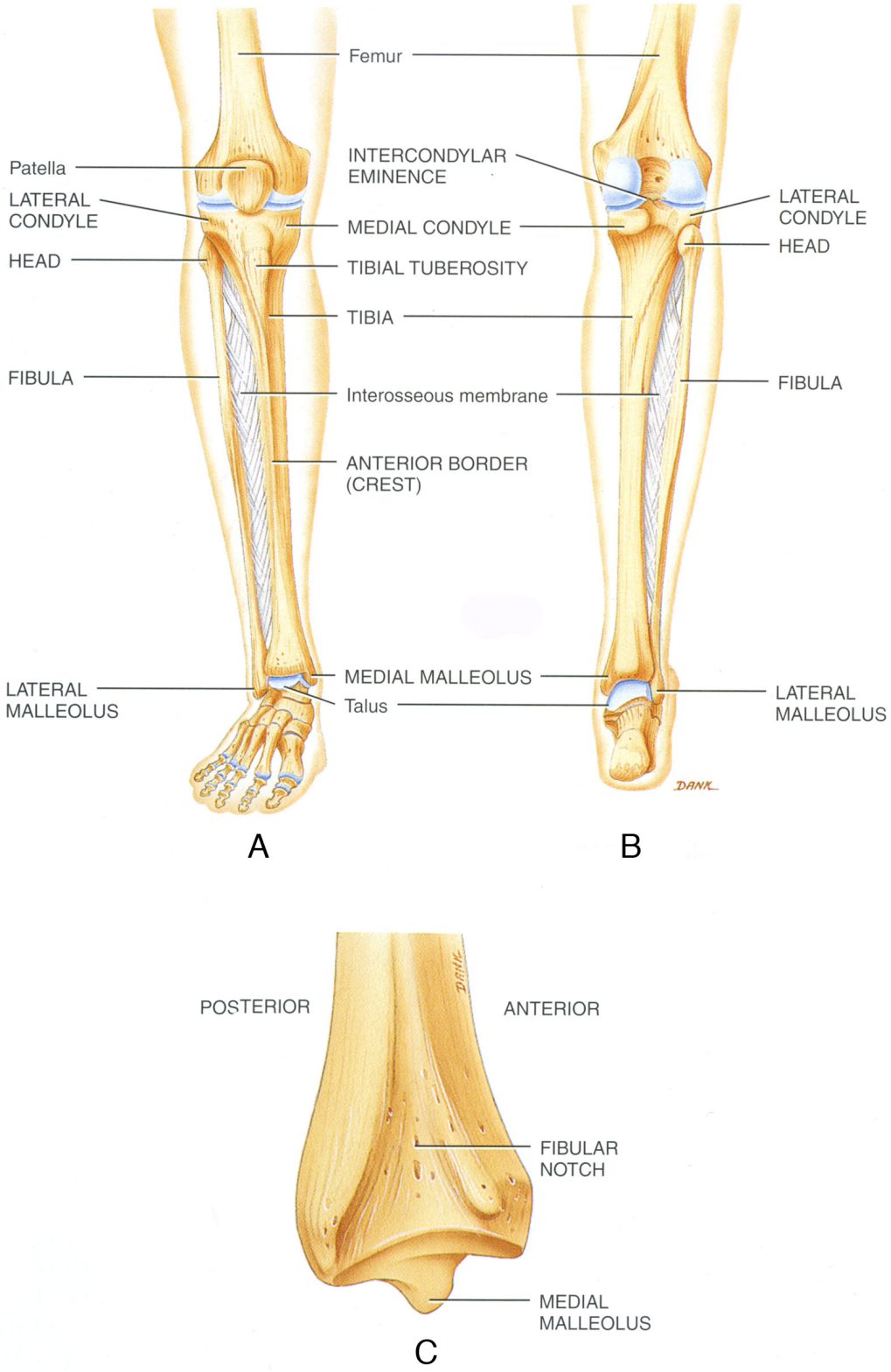

Figure 2-1. (A) Anterior view of the leg bones. (B) Posterior view of the leg bones. (C) Lateral view of the distal end of the tibia. Adapted from [14].

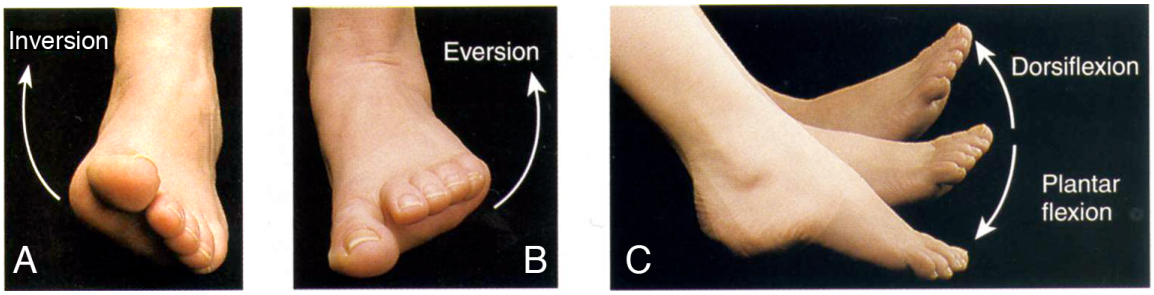

Figure 2-2. Motions of the foot. (A) Inversion: movement of the soles of the feet towards each other. (B) Eversion: movement of the soles of the feet away from each other. (C) Dorsiflexion and Plantarflexion: movement of the foot towards and away from the shin, respectively. Adapted from [14].

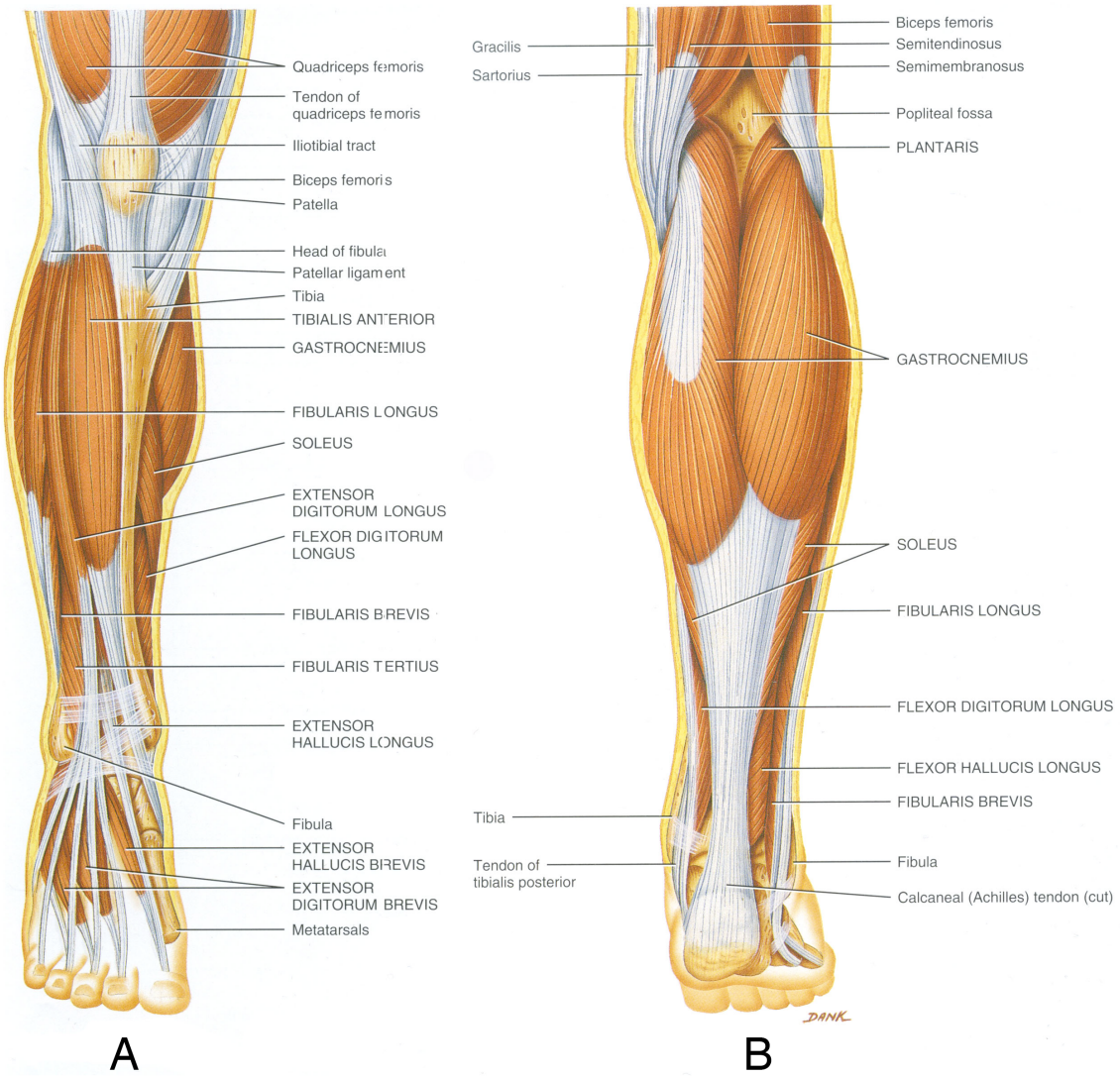

Figure 2-3. Leg muscles. (A) Anterior view. Notice the Tibialis Anterior (Shin muscle). (B) Posterior view. Notice the Gastrocnemius (calf muscle) and Soleus. Adapted from [14].

There are many muscles involved in the motion of the foot, but the three major muscles for dorsi- and plantarflexion are the tibialis anterior, gastrocnemius, and soleus (see Figure 2-3). The tibialis anterior (TA) is located against the lateral surface of the tibia. It is responsible for dorsiflexion of the foot at the ankle joint and inversion through the intertarsal joints. Gastrocnemius and soleus, collectively referred to as the triceps surae (TS), are located on the posterior aspect of the leg. TS produces plantarflexion of the foot through the ankle joint and eversion through the intertarsal joints [14].

2.1.1. Function of the Ankle Joint

The ankle plays a role in both locomotion and posture. During activities such as walking, running, and cycling the triceps surae and tibialis anterior aid movement by dorsiflexing or plantarflexing the foot. TA is used to decelerate the body, while TS produces the majority of forward and vertical propulsion [15]. During normal gait, the ankle does not use its entire range of motion [16]. Posture and balance are maintained by small coordinated contractions of the leg muscles in response to proprioceptive, visual, and vestibular stimuli [17].

2.2. SOMATIC NERVOUS SYSTEM

The nervous system is responsible for many functions within the body. It enables our special senses, regulates our internal organs, and controls our movements. The nervous system can be subdivided into the central nervous system (CNS) and the peripheral nervous system (PNS). The CNS, made up of the brain and spinal cord, is the main processing center. It processes incoming sensory information (afferent signals) and sends out the command signals (efferent signals) that control muscle contractions. The PNS encompasses all nervous tissue outside the CNS. This includes the cranial nerves, spinal nerves, ganglia and sensory receptors. The functions of the PNS can be subdivided into tasks that are voluntary and those that are not. Involuntary functions are mediated by the autonomic nervous system (ANS) and the enteric nervous system (ENS), while voluntary functions fall under the somatic nervous system (SNS) that consists of motor neurons that convey nerve impulses to muscles that are under voluntary control, i.e. the skeletal muscles. It also includes sensory neurons that relay information about the head,

body wall, limbs, and the special senses.[14] This thesis studies systems involving skeletal muscle control and response, and will therefore focus on the somatic nervous system.

2.2.1. Skeletal Muscle Anatomy and Physiology

Skeletal muscles are made up of hundreds to thousands of cells, called muscle fibres. Muscles cells are elongated, multi-nucleated cells that do not undergo mitosis once they have reached maturity. The muscle fibre is filled with myofibrils, the contractile structures of skeletal muscle. Myofibrils extend the length of the muscle fibre and are only about 2 µm in diameter. They have a striated appearance due to the small structures within them called filaments. There are thin filaments that are 8 nm in diameter and 1-2 µm long, and thick filaments that are 16 nm in diameter and also 1-2 µm long. The thin

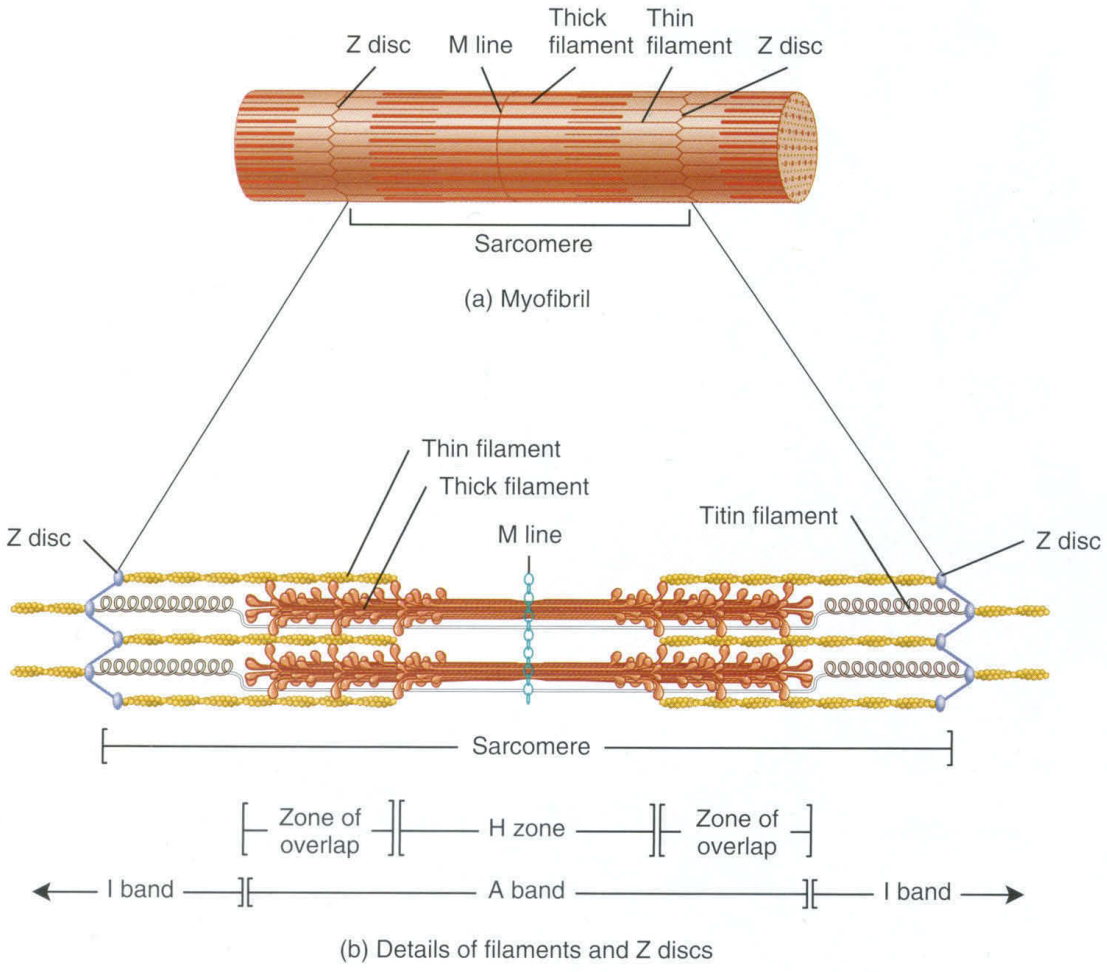

Figure 2-4. (A) A myofibril. Notice the sarcomere. (B) Bands and zones of a sarcomere. The H zone is where there is no overlap between the thin and thick filaments. The A band is the length of the thick filament. The I band is where there are no thick filaments. Adapted from [14].

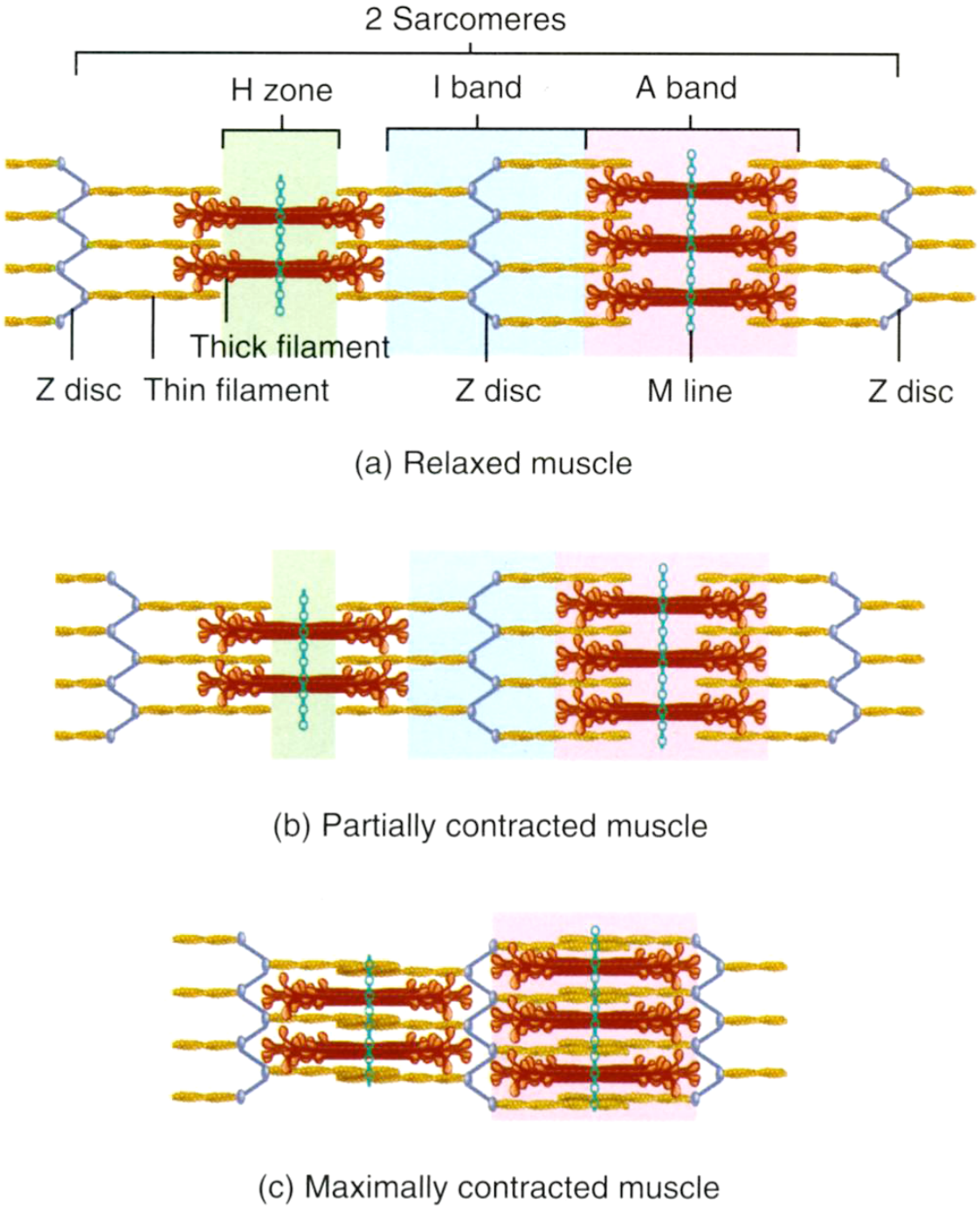

Figure 2-5. (a) Relaxed muscle (b) Partially contracted muscle: the width of the H, I, and A band become smaller as the overlap between the thin and thick filaments increases and the sarcomere shortens (c) Maximally contracted muscle: the A band and H zone are reduced to zero and no further contraction is possible. Adapted from [14].

and thick filaments do not extend the entire length of the myofibril but are arranged in units called sarcomeres. The thin and thick filaments overlap by a variable amount depending on the level of contraction. The pattern of overlap is the source of the striated appearance of the myofibril and can be characterized by bands and zones (refer to Figure 2-4). The dark band in the middle of the sarcomere, called the A band, is due to the presence of the thick filaments. The H zone is the region in the center of the A band where there are no thin filaments. The rest of the A band involves zones of overlap. The I bands, located at the ends of the sarcomere, have a lighter colour than the rest of the sarcomere because they consist of thin filaments only. Z disks separate the sarcomeres, while M lines mark their centre.

The thick filaments (see Figure 2-4) in skeletal muscle are made up of about 300 molecules of the contractile protein, myosin. The thin filaments (see Figure 2-4) are primarily made up of the contractile protein, actin. The actin molecules are connected together to form a helical filament. There are myosin-binding sites on each actin molecule. Muscle contraction results from the interaction between myosin and actin. A myosin molecule is shaped like two golf clubs twisted together; the golf club heads are called the myosin heads, while the twisted shafts are called the myosin tail. A contraction occurs when the myosin head binds to the actin and 'walks' along the thin filament. This occurs at both ends of the sarcomere, causing the thin filaments to be pulled towards the M line (see Figure 2-5). As the thin filaments move inward, the Z disks move closer together, thus shortening the sarcomere. As the sarcomeres shorten, so does the muscle fibre, and the entire muscle. Not all the myosin heads in a thick filament bind at the same time. As some myosin heads are forming crossbridges with the actin and generating force, others are detached and waiting to bind. This is what creates the 'walking' action of the thick filament along the thin filament [14].

2.2.2. Motor Neurons and Motor Units

Skeletal muscles receive commands from the CNS through somatic motor neurons originating in the brain stem or spinal cord. The cell bodies of the neurons that innervate the limbs are located in the spinal cord and their axons can be quite long, as they must reach from the spinal cord to all the skeletal muscles of the limbs. Each axon branches out and

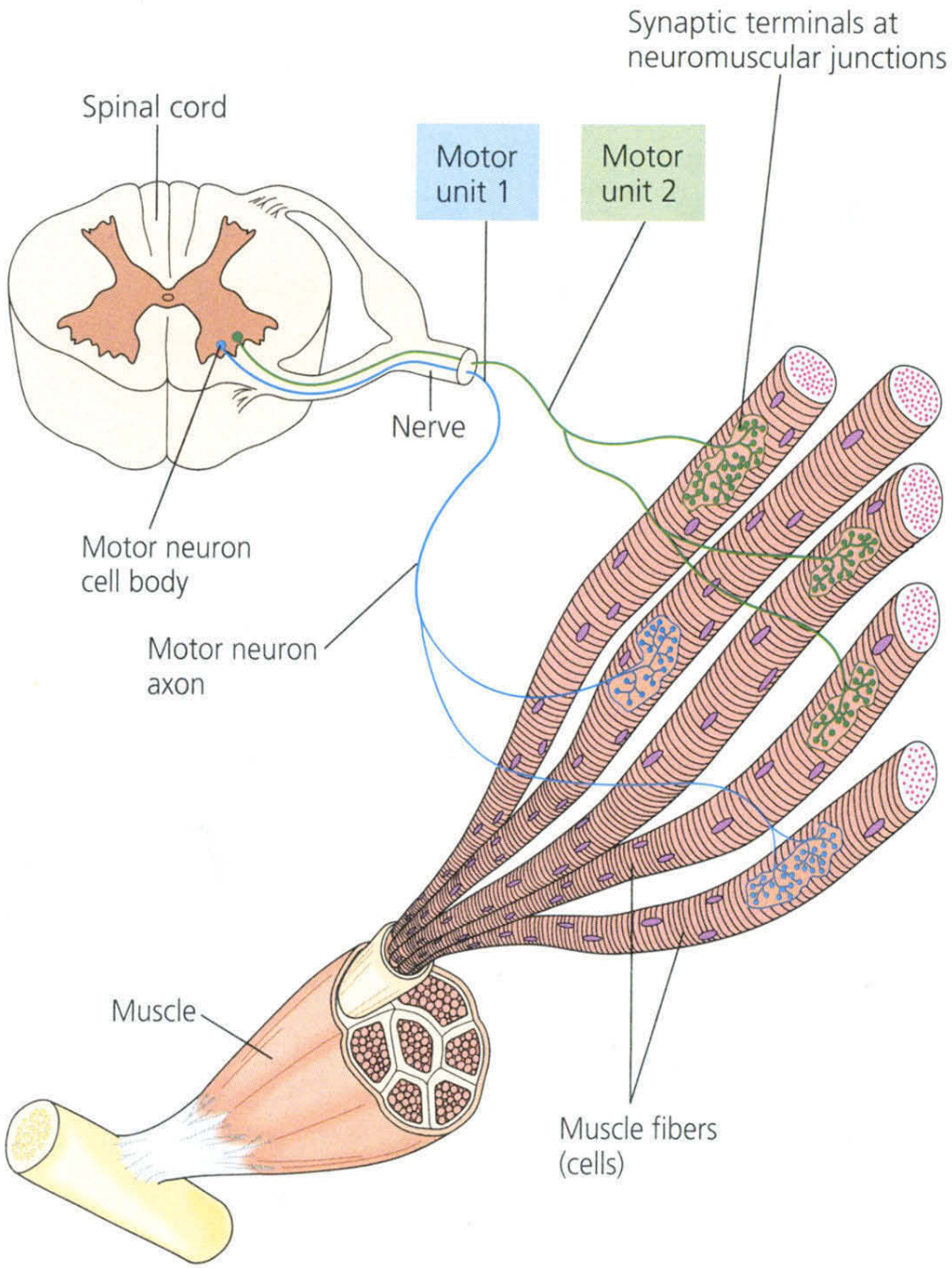

Figure 2-6. Motor Unit. A motor unit consists of a motor neuron and all the muscle fibres that it innervates. A muscle fibre is only ever part of one motor unit. The number of muscle fibres in a motor unit depends on its function. Adapted from [82].

connects with multiple muscle fibres, forming a motor unit. A motor unit consists of one motor neuron and all the muscle fibres it innervates (see Figure 2-6). There are, on average, 150 fibres in one motor unit dispersed throughout the muscle. All fibres in a motor unit contract simultaneously in response to a stimulus. Each muscle fibre receives excitation from only one motor neuron and is therefore part of only one motor unit. Each muscle has multiple motor units, but the number of fibres per unit and the number of units depends on the role of the muscle. Precision muscles have very small motor units, with as few as 2 or 3 fibres; large, powerful skeletal muscles may have as many as 3000 muscle fibres per motor unit. The strength of a contraction is modulated by controlling the number of active motor units and their firing rate [14].

2.2.3. Skeletal Muscle Contraction Mechanics

Movement occurs when the tension generated by the muscle exceeds the resistance of the object to be moved. Contractions can be classified as either isotonic or isometric. A contraction that maintains a constant muscle tension, while the length of the muscle changes, is said to be isotonic. Isotonic contractions produce movement and are classified in two categories: concentric and eccentric. Concentric isotonic contractions are achieved when the muscle tension exceeds the resistance of the environment and the muscle shortens. Eccentric isotonic contractions occur when the opposite is true and the resistance of the environment exceeds the muscle tension causing the muscle to lengthen. A muscle contraction that does not produce movement is called an isometric contraction. In this type of contraction, the length of the muscle does not change, and the muscle tension equals that of the environment.

A muscle contraction is initiated when the muscle fibres are stimulated by a nerve impulse. One nerve impulse from a motor nerve produces a muscle action potential in all the muscle fibres within the motor unit. However, the force generated by that single action potential is not the maximum force that the muscle fibre can produce. Contraction force of a muscle fibre largely depends on the rate at which nerve impulses reach the fibre. The process by which the frequency of stimulation modulates muscle tension is called rate-encoding. The contraction force also depends on the length of the muscle before contraction. The total force produced by a muscle can also be varied by activating

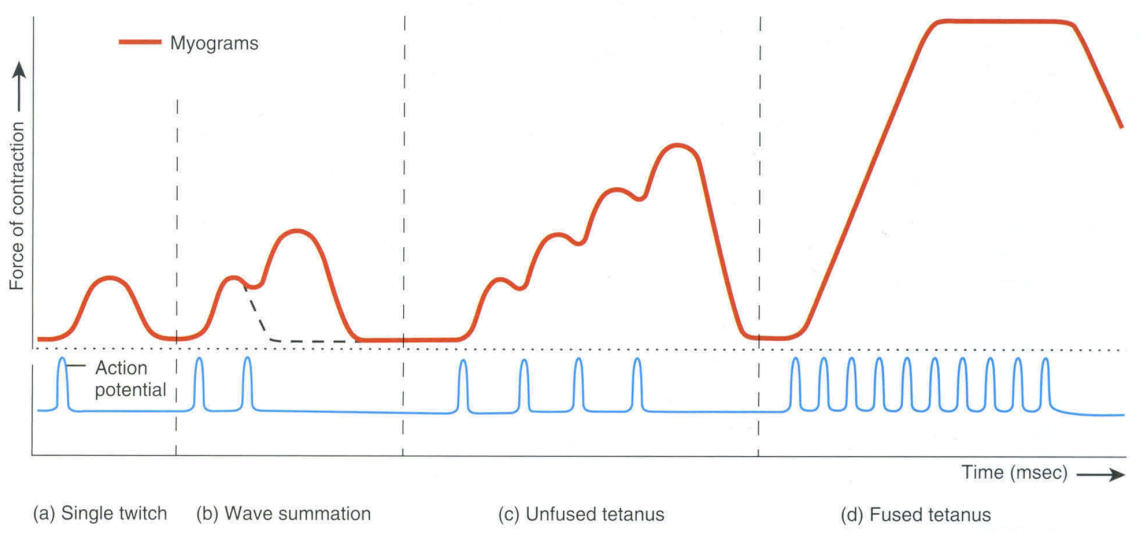

Figure 2-7. Rate Encoding. (a) Single twitch due to a single action potential. (b) Wave summation occurs when a second action potential excites the muscle before it has fully relaxed from the previous stimulus. (c) Unfused tetanus results in a sustained but wavering contraction. (d) Fused tetanus is achieved when the muscle does not relax at all between stimuli. Adapted from [14].

more or less motor units at a time. [14] Each of these effects will be discussed in more detail in the following sub-sections.

2.2.3.1. Rate-encoding

A single stimulus will elicit a twitch contraction lasting from 20 to 200 ms (see Figure 2-7A). There is a small delay between the stimulus and the contraction, as the action potential propagates through the muscle fibre. After this latent period, the contraction phase begins and lasts from 10-100 ms. This is followed by the relaxation period, which also lasts 10-100 ms. After a muscle fibre has been stimulated, there is a period of time where it will not respond to another stimulus, called the refractory period. In skeletal muscle, the refractory period lasts only about 5 ms. A second stimulus applied after the refractory period but before the muscle fibre has completely relaxed will generate a stronger contraction. This is due to a process called wave summation (see Figure 2-7B) that occurs because additional calcium ions, which allow for myosin binding, are released due to subsequent stimuli while there is still a large concentration of calcium ions as a result of previous stimuli. The higher concentration of calcium ions increases the peak tension.

A sustained muscle contraction is achieved by repeated stimulation of a muscle fibre before it has had the chance to relax. If a muscle fibre is stimulated at 20 to 30 times per second it produces a sustained but wavering contraction, called unfused tetanus (see Figure 2-7C). Fused tetanus (Figure 2-7D) is achieved when a muscle fibre does not relax between stimuli. This occurs at stimulation rates of 80 to 100 Hz. Perhaps surprisingly, smooth, sustained contractions of an entire muscle are not ordinarily achieved by fused tetanic contraction of the muscle fibres. Rather, it is produced by unsynchronized, unfused contractions of different motor units within the muscle [14].

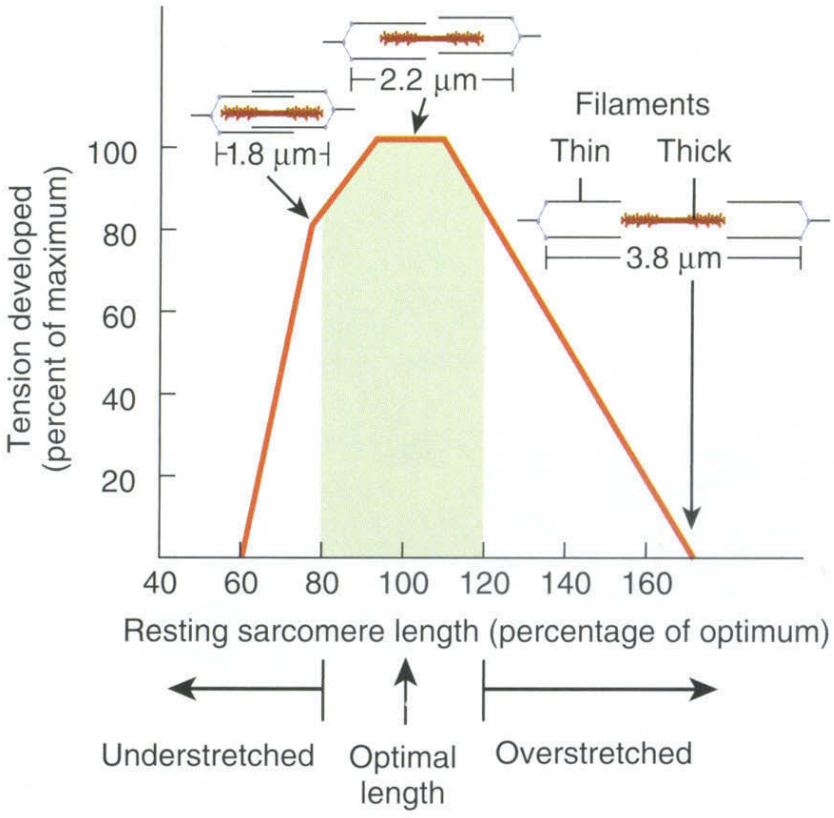

Figure 2-8. Length-Tension relationship. Maximum tension is achieved around 100% of the sarcomere's resting length. Increasing or decreasing the muscle length reduces the tension that can be generated. Adapted from [14].

2.2.3.2. Length-Tension Relationship

The strength of a muscle contraction depends on the sarcomere's length. The length-tension relationship is shown in Figure 2-8. The peak of the curve indicates the optimal length of a sarcomere is at 2.0 – 2.4 μm. This usually occurs when a muscle is at its resting length. At this length, there is the optimal overlap between the thin filaments and the myosin heads. As the sarcomere length increases (moving to the right of the graph), the overlap between the thin and thick filaments decreases and consequently the amount of tension that can be produced decreases. Once a muscle fibre is stretched to 170% of its optimal length, there is no overlap between the thin and thick filaments. This prevents the myosin heads from interacting with the actin filaments and therefore no tension can be produced. Conversely, if the sarcomeres are too short (moving to the left of the graph), the thin filaments overlap and make it more difficult for the myosin heads to bind. In the limit, the Z disks compress and crumple the thick filaments, thereby reducing the number of myosin heads available for binding. [14]

2.2.3.3. Recruitment

The final mechanism for modulating muscle contraction force is motor unit recruitment, the process in which motor units are activated and deactivated as required. Recruitment follows the size principle, which states that smaller motor units are recruited before larger ones. Small motor units are usually composed of slow twitch fibres, while large motor units tend to be made up of fast twitch fibres. Orderly recruitment has several potential functional advantages; it ensures that smaller, more fatigue resistant motor units are recruited first, while the larger, more easily fatigued motor units are reserved for tasks that require a large amount of force for a short period of time. The faster motor units are also the largest and therefore can produce more force than the slower ones. [18]

Smooth movements also result from the size principle. The smaller, slower motor units with the smallest force output are recruited first, and as more force is required, progressively larger motor units are recruited, whose force output is roughly proportional to the force at which they were recruited [18].

Recruitment also plays a role in preventing muscle fatigue. To allow for a contraction to be maintained for long periods of time with limited fatigue, motor units alternate between contracted and relaxed states. Different motor units take turns sustaining the contraction. [14]

2.2.4. Electromyography (EMG)

Electromyography is a measure of the electrical activity of muscles. The electrical activity originates from the impulses traveling along the membrane of the muscle fibres. These action potentials create an electrical field that can be measured by placing an electrode on the surface of the skin or by inserting a needle electrode directly into the muscle. Needle electrodes record motor unit action potentials (MUAP) from a very small volume of tissue and can target deep muscle fibres. Surface electrodes, on the other hand, detect MUAPs in a large volume and primarily record from the superficial muscle fibres. The needle electrode measurement technique provides more precise, targeted readings, yet it is the less common method because of the ease of use and the non-invasive nature of the surface electrode.[19] Furthermore, surface electrode recordings may be preferable if the goal is to record the overall muscle activity.

With EMG recording, there is a layer of tissue between the muscle fibres, the source, and the electrode, which changes the properties of the signal. This tissue acts as a volume conductor, and the properties of this conductor determine many features of the signal, such as its frequency content. In general, the biological tissue acts as a spatial low-pass filter on the distribution of electrical potentials from the muscle fibres. The electrode's size and dimensions also affect the features of the detected signal. The potential measured by the electrode is the average of the potential distribution over the skin under it. So the electrode also acts as a spatial low-pass filter.[19]

Crosstalk is a common problem with surface electrodes. Crosstalk is the interference of signals from nearby muscles other than the one of interest. It occurs because of volume conductor properties and source properties. It leads to frequent interpretation errors, such as muscles being incorrectly identified as active, when they are at rest, while a nearby muscle is active.

Since EMG represents the level of muscle activation, it would follow that it represents force output. In general, with isometric contractions, EMG has been found to vary monotonically with force. One study found that under static conditions the dynamic EMG/force relationship is well described by a second-order low-pass filter. However, they also found that the parameters of the filter varied greatly with the type of movement being executed, making it very difficult to create a general model. [20] The EMG-force relationship during isotonic contractions is much more complex. One particular study examined EMG and torque during an imposed walking movement and found that at a point of peak EMG no discernible torque was generated [21]. The relationship is more difficult to generalize because of the change in muscle length and the effect of the rate of change of length on the output torque. Therefore, caution should always be taken when interpreting the functional significance of EMG recordings during tasks involving isotonic contractions.

2.2.5. Peripheral Sensory Receptors

The efferent pathways of the somatic nervous system (SNS) were discussed in detail in the previous sections. In addition, the afferent pathway plays an important role in reflexes and the control decisions made by the CNS. The afferent pathway relays sensory information about the head, body walls, and limbs. This sensory information gives rise to the sense called proprioception, which indicates limb position and velocity. The sensors responsible for this sense are broadly termed proprioceptors. They are imbedded in muscles and tendons and provide information about the length of a muscle and the tension in the tendons. The brain constantly receives impulses from the proprioceptors, which allows it to produce coordinated muscle movements [14]. The muscle spindles, proprioceptors involved in the stretch reflex, and the Golgi tendon organs, which detect muscle tension, are discussed in the following sections.

2.2.5.1. Muscle spindles (Length-monitoring)

Muscle spindles are small proprioceptors; they have a fusiform shape and are found imbedded throughout the fleshy part of the muscle. Their main purpose is to monitor length changes in skeletal muscles. They are also vital to the stretch reflex (see Section

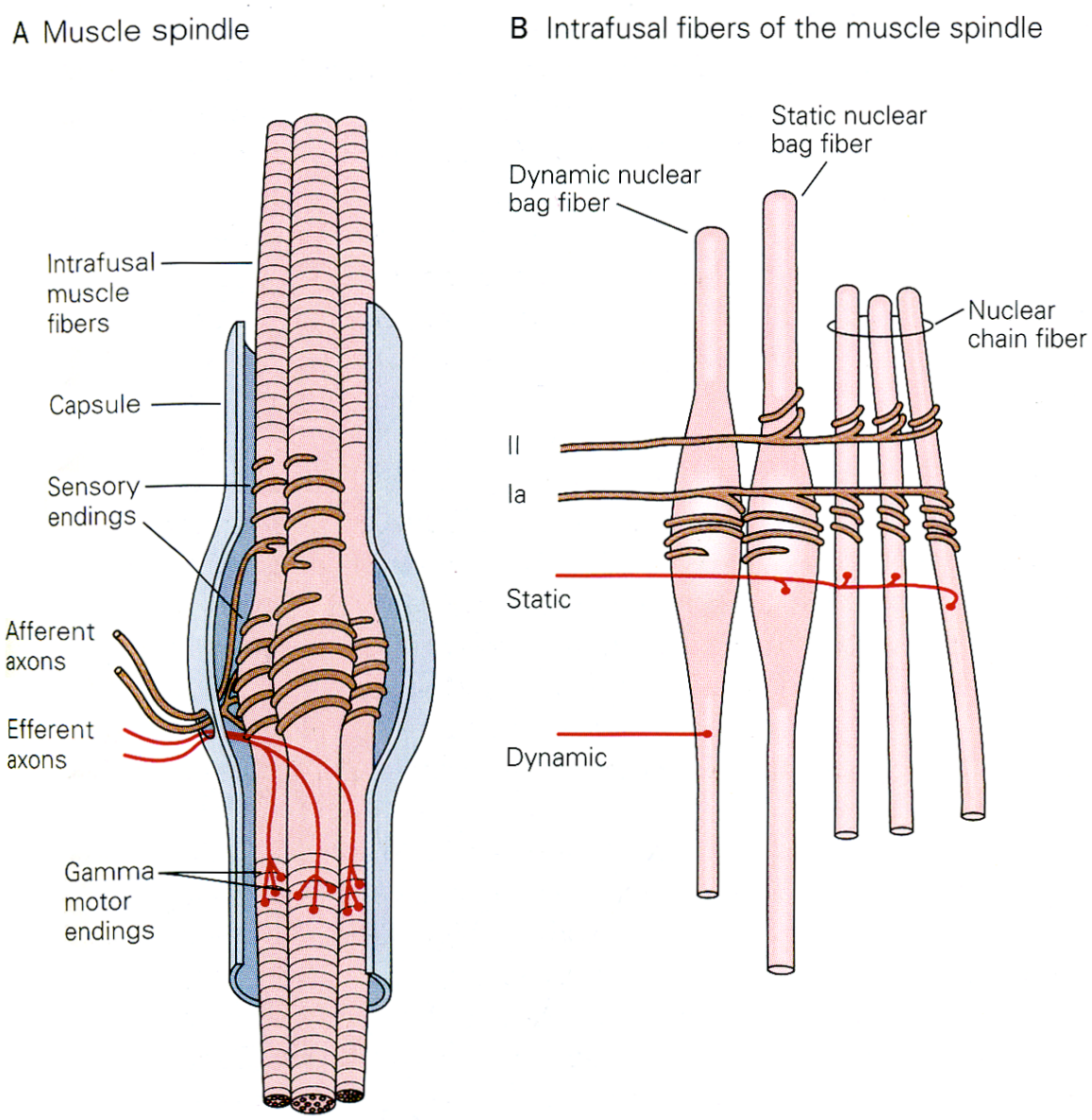

Figure 2-9. (A) Muscle spindle. Intrafusal muscle fibres are located within a capsule and innervated by afferent and efferent axons. Sensory endings wrap around the non-contractile centre of the intrafusal muscle fibres. The gamma motor endings innervate the contractile ends of the fibres. (B) Types of intrafusal muscle fibres and the types of neurons that innervate them. Adapted from [22].

2.2.6.1). Muscles involved in precisely controlled movements, such as in the fingers, have many muscle spindles. Conversely, there are fewer muscle spindles in muscles involved in coarser movements, such as the quadriceps and the hamstring muscles [14]. Muscle spindles have three main components (refer to Figure 2-9A):

1. A group of specialized muscle fibres, called intrafusal muscle fibres, with non-contractile central regions.

2. Sensory nerve endings.

3. Motor nerve endings.

The intrafusal fibres are enclosed in a capsule and run parallel to the regular muscle fibres, called extrafusal muscle fibres. There are three types of intrafusal fibres: dynamic nuclear bag fibres and static nuclear bag fibres, which have a bulbous centre region, and nuclear chain fibres, which have a more uniform cross-section (refer to Figure 2-9B). A muscle spindle usually has 2-3 nuclear bag fibres, and 5 nuclear chain fibres. These different fibre types have different functions, which are also in part dictated by the type of innervation they receive [22].

There are two types of sensory endings (refer to Figure 2-9B). The Ia sensory fibre is a large diameter (12-20 μm), myelinated neuron that innervates all three types of intrafusal muscle fibres. It wraps around the central regions of the intrafusal fibres to form the only primary sensory ending. The secondary sensory endings, formed by smaller diameter (6-12 μm) group II fibres, are located adjacent to the central regions of the static nuclear bag fibres and nuclear chain fibres. When the intrafusal fibres are stretched, the sensory endings are distorted, and increase their firing rate. When the stretch is relieved, the activity decreases. [22] The extrafusal muscle fibres are innervated by large diameter alpha motor neurons. When the extrafusal fibres are stimulated and contract, gamma motor neurons prevent slack in the muscle spindles, which would reduce their sensitivity. The small diameter gamma motor neurons innervate the polar contractile ends of the intrafusal muscle fibres and cause them to contract, helping to maintain their sensitivity. In fact, alpha and gamma motor neurons are often activated at the same time during

normal activity; this is referred to as alpha-gamma coactivation. The action of the gamma motor neurons does not contribute to the overall force output of the muscle but functions to adjust muscle spindle sensitivity. [22]

There are two types of gamma motor neurons, dynamic and static, that affect the sensitivity of the afferent sensory neurons differently. Dynamic gamma motor neurons innervate the dynamic nuclear bag fibres which only have a primary sensory ending. The *dynamic* gamma motor neurons are so called because they increase the primary afferents response to *dynamic* length changes during a ramp stretch. Static gamma motor neurons innervate both the static nuclear bag fibres and the nuclear chain fibres, which have both primary and secondary endings (refer to Figure 2-9B). The static gamma motor neurons increase the sensory endings steady-state response to a ramp stretch. However, the dynamic response of the afferents is much more complex than can be deduced from a simple ramp stimulus. [23]

Figure 2-10A shows the response amplitude (impulses/s) of primary and secondary endings to different stretch amplitudes (mm) at 1 Hz. Primary endings clearly have a much greater sensitivity (impulse/s/mm) to small amplitude stretches than do secondary endings and also have a very small linear range. Secondary endings have lesser sensitivity but have a much larger linear range. At larger stretch amplitudes, the difference in sensitivity of the primary and secondary afferents is insignificant. Figure 2-10B shows the sensitivity of primary and secondary endings to stimuli of different frequencies. Both primary and secondary endings have a similar highpass response; the sensitivity of the secondary ending is only an absolute order of magnitude lower. The primary afferent's sensitivity increases more quickly at higher frequencies, which may suggest some acceleration response as well **[23]**. The muscle spindles are very tunable structures. Their response to changing length of the parent muscle is largely determined by the gamma motor neuron activity. The dynamic response and sensitivity of the muscle spindle can be modified by selective stimulation by the gamma motor neurons **[22]**.

Spindle information about muscle stretch goes to three places: (1) the spinal cord, which mediates the stretch reflex, (2) the sensory areas of the cerebral cortex, which allow for

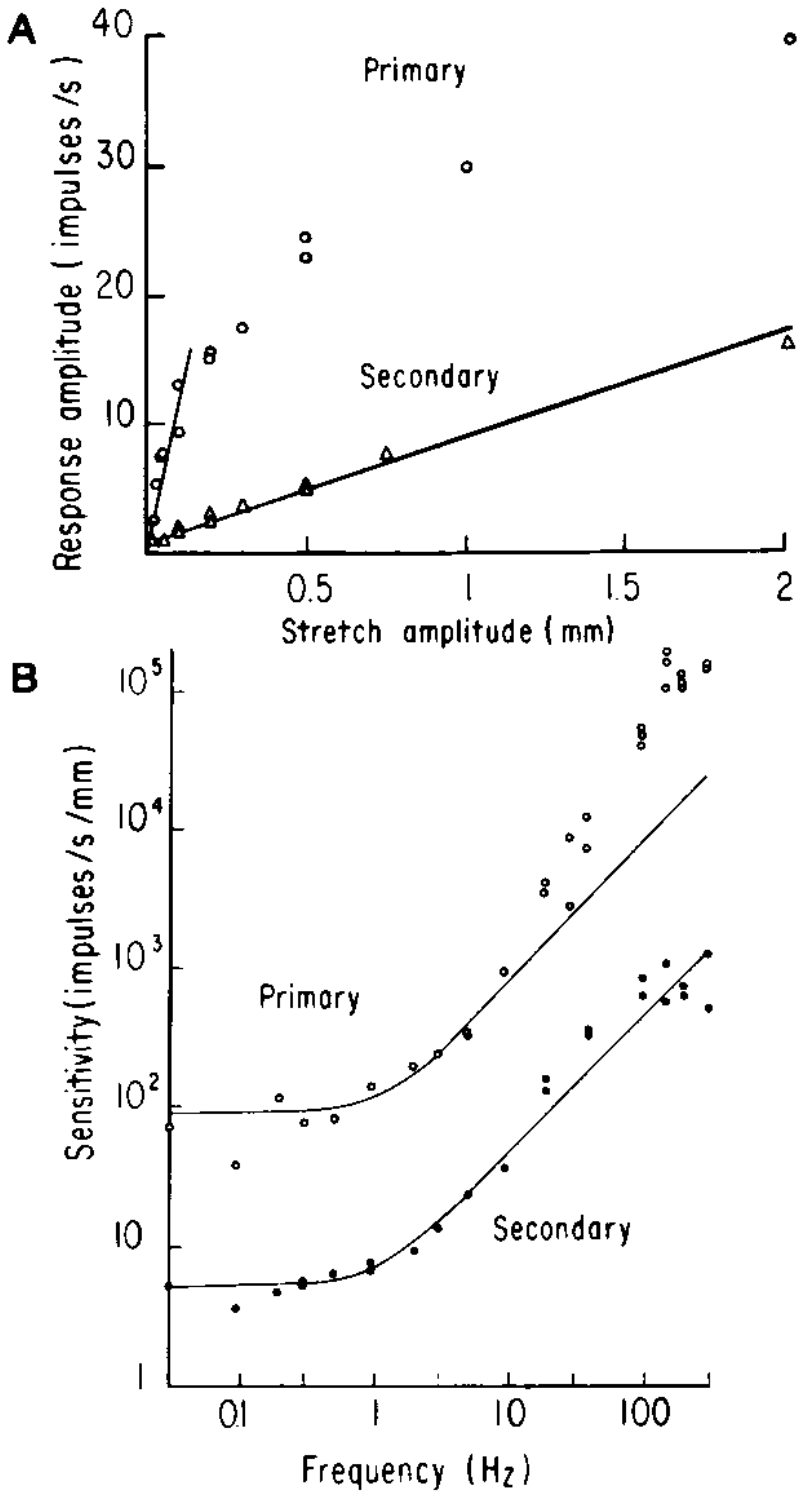

Figure 2-10. (A) Response amplitude vs. Stretch amplitude. The slope of the lines represents the sensitivity. Primary endings have a much greater sensitivity to small stretch amplitudes than secondary endings and also have a small linear range. (B) Sensitivity vs. Frequency. Primary and secondary endings both have a similar highpass response with only an order of magnitude difference. The primary ending's sensitivity increases faster at high frequencies, which may indicate an acceleration sensitivity. Adapted from [23].

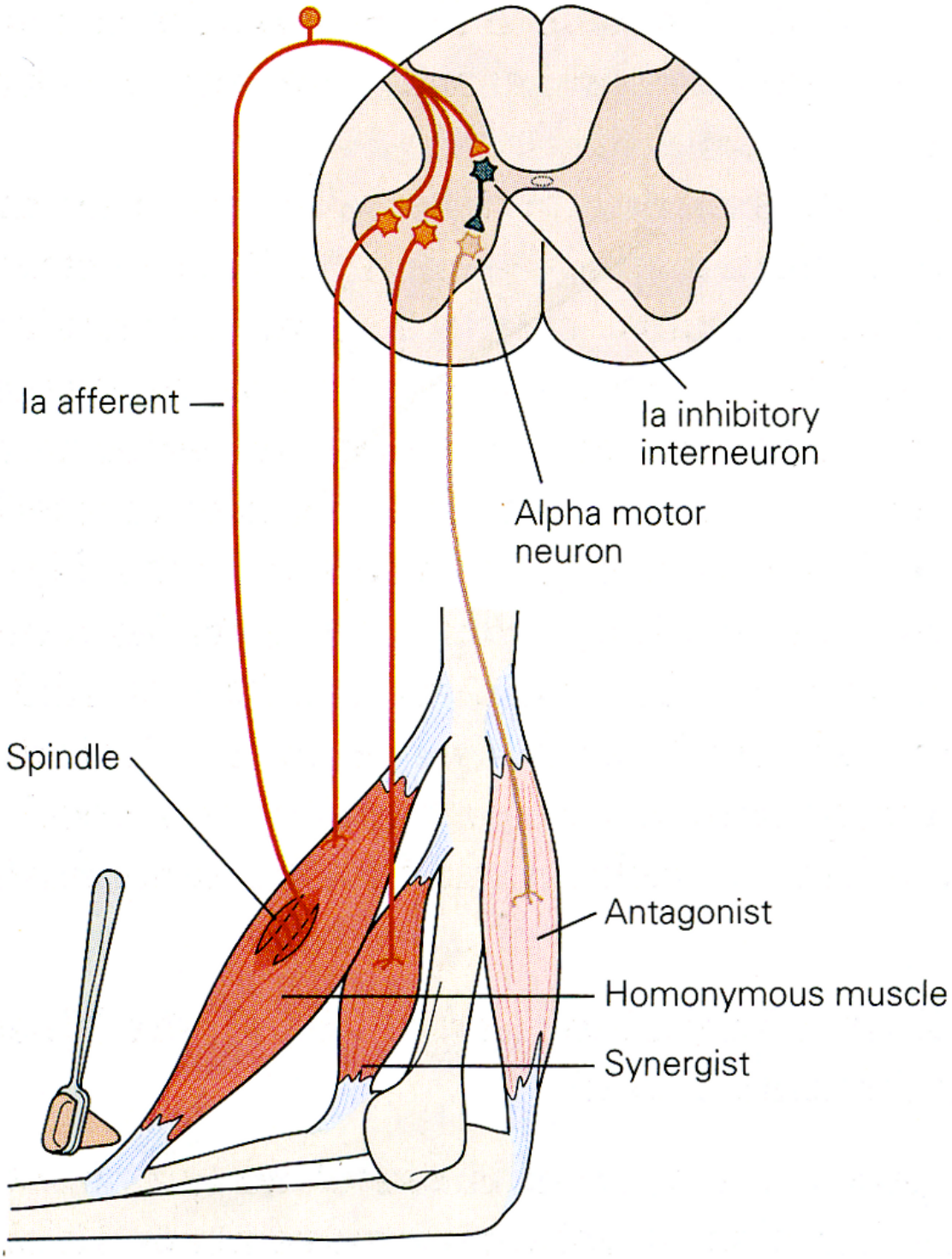

Figure 2-11. Stretch reflex pathway. A muscle stretch causes a response in the muscle spindle. This response travels up the Ia afferent and synapses in two places. It connects directly to alpha motor neurons of the homonymous and synergist muscles, forming a monosynaptic connection, which causes those muscles to contract. It also synapses onto the Ia inhibitory interneuron which connects to the alpha motor neuron of the antagonist muscle and causes it to relax. This reciprocal innervation prevents the antagonist muscles from interfering with the agonist muscle contraction that relieves the stretch. Adapted from [22].

conscious perception of muscle position, and (3) the cerebellum, which helps coordinate muscle contractions. [14] At the spinal level (see Figure 2-11), the Ia afferent fibres synapse directly onto the alpha motor neurons of the same muscle, forming a monosynaptic connection. They also synapse onto agonist muscles that produce the same action. This causes the muscles to contract and relieve the stretch. The Ia fibres also activate a polysynaptic inhibitory pathway by synapsing onto the Ia inhibitory interneurons, which synapse onto the alpha motor neurons of the antagonist muscles and cause them to relax. This prevents conflict between the muscle groups and coordinates the limb movement. This mechanism is referred to as reciprocal innervation, when a muscle is stretched, its antagonist relaxes.[22] The stretch reflex will be discussed in more detail in Section 2.2.6.1.

2.2.5.2. Golgi Tendon Organs

Golgi tendon organs (GTO) are small sensory receptors that detect tension in the muscle. They are located at the junction between muscle fibres and the tendon, placing them in series with a group of muscle fibres (refer to Figure 2-12). Since they are in series with the muscle fibres, they become taught when the muscle contracts, which is the opposite of the muscle spindles, which slacken when the muscle contracts. The GTO is an encapsulated structure that contains braided collagen fibres. Each GTO is innervated by a single group Ib sensory neuron. The Ib axon enters the capsule, after which it loses its myelination and branches into many small nerve endings, which intertwine with the collagen fibres. Stretching the capsule straightens the collagen fibres, compresses the free nerve endings, and causes them to fire. [22] The GTO are not very sensitive to passive force because the overall tension is distributed over all the receptors, so the tension sensed by each is very small. However, their structure makes them very sensitive to force in the muscle fibers to which they are connected, which makes them very sensitive to active contractions. Studies have shown that the average level of activity of the GTO of a contracting muscle gives a good measure of the total force it generates.

The Ib afferent axons synapse onto the Ib inhibitory interneurons, causing inhibition of homonymous muscles. In other words, when tension is sensed in a muscle, the GTO

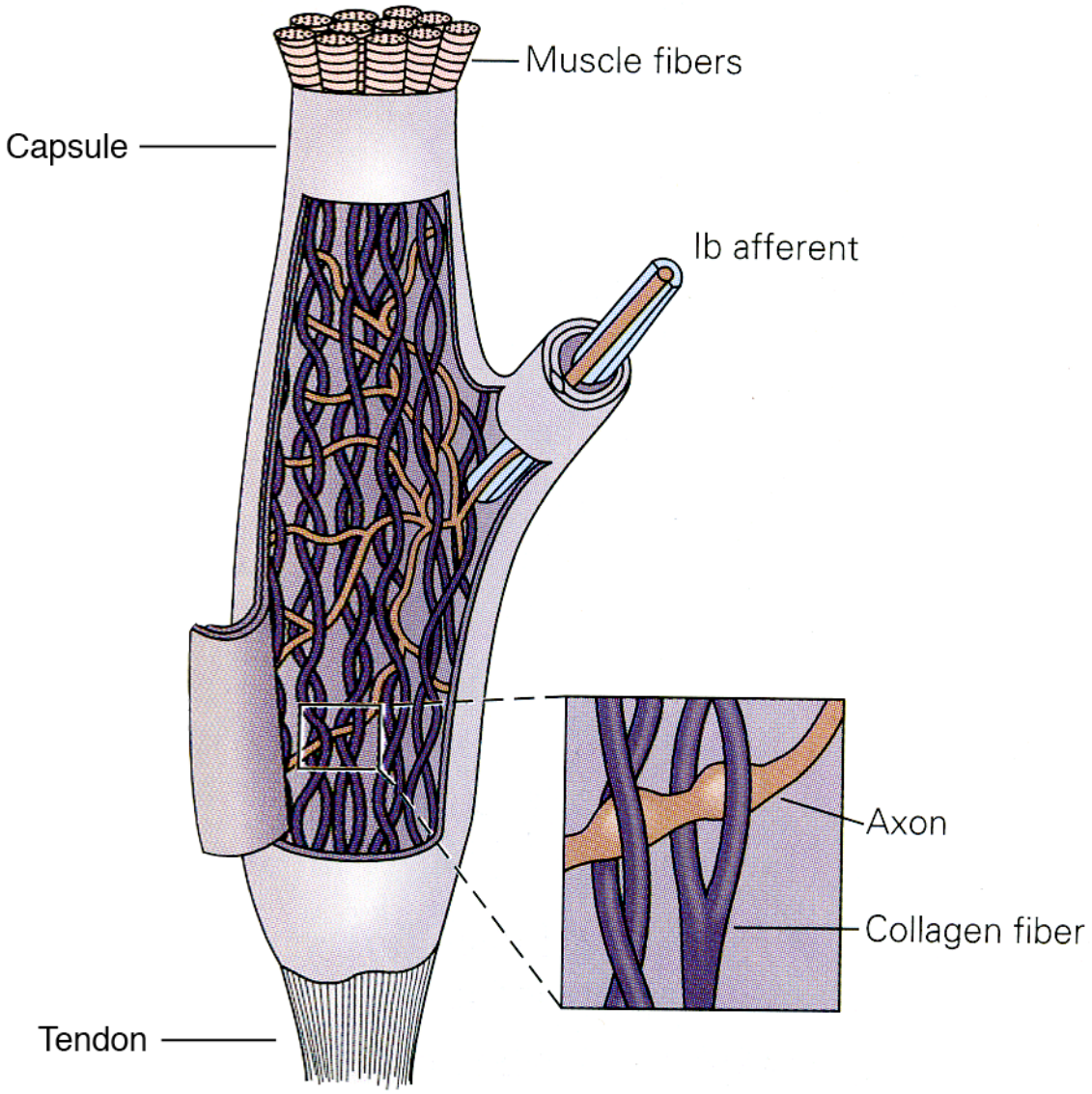

Figure 2-12. Golgi Tendon Organ. The Golgi tendon organ is located at the junction between the muscle fibres and the tendon. It consists of braided collagen fibres enclosed in a capsule. A Ib afferent innervates the structure. The single sensory neuron splits into small endings that are intertwined with the collagen. Tension in the muscle fibres stretches the capsule and straightens the collagen fibres, which pinch the nerve endings causing them to fire. Adapted from [22].

trigger a response that causes the muscle to relax and thus, alleviate the tension. The action of the Ib fibres is more complex than that explanation indicates. The interneurons that mediate their response, also receive input from the Ia muscle spindle fibres, afferent fibres from cutaneous receptors and joints, and excitatory and inhibitory inputs from multiple descending pathways, which will all contribute to the final response. Furthermore, the Ib fibres also form multiple connections to motor neurons of other joints, which has led to the speculation that the tendon reflex is part of a network that regulates whole limb movement. [22]

2.2.6. Peripheral Reflexes

A reflex is a rapid series of actions elicited in response to a specific stimulus. It is unplanned and automatic, such as pulling away from a hot surface. Since the processing of reflex responses needs to happen quickly, the brain is not directly involved, rather it is the spinal cord or brain stem that determines the response [14]. Of primary interest to this thesis are the reflexes classified as somatic, which involve the contraction of skeletal muscles. The following subsection looks at the response of one spinal reflex, the stretch reflex.

2.2.6.1. Stretch Reflexes

Stretch reflexes resist stretching of the muscle by causing the stretched muscle to contract, and thus, shorten. Section 2.2.5.1 discussed the action of the muscle spindle. The basic stretch reflex response involving the monosynaptic and reciprocal innervation, is seemingly very simple but can produce a broad range of responses. The reflex response is highly adaptable and can produce task appropriate responses [9, 10, 22]. In fact, the stretch reflex does not always cause the antagonist muscles to relax; during a ball catching task, both the agonist and antagonist muscles contract in response to a stretch [24]. The stretch reflex can also have more far reaching consequences and can cause muscles in other limbs to contract as well [22]. Furthermore, reflex strength can be voluntarily modulated, although whether we do this during normal function is not certain [8]. From these examples it is clear that the stretch reflex response is highly modulated in a functionally significant way.

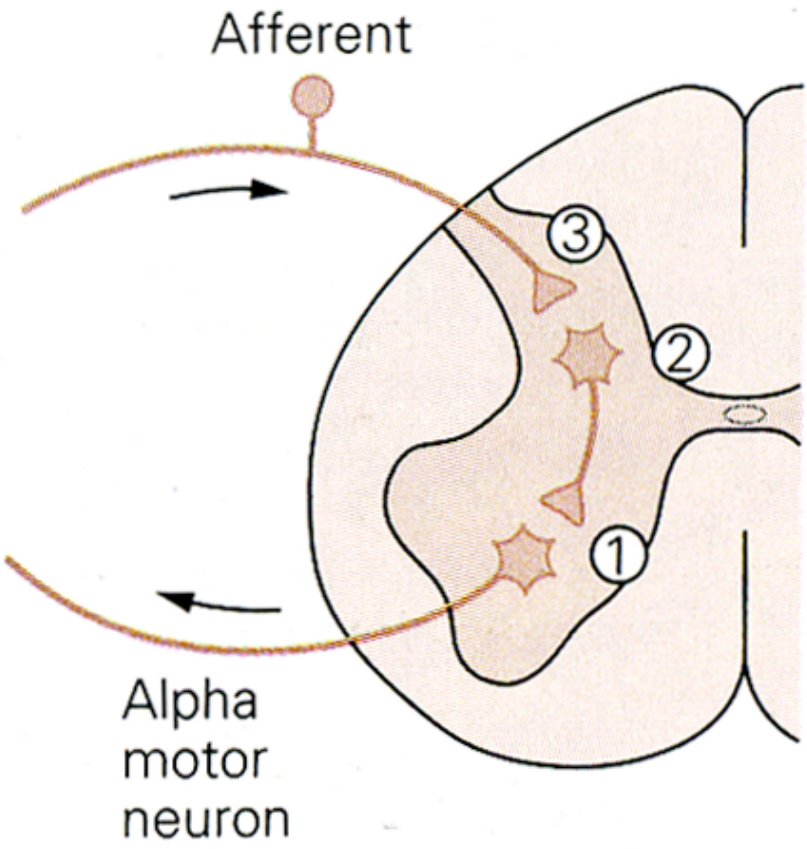

Figure 2-13. The magnitude of the stretch reflex response can be modulated at three locations in the spinal cord. Descending signals from regions of the upper nervous system and from other parts of the spinal cord synapse at those locations. (1) the alpha motor neurons, (2) the interneurons, and (3) the presynaptic terminals of the afferent fibres. Adapted from [22].

There are three main ways in which the stretch reflex can be modulated:

1. The sensitivity and dynamics of the muscle spindles can be regulated by the action of the gamma motor neurons, as discussed in Section 2.2.5.1.

2. The state of the joint, about which the reflex acts, affects its response. In fact, the strength of the reflex response changes with joint position[5], the level of torque acting about the joint [5, 25] and the mean average velocity with which the joint is perturbed [26].

3. The reflex response can be modulated at three sites in the spinal cord (refer to Figure 2-13): the alpha motor neurons, the interneurons, and the presynaptic terminals of the afferent fibres. Descending signals from regions of the upper nervous system and from other parts of the spinal cord synapse at those locations. They may regulate the strength of the reflexes by changing the background level of activity. For example, by

increasing the background activity of the alpha motor neurons, the neuron is closer to its firing threshold and will respond to smaller inputs from the Ia fibres [22].

There are clearly many ways in which the stretch reflex response can be modulated and adapted. The stretch reflex response has also been shown to be large and malleable enough to play a significant role in many day-to-day activities [26]. Exactly how and how much reflexes contribute is still unclear. The remainder of this chapter is dedicated to a discussion of past studies of dynamic joint stiffness that have worked to shed some light on motor control strategies.

2.3. DYNAMIC JOINT STIFFNESS

Dynamics deal with the forces acting on a body and the resulting movement [1]. This thesis is primarily concerned with the dynamics of human joints, which is defined as the dynamic relation between joint position and the torque acting about it[3]. It can be separated into two components[1]:

1. Intrinsic stiffness: due to the mechanical properties of the joint, active muscle fibers, and passive, visco-elastic tissues.

2. Reflex stiffness: due to the change in muscle activation mediated by the stretch reflex.

Joint stiffness plays an important role in the control of movement; it determines the force needed to achieve the desired final position of the limb and the movement that will result from an external perturbation [3]. However, the exact role of joint stiffness, and in particular, reflex stiffness, in movement and posture is still under debate.

There are a number of opposing motor control theories but they can generally be grouped in two categories: internal model control or equilibrium point control [27-30]. The internal model theory postulates that the CNS includes either inverse or forward models that predict the neural activation pattern needed to produce a specified movement [30, 31]. This theory must assume that the CNS accounts for the dynamics of the limb and external loads [30]. Within this category, certain theories postulate that the brain encodes movement parameters, such as position and velocity [32-35], and that

these are later converted to joint torques and muscle activations via an internal model [36]; others believe that muscle activation is directly encoded using built in knowledge of system dynamics [37, 38]. However, with both groups, once the neural signal reaches the spinal level it encodes for muscle activation, which in turn affects joint stiffness. Feedback from peripheral sensory receptors is used to update the internal models [28], but the role of the monosynaptic stretch reflex in movement is not clearly defined. This is problematic since the absence of reflexes has been shown to severely impair movement [39], indicating that they must play an integral role in any motor control theory. The internal model control theories also fall short when attempting to explain the transition from posture control to movement [30]. During postural control, reflexes work to return the body to a stable position. Without any reflex control, voluntary movements would trigger resistance, as the reflexes attempted to move the body back to a stable position [30].

The equilibrium-point (EP) hypothesis addresses this problem. The EP theory postulates that the brain sets various equilibrium points for the limbs. When a body part moves away from its equilibrium point, reflexive processes work to bring it back. Movement is generated by changing the EPs [40]. Both central commands and feedback from muscle spindles work together to set the EPs by modifying the threshold value, λ [41, 42]. In the EP theory, muscle forces are not computed explicitly by the brain, but are a consequence of the limb not being in the equilibrium position [29]. This could account for the severe motor control impairment seen in deafferented patients [30]. The progress of the EP hypothesis has been stalled by the difficulty of estimating λ. Attempts have been made to discredit this theory by modeling joint stiffness using a inertial-viscous-elastic model and converting it to an EP trajectory [43, 44]. However, it appears that the method did not estimate joint stiffness correctly and consequently, modeled the EP trajectory incorrectly [29]. The study of dynamic joint stiffness using more comprehensive models, such as the one explored in this thesis, may help clarify the role of joint stiffness in movement, and help shed some light on the motor control debate.

Ultimately, understanding the role of joint stiffness in movement will greatly improve the design of prosthetic devices and human-machine interfaces. It will also provide a more

quantitative means of evaluating the progression and rehabilitation of neurological diseases [2]. The following section examines research in the field of dynamic joint stiffness.

2.3.1. Studies in joint dynamics

Early studies in joint dynamics often referred to joint stiffness as a whole, and did not differentiate explicitly between intrinsic and reflex stiffness [2, 3, 45, 46]. However their methods limited them to the study of intrinsic stiffness, because they examined the linear dynamic relationship between position and torque, and as discussed below, reflex stiffness is highly non-linear.

Hunter and Kearney [3] developed an intrinsic stiffness model to quantify joint stiffness properties. This model relates position to torque through a linear, 2nd-order transfer function:

$$\frac{TQ(s)}{P(s)} = Is^2 + Bs + K$$

where K, B, and I are the elastic, viscous and inertial parameters, respectively. Using this model, it was shown that intrinsic stiffness varied with many conditions, such as joint position [5, 45, 46], the mean ankle torque [3, 5], and the perturbation displacement amplitude [2]. Specifically, ankle stiffness was found to increase (i.e. K and B increased) with increasing levels of voluntary contraction [3, 45] and with progressive ankle dorsiflexion [45, 46] (see Figure 2-14). These results show that more force is required to rotate the ankle when the muscles are contracted than when they are relaxed (Figure 2-14B), and that it becomes increasingly difficult to rotate the ankle as it approaches the limits of its range of motion (Figure 2-14A). It has also been shown that ankle stiffness has a strong non-linear dependence on the amplitude of the perturbations used to identify it; increasing displacement amplitude decreased ankle stiffness [2]. Since stiffness is highly dependent on the state of the joint it is difficult to create a model that describes its behavior under all circumstances.

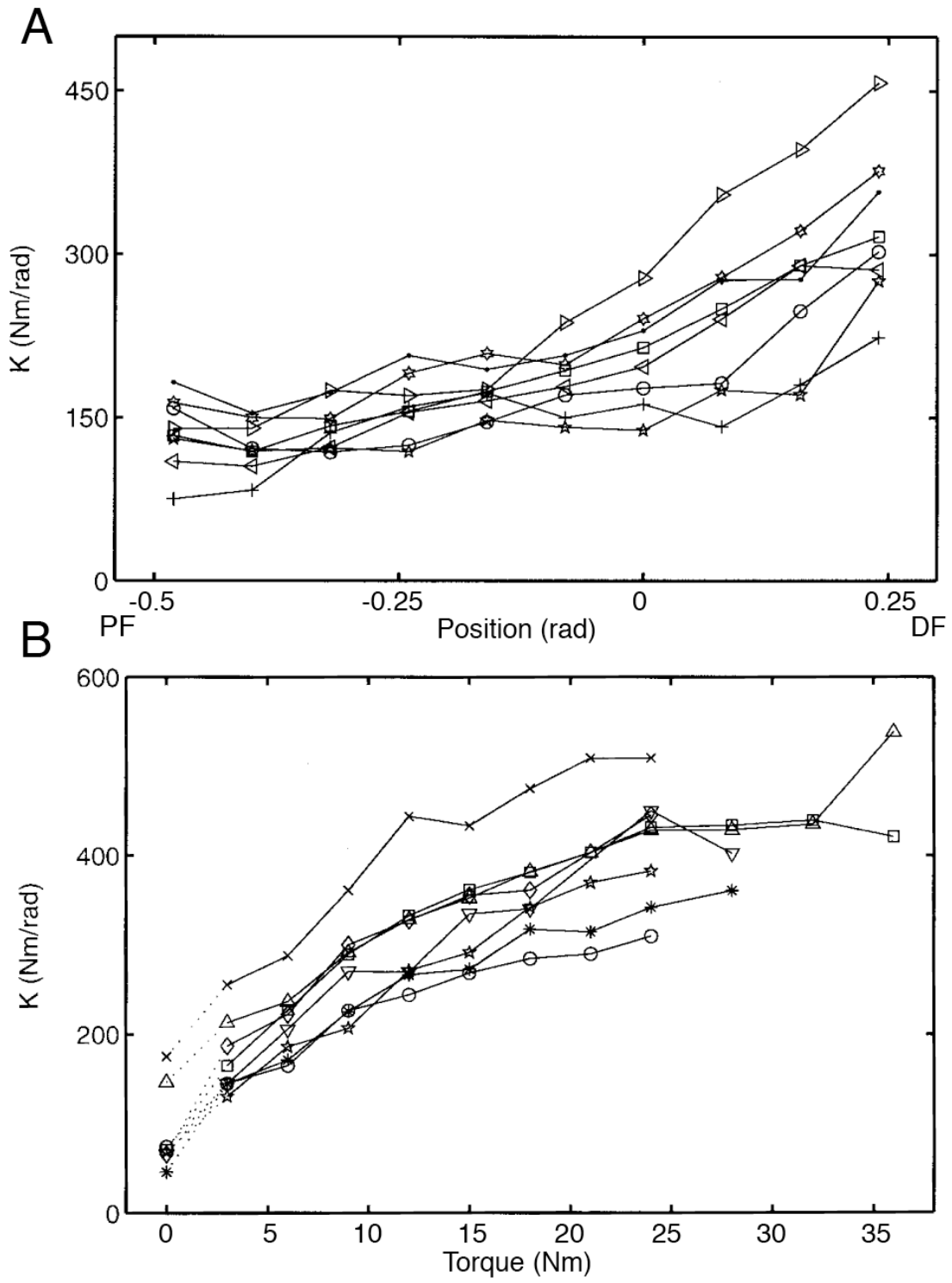

Figure 2-14. (A) Intrinsic gain, K, versus position for 8 subjects. As ankle moves from a plantarflexed position to a dorsiflexed position, K increases. (B) Intrinsic gain, K, versus plantarflexing torque for 7 subjects. As the voluntary torque increases so does K. Adapted from [5].

2.3.1.1. Stretch Reflex Dynamics

2.3.1.1.1. Reflex Stiffness model

Relatively few studies have examined reflex stiffness because reflex torque cannot be recorded separately from intrinsic torque, making it difficult to isolate the reflex stiffness contribution. Attempts were made to circumvent this problem by blocking the reflex response by using electrical stimulation [47-49], nerve block [50], or deafferentation [51, 52] to record a reflex-free baseline response, which could later be removed from the total torque to isolate the reflex response. The technique could potentially lead to over or underestimation of the reflex contribution if there were changes in the intrinsic baseline [5]. Other studies have avoided the problem completely by focusing on the reflex EMG response instead of the reflex torque response, because the EMG does not have a mechanical intrinsic component and can, therefore, be described more directly. Ideally, both intrinsic and reflex stiffness components must be identified simultaneously. Kearney et al. [4] developed a parallel-cascade system identification technique (described in Section 3.5) to do this. The parallel-cascade model of ankle stiffness incorporates the intrinsic stiffness model, described in the previous section, and also includes a model of reflex stiffness dynamics.

Studies of reflex EMG dynamics at the ankle were able to establish that there is a 40 ms delay from the onset of the stretch to the change in EMG, and that the stretch reflex has a strong non-linear dependence on velocity [25], correlating well with delayed, half-wave rectified velocity. Furthermore, reflex EMG dynamics were particularly well modeled by a Hammerstein system [53], consisting of a static non-linearity followed by a linear filter.

This knowledge was used to build the reflex stiffness model, which relates position to torque through a differentiator, followed by a delay and a Hammerstein system [4]. The implementation of this model and the identification procedure yielded good system estimates, and were able to confirm the uni-directional rate sensitivity of the reflex response, as well as the response delay of 40-50 ms. Reflex torques were found to be significant only over a limited frequency band (5-10 Hz).

2.3.1.1.2. Reflex stiffness - Static conditions

Studies have examined reflex stiffness and reflex EMG dynamics under various stationary conditions and have found that reflex gain is highly dependent on ankle position [5, 25, 26, 54], the level of voluntary contraction [5, 26], and the properties of the input pulse used to identify it, such as the velocity, amplitude, duration, and direction [26]. Mirbagheri et al. [5] studied the effect of position and the level of voluntary contraction on reflex stiffness gain, using multiple subjects. Figure 2-15 shows reflex gain versus position and voluntary torque. Figure 2-15A shows that there is little change in stretch reflex gain as the ankle moves from near the neutral position to a more plantarflexed position. There is, however, a large increase in reflex gain as the ankle is dorsiflexed. This is likely due to the effect of changing muscle length; changing the stretch of the muscle will affect the spindle sensitivity. Plantarflexion reduces the muscle length, which, without any modification from central commands, would reduce muscle spindle activity. Dorsiflexion stretches the muscle and therefore, increases muscle spindle activity. This same position dependence has been observed in the reflex EMG response [25, 26, 54].

The functional consequences of changing the level of voluntary contraction on the reflex response is more disputed. Early studies that examined the reflex EMG dynamics concluded that reflex gain increased monotonically as the level of voluntary contraction increased [25, 26, 49]. This is what we would expect since increasing the activation level of a muscle increases the number of motor neurons close enough to threshold to be activated by the stretch [26]. However, this increase in reflex EMG gain does not translate into increased reflex stiffness. Figure 2-15B shows the results of a study examining reflex stiffness gain with various levels of torque. This figure shows a large increase in reflex stiffness gain in the transition from rest to low contraction levels followed by a gradual drop in reflex gain as the voluntary torque continues to increase. This behavior was also observed by Toft et al. [48]. These studies show that the behavior of reflex EMG dynamics cannot predict reflex stiffness dynamics. Stiffness dynamics are more representative of reflex functionality than reflex EMG dynamics, because they represent the actual mechanical output of the muscle, not only its activation. As discussed in Section 2.2.4,

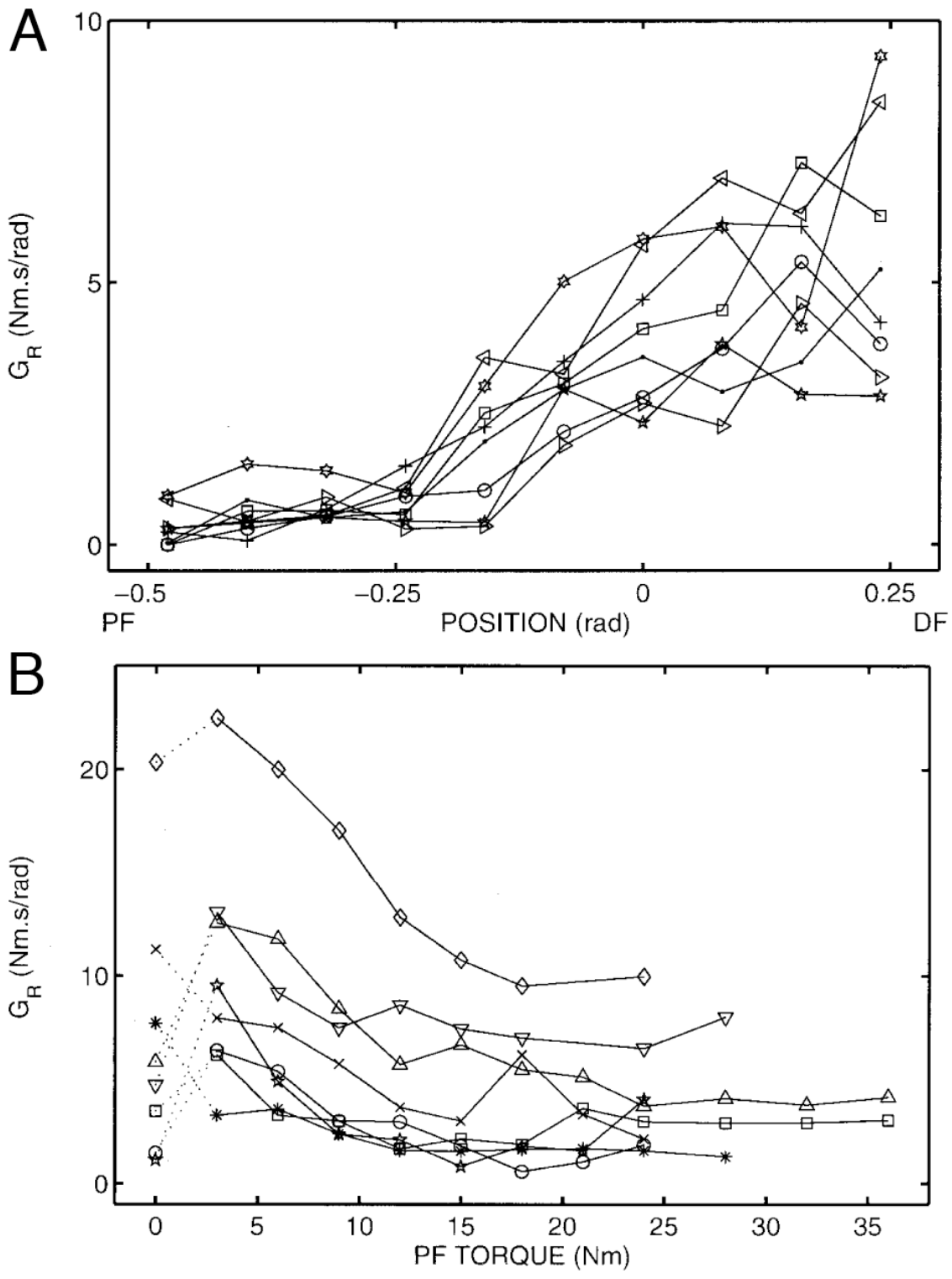

Figure 2-15. (A) Reflex gain, G_R, versus position. As the ankle moves from a neutral position to a dorsiflexed position the reflex gain increases. There is little change from a plantarflexed position to a neutral position. (B) Reflex gain versus plantarflexing torque. The reflex gain peaks at a low torque, about 3 Nm, and decreases as further torque is generated. Adapted from [5].

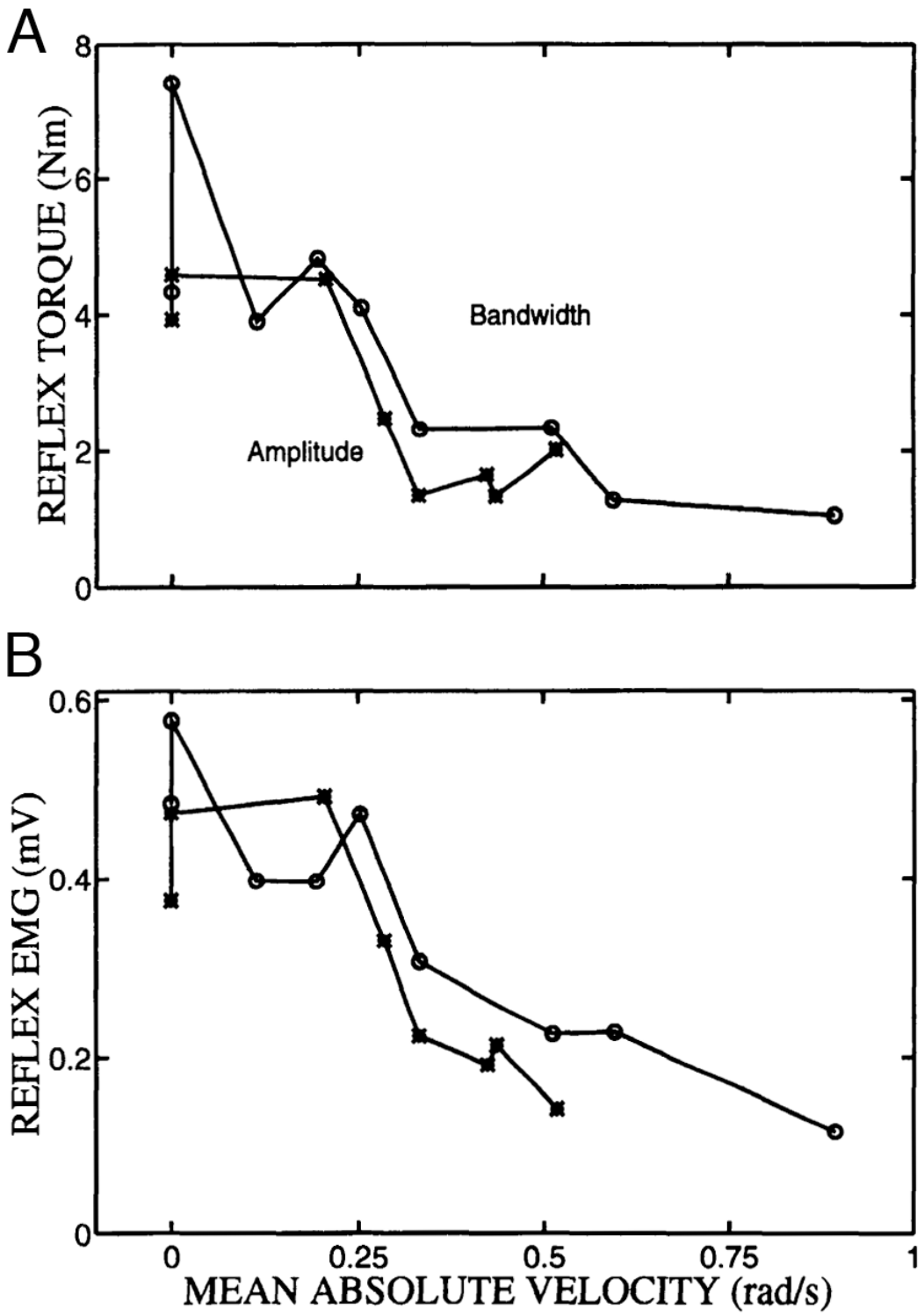

Figure 2-16. Reflex torque (A) and reflex EMG (B) versus the mean absolute velocity (MAV) of the perturbation. The amplitude of the reflex response tends to decrease as the MAV of the perturbation increases. Adapted from [26].

EMG does not directly correlate with the tension produced in the muscle under all conditions.

The gain of the stretch reflex has also been shown to be highly dependent on the properties of the input perturbation; the mean average velocity of the perturbation sequence being the most important of these properties [26]. Figure 2-16 shows the magnitude of the reflex torque and EMG versus the mean absolute velocity (MAV). The reflex EMG and torque responses are strongest for MAVs below 0.25 rad/s. This tells us that sustained movement suppresses reflexes. Any type of movement, therefore, will likely have a substantial effect on reflex gain. The following section examines the way reflexes change during motion and what role they may play.

2.3.1.1.3. Stretch Reflex and Movement

The stretch reflex can generate torques as large as 30-50% of a muscle's maximum voluntary contraction [47]. This is large enough to contribute significantly to voluntary movements [26]. Section 2.2.6.1 discussed several ways in which the reflex gain could be modulated. The question, therefore, is whether the brain modifies reflex gain depending on the task being performed. Many studies have shown that reflexes are modulated in a way that meets the functional requirements of a movement [10, 55-57], which supports the idea of central control of reflex gain. Furthermore, Ludvig et al. [8] showed that reflex stiffness could be voluntarily modulated independently of intrinsic stiffness. Whether this is a technique employed by the nervous system is still unclear.

Most studies of reflexes during movement and other time-varying tasks examined the EMG response, not reflex stiffness. The functional significance of their results should be interpreted with caution because the amplitude of EMG during movement does not directly correlate with torque output [21]. The Hoffman (or H-) reflex has been used extensively to study reflex modulation during movement in human subjects [10, 55, 57]. The H-reflex involves electrical stimulation of the muscle spindle afferents and is used to study the modulation of reflexes by central mechanisms [39]. They differ from the stretch reflex in that they do not include the effect of peripheral mechanisms [39]. The use of this method has produced interesting results. Capaday and Stein [9, 10] studied

the amplitude of the EMG elicited by the H-reflex in the soleus muscle during standing, walking, and running tasks. In walking and running tasks, they found that the reflex EMG amplitude was largest during the late stance phase, when it would assist in forward propulsion and in lifting the body. The reflex response was virtually absent during the swing phase, when it would oppose ankle dorsiflexion. However, the H-reflex was on average smaller during running than walking [10]. Similarly, the reflex response was in general larger during standing than walking for matched background EMG and stimulus levels. Similarly, a study performed by Grey et al. [55] showed that the EMG amplitude elicited by the H-reflex and the stretch reflex were largest during the down-stroke (power phase) of the crank cycle in a cycling task. The reflexes were smallest during the recovery phase, when they would be less useful.

Kimura et al. [56] examined the magnitude of the stretch reflex response in the soleus during a gradual increment and decrement of isometric force, and found that for matched torque levels the stretch reflex EMG amplitude was larger during the increasing phase than the decreasing phase. They speculated that a reduced reflex response during relaxation would lower the level of muscle activity and thus allow for a smoother force decrement. This coincides with the results of the studies mentioned above that found that reflexes were largest during the late stance phase of walking and the power phase of cycling, during soleus contractions, and smallest immediately afterwards, as the soleus relaxed.

Kirsch et al. [58] performed a similar experiment and found that the reflex EMG gain was largest just prior to the onset of the contraction and was depressed just prior to relaxation. The changes in reflex EMG gain closely followed the changes in background EMG but not the level of voluntary torque. This indicates that, at least for this task, the reflex gain was primarily modulated by the level of muscle activation, regardless of the output torque. In a related study, Kirsch and Kearney [59] found that reflex gain did not follow the background EMG changes as closely during a rapid imposed movement. This shows that there are many ways to modulate the reflex response, and one mechanism cannot predict the response in all situations.

The above studies do not conclusively determine the cause or purpose of reflex modulation. Both peripheral and central mechanisms have been shown to modify reflex gain, and it has also been shown to be task dependent. What is clear, however, is the importance of reflexes. Sinkjaer et al. [60] studied reflex modulation in multiple sclerosis patients and found that it was impaired when compared to normal function. This contributed to severe dysfunction during normal gait, demonstrating that reflexes play an important role in locomotion. Other studies also found that reflexes may play a role in stumble correction, stabilization of body posture over an uneven surface and restoration of balance during locomotion in the face of external perturbations [39]. Further study of reflex stiffness during movement is required to determine the functional significance of the stretch reflex in day-to-day tasks.

2.3.1.2. Relative Importance of Intrinsic and Reflex Stiffness

Both intrinsic and reflex mechanisms contribute to the total joint stiffness; however, their importance is determined by their relative contribution to the total output torque. Knowing how reflexes are modulated during movement would not be important if they contributed little to the total output torque. To determine the relative importance of each component, they must be identified simultaneously. A parallel-cascade system identification technique (described in detail in Section 3.5) was developed in our lab to do this [4]. Using this technique, it was shown that the reflex component dominates at 5-10 Hz, while the intrinsic component dominates at higher frequencies. The reflex contribution was largest when stimulated with a perturbation with a low mean average velocity.

Mirbagheri et al. [5] used this technique to investigate the effect of position and the level of voluntary torque on the relative contribution of intrinsic and reflex stiffness; Figure 2-17 shows the results. They found that although both intrinsic and reflex gain increased with ankle dorsiflexion, the reflex contribution was largest at a neutral position. Furthermore, intrinsic gain increased with the level of voluntary contraction, while the reflex gain was largest at a low contraction level, making the reflex contribution greatest at low contraction levels. From this study, we can see that the stretch reflex is likely to be more significant near a neutral position and with low contraction levels, near 3 Nm.

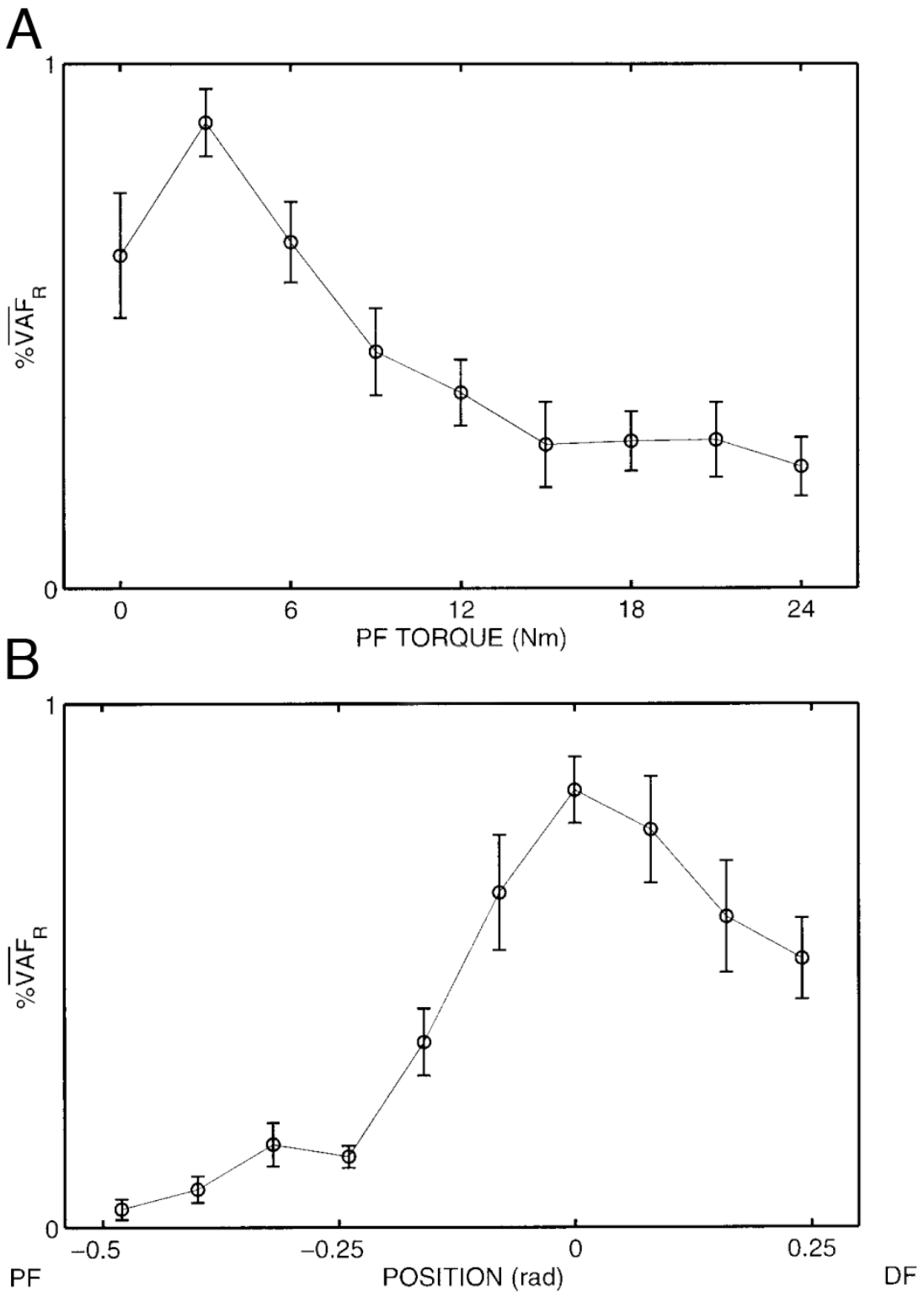

Figure 2-17. The average percent variance accounted between the reflex torque and the total torque versus plantarflexion torque (A) and position (B). The relative contribution of the reflex pathway peaks at approximately 3 Nm and near the neutral position. Adapted from [5].

2.4. THESIS RATIONALE

It is well established that impaired ankle reflexes lead to dysfunction in gait [39, 60] but their role in normal movement [9, 10, 21] and how they are controlled [56, 58] is still under debate. Previous studies of ankle reflexes lacked adequate means of separating mechanical stiffness from reflex generated stiffness, and instead relied on baseline, reflex-free recordings [50-52, 61]. To solve this problem our lab developed a parallel-cascade algorithm to simultaneously identify intrinsic and reflex stiffness [4]. This algorithm was applied to many time-invariant studies of ankle stiffness [5-8] but the ultimate goal was to examine ankle stiffness under time-varying conditions, where the position and torque of the ankle are changing.

An ensemble identification method was developed to study time-varying total joint stiffness [62]. However, this method did not distinguish between intrinsic and reflex stiffness [63]. That is why our lab further developed the time-varying, parallel-cascade (TVPC) algorithm to study intrinsic and reflex stiffness during time-varying tasks [13]. The TVPC algorithm incorporates ensemble identification techniques and will be able to accurately track ankle stiffness during a variety of tasks.

A thorough study of time-varying ankle stiffness will provide a clearer understanding of the role of reflex stiffness in motor control. The TVPC algorithm could be used to establish the normal pattern of reflex modulation for a variety of tasks. Once the modulation pattern is known, reflex impairment could be more objectively and precisely characterized. Current methods rely on a clinician's subjective assessment of the joint's resistance to passive manipulation and therefore, do not provide much insight into the progression of neurological diseases or effectiveness of a treatment program [1]. Furthermore, an in-depth understanding of joint stiffness modulation patterns would improve the design of limb prothesis and robotic control [1].

2.4.1. Thesis objectives

The goals of this research were the following:

1. Improve and debug the existing implementation of the TVPC algorithm.
2. Verify the algorithm's ability to track rapid, time-varying changes in system dynamics.

3. Assess the algorithm's noise performance and evaluate the effect of changing the relative contribution of the reflex pathway to the output.
4. Determine the effect on the quality of the identification of changing the number of realizations in the data ensembles.
5. Apply the TVPC algorithm experimentally to confirm that it can produce good results using real data.

Goals 1-4 are accomplished through a simulation study involving a realistic simulation of ankle stiffness. Goal 5 is achieved by applying the TVPC algorithm experimentally to track changes in intrinsic and reflex stiffness during a time-varying torque matching task.

3. System identification and the time-varying, parallel-cascade algorithm

System identification tackles the problem of developing a mathematical model of a system knowing only its inputs and outputs [64, 65]. This is a useful tool in the study of joint stiffness, since, in humans, joint position and torque are most easily recorded. This chapter gives an overview of system identification methods, focusing specifically on the techniques relevant to this thesis. This will provide the background necessary to understand the following chapters, which apply the TVPC algorithm to simulation and experimental data. The methods of identifying linear and non-linear, time-invariant systems are discussed, followed by a description of the parallel-cascade algorithm used to separate and identify intrinsic and reflex stiffness. A review of time-varying system identification techniques follows; ensemble methods are presented in detail. It is then shown how the ensemble methods are incorporated into the parallel-cascade algorithm to study time-varying joint stiffness. The last section discusses improvements made by the author to the time-varying, parallel-cascade (TVPC) algorithm's implementation, as part of this thesis research.

3.1. System Identification

There are many types of systems and many ways of representing them. A system can be either linear or nonlinear, time-invariant or time-varying. It can be represented either in the time domain using an impulse response function, or in the frequency domain using a frequency response function.

A mathematical model can also be either parametric or non-parametric. Parametric models are represented by an analytic expression that contains a limited number of parameters. The parameters are often chosen to represent certain physical properties and therefore, have actual physiological meaning. However, parametric modeling is only successful when the underlying model is chosen correctly, and this requires *a priori* knowledge about the system structure. If the model parameters are chosen incorrectly they will be meaningless. Unfortunately, biological systems are often very complex and a large number of parameters would be needed to accurately represent them, which is what parametric modeling aims to avoid. [1] For this reason, non-parametric methods are

more suitable for identifying unknown systems, even though they require a "large" number of parameters. Non-parametric models make few assumptions as to the structure of the system and are represented using frequency response functions, or impulse response functions (IRFs); the latter is described in the following section. An analytic expression can be fit to the IRFs or frequency response functions following the initial identification to reduce the number of parameters required. This is the method used in this thesis.

3.2. Impulse Response Function

The impulse response function (IRF) is a fundamental tool in system identification and can be used to predict a linear system's output due to any input. The IRF is the response evoked by applying a unit impulse to a system; since all frequencies are excited by an impulse, an IRF fully characterizes the dynamics of a linear system. Given the input, $x(t)$, and the system IRF, $h(t)$, the output, $y(t)$, is given by the convolution integral:

$$y(t) = \int_{-\infty}^{\infty} h(\tau)x(t-\tau)d\tau \tag{1}$$

The IRF may have positive lags that represent 'system memory' and negative lags that represent 'system anticipation'. Typically, a system has 'finite memory', and so has very small or zero values for large lags, defined by the limits $\tau < \tau 1$ and $\tau > \tau 2$. The above integration limits can then be set from $\tau 1$ to $\tau 2$ [66]. Equation 1 is more practically written in the discrete-time format, with sampling interval Δt, as follows:

$$y(i) = \Delta t \sum_{j=T1}^{T2} h(j)x(i-j) \tag{2}$$

where, i, is the discrete-time index, j, is the lag index, and $T1$ and $T2$ are equal to $\tau 1 / \Delta t$ and $\tau 2 / \Delta t$, respectively. The discrete-time formulation assumes that Δt is small compared to the fastest fluctuations of the system, so that the rectangular integration gives satisfactory results.

The basic IRF can only describe linear systems; more complex formulations are necessary for non-linear cases. If the system is stationary and linear about a particular operating point, a quasi-linear model can be used, which is described by an IRF that depends on the operating point, as follows [1]:

$$y(i) = \Delta t \sum_{j=T1}^{T2} h(j,\lambda)x(i-j) \tag{3}$$

where λ represents the operating point. This model can be used to represent linear, quasi-stationary system. If the system is not stationary long enough to estimate the IRF, this model cannot be used; time-varying identification methods will be necessary.

Cascade models can be used to model non-linear systems, which is the method used in this thesis. These models consist of a cascade of linear and non-linear elements; the simplest being the Wiener (linear – nonlinear) and the Hammerstein (nonlinear – linear) models. The Hammerstein model, as previously mentioned, can be used to model reflex dynamics. The procedure for identifying a Hammerstein model is discussed in Section 3.4. The following section describes a technique for identifying linear systems using a correlation-based method.

3.3. Correlation function approach to linear, time-invariant system identification

There are many techniques for solving the linear, time-invariant convolution equation for the impulse response function. This section presents a technique that uses a correlation function approach. This method involves solving a matrix equation expressed as a function of the input autocorrelation and the impulse response function; it is derived as follows [66]. Substitute $i + k$ for i into Equation 2 to get the following:

$$y(i+k) = \Delta t \sum_{j=T1}^{T2} h(j)x(i+k-j) \tag{4}$$

Multiply Equation 4 by $x(i)$ and sum both sides from $i = 1$ to N to get:

$$\sum_{i=1}^{N} x(i)y(i+k) = \Delta t \sum_{j=T1}^{T2} h(j) \sum_{i=1}^{N} x(i)x(i+k-j) \tag{5}$$

The left hand side of Equation 5 is a biased estimator of the cross-correlation function:

$$c_{xy}(k) = \frac{1}{N} \sum_{i=1}^{N} x(i)y(i+k). \tag{6}$$

The rightmost sum is a biased estimator of the autocorrelation function:

$$c_{xx}(k) = \frac{1}{N} \sum_{i=1}^{N} x(i)x(i+k). \tag{7}$$

Equations 6 and 7 are substituted back into Equation 5 and rewritten in matrix form, as follows:

$$\boldsymbol{C}_{xy} = \Delta t \mathbf{C}_{xx} \boldsymbol{H} \tag{8}$$

where $\boldsymbol{C}_{xy}$ is a T2-T1+1 length vector with i^{th} element $c_{xy}(T1+i-1)$, $\mathbf{C}_{xx}$ is a T2-T1+1 square matrix with i, j^{th} element $c_{xx}(i-j)$, and $\boldsymbol{H}$ is a T2-T1+1 length vector with i^{th} element $h(T1+i-1)$. Rearranging Equation 8 for $\boldsymbol{H}$ gives:

$$\boldsymbol{H} = \frac{1}{\Delta t} \boldsymbol{C}_{xx}^{-1} \boldsymbol{C}_{xy} \tag{9}$$

Using a simple matrix inverse to solve the above equation can lead to large random errors when the output SNR is low and the input is coloured [67, 68]. A pseudoinverse provides more reliable results in those situations. The pseudoinverse method removes terms from the calculation that don't contribute significantly to the output [11], thus providing better results.

3.4. Time-Invariant Hammerstein Identification Technique

Biological systems are very often non-linear and require specialized techniques to identify them. Certain non-linear systems can be represented using a Hammerstein cascade

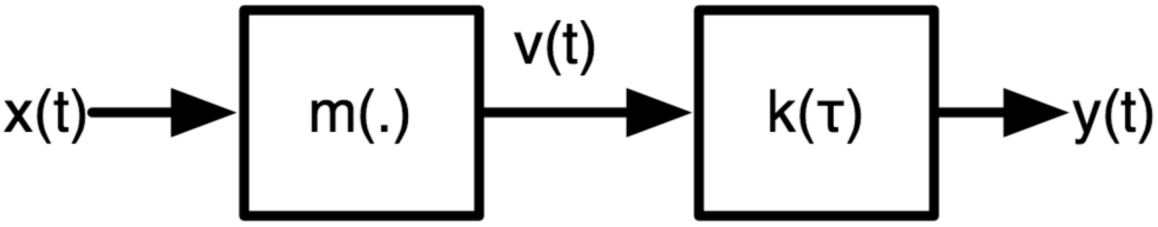

Figure 3-1. Non-linear Hammerstein cascade model.
x(t) - input
m(.) - non-linear function
v(t) - intermediate signal modified by the non-linear function
k(τ) - linear subsystem
y(t) - output

system (see Figure 3-1), as is the case with ankle reflex stiffness. Hunter and Korenberg [64] describe an iterative technique to identify time-invariant Hammerstein systems. The technique iterates between the identification of the linear element and the non-linear element as follows (refer to Figure 3-1):

1. Generate a linear estimate of the inverse of k, denoted ik, between y and x using linear correlation system identification techniques. Note that this is made possible by Bussgang's theorem, which states that for two Gaussian signals, the cross-correlation, calculated after one of them has undergone a nonlinear amplitude distortion, is identical to the cross-correlation calculated before the distortion was applied, except for a factor of proportionality [69].

2. Predict v (denoted $\hat{v}$) by convolving y with ik.

3. Estimate the non-linear function, m, by fitting a high-order polynomial between x and $\hat{v}$, and set $\hat{v}$ to be the value predicted by the polynomial.

4. Re-estimate ik between y and $\hat{v}$.

5. Re-estimate $\hat{v}$ from the convolution of ik and y.

6. Continue iterating at step 3 to improve the estimates or generate the final estimate by continuing at step 7.

7. Re-estimate the non-linear function, m, by fitting a high-order polynomial between x and $\hat{v}$, and set $\hat{v}$ to be the value predicted by the polynomial.

8. Estimate k between $\hat{v}$ and y.

9. Generate a prediction of y by convolving the estimate of k with $\hat{v}$.

This method has been used to model dynamic reflex stiffness [5]. It has also been adapted for time-varying Hammerstein systems [12], as discussed in Section 3.6.3.

3.5. Parallel-Cascade System Identification of Ankle stiffness

Joint stiffness consists of both intrinsic and reflex components. Identifying one component while excluding the other can lead to biased results. Our lab developed a time-

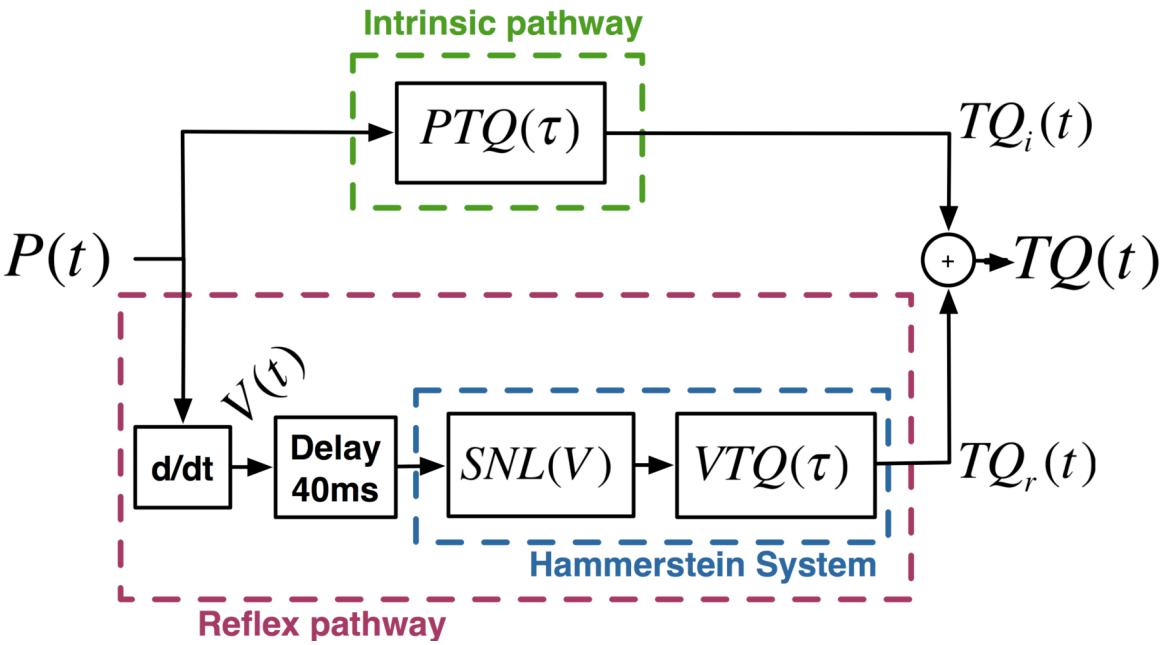

Figure 3-2. Model of ankle stiffness used in the parallel-cascade system identification algorithm. The upper pathway represents intrinsic stiffness. The lower pathway is the reflex stiffness. The torques resulting from each pathway combine additively to give the total output torque.

P(t) - Position
TQ(t) -Total output torque
$TQ_i(t)$ and $TQ_r(t)$ - Intrinsic and Reflex torque, respectively
V(t) - Velocity
PTQ(τ) - Intrinsic stiffness IRF
SNL(V) - Non-linear function of reflex stiffness Hammerstein system
VTQ(τ) - Linear subsystem IRF of reflex stiffness Hammerstein system

invariant, parallel-cascade identification technique to separate and identify the two components [4]. The parallel-cascade model used in the identification of reflex and intrinsic stiffness is shown in Figure 3-2**.**

The upper pathway represents the intrinsic component of joint stiffness, which relates position to torque via a linear, dynamic system. The lower pathway, representing reflex stiffness, relates joint velocity to torque through a delay followed by a Hammerstein system. The two pathways are assumed to contribute linearly to the total output torque. Each pathway of the parallel-cascade model is separated and identified using the following iterative technique:

1. First, an estimate of the intrinsic stiffness, $P\hat{T}Q$, is generated by estimating the IRF between input position, P, and total output torque, TQ, using the correlation method described in Section 3.3. The length of the intrinsic IRF is fixed to be shorter than the reflex delay, to avoid any correlation between the reflex component and the input. $P\hat{T}Q$ is then convolved with P to generate an estimate of the intrinsic torque, $T\hat{Q}_i$.

2. The intrinsic residuals, $T\hat{Q}_{iR}$ are calculated by subtracting the predicted intrinsic torque from the total torque, as follows: $T\hat{Q}_{iR} = TQ - T\hat{Q}_i$. $T\hat{Q}_{iR}$ is used as the output for the reflex identification. Using the residual signal instead of the total output torque increases the SNR of the reflex identification by eliminating the component of the signal due to the intrinsic pathway.

3. The static non-linearity, $S\hat{N}L$, and the linear subsystem, $V\hat{T}Q$, of the Hammerstein system are estimated between the joint velocity, V, and $T\hat{Q}_{iR}$ using the Hammerstein identification method described in the previous section. The estimated Hammerstein system is used to predict the reflex torque, $T\hat{Q}_r$.

4. An estimate of the total output torque, $T\hat{Q}$, is calculated by summing $T\hat{Q}_i$ and $T\hat{Q}_r$.

5. The quality of the identification is evaluated by computing the percent variance accounted for (%VAF) between TQ and $T\hat{Q}$. The general %VAF equation between an observed signal, X, and its estimate, $\hat{X}$, is as follows:

$$\%VAF(X,\hat{X}) = 100\left(1 - \frac{\mathrm{var}(X - \hat{X})}{\mathrm{var}(X)}\right) \quad (9)$$

6. The procedure continues back at step 1, where a new estimate of intrinsic stiffness is generated using reflex residuals as the output.

7. Iteration continues until the %VAF fails to increase.

Following the identification, intrinsic stiffness is converted to compliance, $T\hat{Q}P$, since it is more readily interpreted.

The time-invariant, parallel-cascade identification procedure has been successfully applied in many studies [5-8] to examine ankle stiffness about a fixed operating point, (i.e. when torque and position are fixed). This model does not describe joint stiffness under all conditions, such as when position or torque are changing. Therefore, for this model to hold, it is important to use a small position perturbation to identify the system, such that it minimizes the non-linear effects of changing position and torque. For example, intrinsic mechanisms are modeled here as linear even though muscle and joint properties are known to be non-linear. This model holds as long as the position input used to identify the system is small enough, such that it doesn't affect the system parameters. A small amplitude (usually 0.03 rad) pseudo-random binary sequence (PRBS) about the operating point is used, as it satisfies this requirement and has a wide enough bandwidth to identify the system dynamics.

Similarly, reflex stiffness is only modeled in terms of its velocity-torque relationship. However, the parameters of the model change with changing position and torque [5] but by identifying it about a fixed operating point with small position perturbations this simplified model can be used. A more complete model would be required to account for all

the non-linearities of this complex system. Unfortunately, is not yet possible to develop an overall model of joint stiffness.

The system parameters that change due to the non-linearities of ankle stiffness can instead be modeled as functions of time. Their changes through time can be described for a specific task. This will not provide insight into other tasks but can be used to describe the role of reflexes in specific situations. This simplifies the modeling task, as the non-linear properties and interactions between the intrinsic and reflex pathways do not need to be described explicitly.

To identify ankle stiffness as a time-varying system, Mackenzie Baker, adapted the time-invariant, parallel-cascade identification algorithm for the time-varying case, as the topic of her master's thesis [70]. The time-varying, parallel-cascade algorithm is discussed in Section 3.6.4.

3.6. Time-varying system identification

Time-varying systems provide an added challenge in system identification because their dynamics change with time. Many system identification methods assume time-invariant systems, however, most biological systems are time-varying to some degree. For this reason, traditional, time-invariant methods cannot be used to identify them. [62] This has limited most of the study of motor control system to static conditions [1, 3, 5, 53], or physical models [55, 57], which can describe the system behavior for a particular task but have no general predictive abilities [1]. These studies provide insight into motor control strategies, but will always be lacking because most of motor control involves movement of some kind.

For certain applications, which deal with slowly time-varying systems, adaptive methods are appropriate. Adaptive methods use recursive algorithms that progressively change parameters in a parametric model such that they reduce the output error. They are often applied in tracking applications of slowly varying systems. Like with time-invariant parametric modeling, the system structure must be known *a priori*, which limits its usefulness. [62] A recent improvement to this tracking method blends parametric and non-parametric modeling to reduce the need for *a priori* information about the system while

remaining computationally efficient [71]. Adaptive methods are generally used for control purposes and there is no guarantee that the estimates accurately track the actual system dynamics during the adaptation process.

Further development of methods for the identification of linear and non-linear time-varying systems has been approached in several different ways. State-space methods are common because they provide reliable models for complex multivariable dynamic systems [72]. Kameyama and Ohsumi [73] recently developed a subspace method capable of tracking fast-varying systems by using a predictive approach, making it far superior to other state-space methods, which use step-wise approximation to model the time-variations [74], or require some *a priori* knowledge of the general shape of the time-variations [75]. This method has yet to be applied to the study of biomedical systems.

Ensemble methods identify time-varying systems from sets of responses that exhibit the same underlying time-varying behavior. Time-invariant identification techniques are used to identify an IRF at each time point by forming the input and output from points chosen at a particular point in the TV behavior instead of from a single response. In other words, the identification is performed across the ensemble instead of in time. This method has the advantage of being able to track rapid changes in system behavior and requires no *a priori* information about the system order or the nature of the TV behavior. The major disadvantage of this method is that it requires the acquisition and analysis of large data sets. This can make it challenging to acquire the necessary data experimentally. In spite of this, ensemble identification is the method of choice for studying real-world movements, since it does not impose restrictions on the type of movement studied. [62] For this reason, this is the method used in this thesis to study TV behavior.

3.6.1. Ensemble methods

Ensemble methods provide a robust means of identifying TV joint dynamics, and have been used to study many biological systems [24, 58, 76-78]. The ensemble technique was pioneered by Soechting et al. [77]. The original method imposed strict timing between the input sequence and the movement studied, requiring that with each repetition of the movement the input sequence be shifted by one element. To generate the

desired ensemble of data, extreme consistency between each trial of the movement was required. Time-invariant, cross-correlation system identification techniques were applied across the ensemble of data to calculate the IRF for every time point. Thus changes in system dynamics could be visualized via a surface of IRFs. Despite the timing restriction, this method was used successfully to study the myotatic response in the arm [77], and reflex changes during a simple ball catching task [24].

Seeing the advantages of the ensemble approach, researchers sought to modify the technique to remove the strict timing requirements. Verhaegen and Yu [79] developed a state-space formulation of the ensemble method, but it required some knowledge of the time-variations to generate the state-space model. Bennett et al. [76] developed a parametric ensemble method based on the autoregressive moving average (ARMA) model. The time-varying ARMA parameters were considered fixed for a particular time point, and were solved for using an unbiased estimation procedure. Xu and Hollerbach [78] also developed a parametric ensemble identification technique that used a model of forearm dynamics. The advantage of using a parametric model with the ensemble technique is that the models have fewer parameters, and therefore fewer movement trials are required to identify them. On the other hand, parametric models also assume a system structure and are therefore less general.

Our lab developed a non-parametric, least-squares ensemble method based on singular value decomposition (SVD) [62]. This method doesn't impose any timing requirements between the input sequence and the time-varying behavior, nor does it require the input to be white. This method is based on time-varying convolution. The discrete-time, time-invariant convolution equation (Equation 2) is extended to the time-varying case by making the IRF time-dependent, as follows [62]:

$$y(i) = \Delta t \sum_{j=M1}^{M2} h(i,j)x(i-j) \tag{10}$$

where *i* is the discrete-time index and *j* is lags. The time-varying IRF, $h(i,j)$, describes the instantaneous system dynamics at each time, and can be expressed in matrix form, as

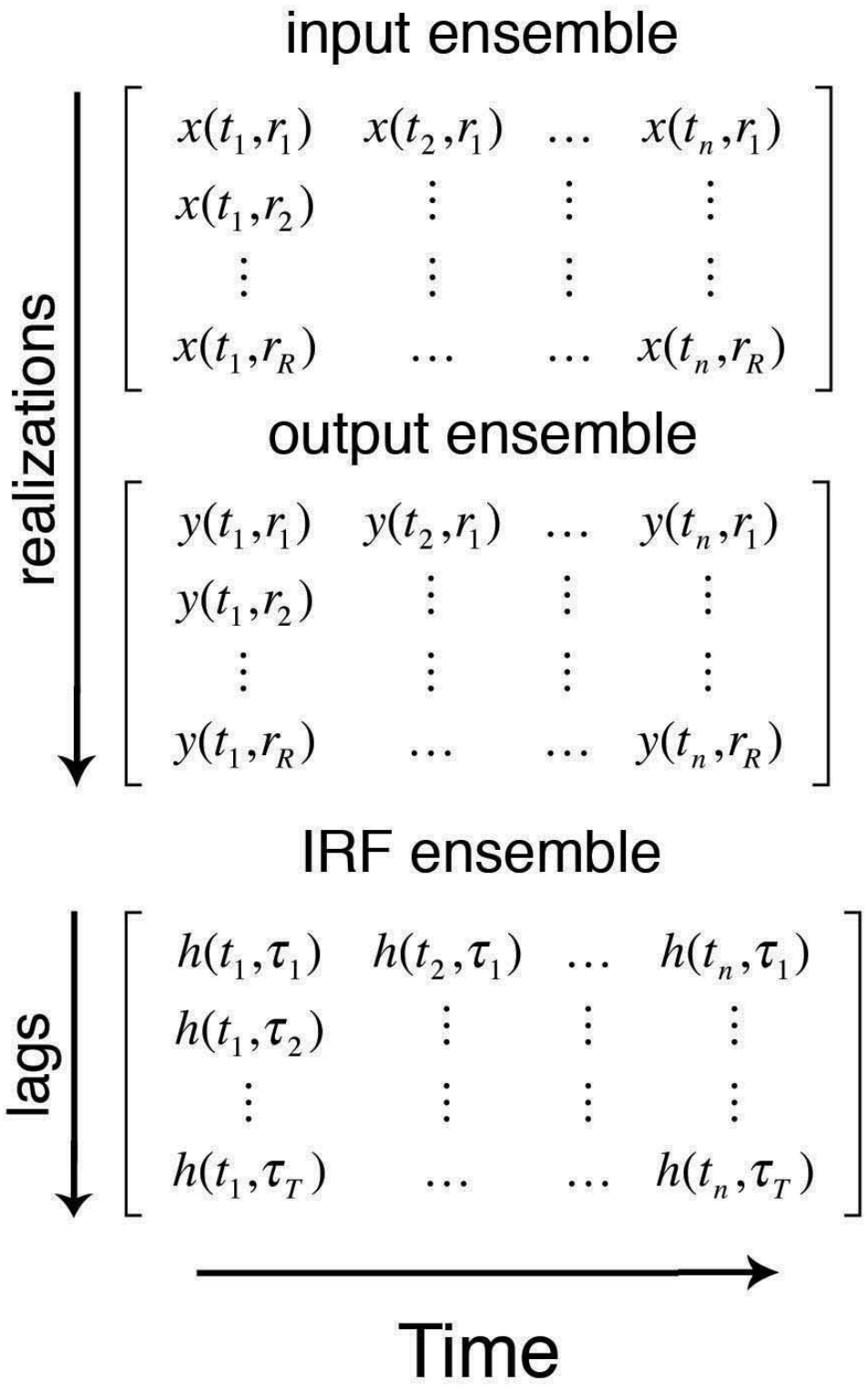

Figure 3-3. Data ensembles. The input and output ensembles are functions of time and realizations. For each time point, there is an IRF that describes the instantaneous system dynamics, which is a function of lags.

shown in Figure 3-3. Large ensembles of input and output data generated by recording multiple trials of the same time-varying behavior are required to identify the time-varying IRF ensemble. Ensemble methods assume that (1) the input trials are uncorrelated with each other, and (2) the system undergoes the same time-variations during each realization. The data is organized in matrix form, as shown in Figure 3-3. In theory, the number of trials needed is equal to the number of points in the IRF. However, since there is noise in practice, more trials are necessary. This makes the problem overdetermined, and a unique solution will not exist. A solution is found by minimizing the squared error between the observed and predicted output using SVD.

3.6.2. TV linear pseudoinverse approach

Our lab developed a method for the identification of linear time-varying (TV) system based on the correlation method, originally applied to time-invariant systems [11]. For an ensemble of input and output realizations exhibiting the same time-varying behavior, the discrete convolution equation (Equation 10) for a realization is:

$$y_r(i) = \Delta t \sum_{j=M1}^{M2} h(i,j)x_r(i-j) \tag{11}$$

$$\hat{\mathbf{\Phi}}_{xx}(i) = \begin{bmatrix} \hat{\phi}(i-M1,0) & \hat{\phi}(i-M1,-1) & \dots & \hat{\phi}(i-M1,M1-M2) \\ \hat{\phi}(i-M1-1,1) & \hat{\phi}(i-M1-1,0) & \dots & \hat{\phi}(i-M1-1,M1-M2+1) \\ \vdots & \vdots & \vdots & \vdots \\ \hat{\phi}(i-M2,M2-M1) & \hat{\phi}(i-M2,M2-M1-1) & \dots & \hat{\phi}(i-M2,0) \end{bmatrix}$$

$$\hat{\boldsymbol{\phi}}_{yx}(i) = \begin{bmatrix} \hat{\phi}_{yu}(i,-M1) & \hat{\phi}_{yu}(i,-M1-1) & \dots & \hat{\phi}_{yu}(i,-M2) \end{bmatrix}^T$$

$$\mathbf{h}(i) = \begin{bmatrix} h(i,M1) & \dots & h(i,0) & \dots & h(i,M2) \end{bmatrix}^T$$

Figure 3-4. Form of the matrices used to solve for a TV linear system.

$\hat{\mathbf{\Phi}}_{xx}(i)$ - matrix of unbiased auto-covariances

$\hat{\boldsymbol{\phi}}_{yx}(i)$ - vector of unbiased cross-covariances

$\mathbf{h}(i)$ - IRF for time i

where the subscript, r, indicates the realization number. The derivation of the TV correlation method is similar to that described in Section 3.3. By multiplying both sides of the above equation by $x_r(-i-k)$, summing over all realizations and dividing by the total number of realizations, Equation 11 can be expressed in terms of covariances, as follows:

$$\hat{\boldsymbol{\phi}}_{yx}(i,-k) = \Delta t \sum_{j=M1}^{M2} \boldsymbol{h}(i,j)\hat{\boldsymbol{\phi}}_{xx}(i-k,k-j) \tag{12}$$

where $\hat{\boldsymbol{\phi}}_{xx}(i-k,k-j)$ is the unbiased auto-covariance of the input at time $i-k$ and the input at time $k-j$, as follows:

$$\hat{\boldsymbol{\phi}}_{xx}(i-k,k-j) = \frac{1}{R}\sum_{r=1}^{R} x_r(i-j)x_r(i-k) \tag{13}$$

and $\hat{\boldsymbol{\phi}}_{yu}(i,-k)$ is the unbiased cross-covariance of the output at time i and the input at time $i-k$, as follows:

$$\hat{\boldsymbol{\phi}}_{yu}(i,-k) = \frac{1}{R}\sum_{r=1}^{R} y_r(i)x_r(i-k) \tag{14}$$

By letting k take on values from M1 to M2, Equation 12 can be rewritten in matrix form:

$$\Delta t\hat{\Phi}_{xx}(i)\mathbf{h}(i) = \hat{\boldsymbol{\phi}}_{yx}(i) \tag{15}$$

The complete forms of the matrices are shown in Figure 3-4. Equation 15 is solved for **h***(i)* by replacing matrix inverse of $\hat{\Phi}_{xx}(i)$ by a pseudoinverse.

Kirsch et al. successfully applied this technique in two studies [58, 59, 63]. The first study looked at reflex EMG gain changes during an isometric contraction/relaxation task [58]. The second study examined changes in reflex EMG dynamics and intrinsic stiffness during a rapid imposed movement while a constant contraction level was maintained [59, 63].

3.6.3. TV Hammerstein system identification

As previously mentioned, reflex stiffness is well modeled by a Hammerstein system, which is a cascade of a static non-linearity and a linear subsystem [25]. Mireille Lortie, from our lab, extended Hunter and Korenberg's iterative technique [64] to the time-varying case with the use of ensemble data [12]. The discrete-time relationship between the input $x(t)$ and the output $y(t)$ for a time-varying Hammerstein system is expressed as follows:

$$y(i) = \Delta t \sum_{j=M1}^{M2} h(i,j)g(i,x(i-j)) \tag{16}$$

where $g(i,\cdot)$ is the time-varying non-linear mapping function represented by a polynomial, and $h(i,j)$ is the time-varying IRF. Input and output ensembles are required to predict the non-linear mapping function and IRF at each time. The iterative procedure for

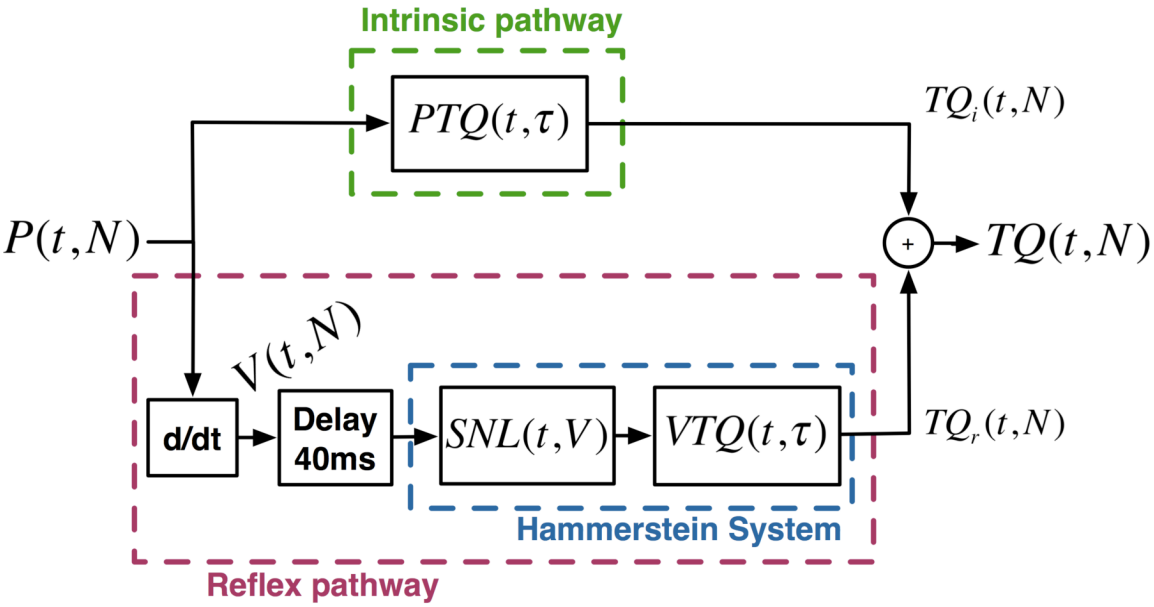

Figure 3-5: Model of ankle joint stiffness used in the time-varying, parallel-cascade identification algorithm. All variables are the same as for the time-invariant case with some slight changes.

PTQ and VTQ are now a function of lags, τ, and time. There is a separate IRF to describe the instantaneous system dynamics at every time. SNL is also a function of time; the non-linear function may be different at every time point.

P, TQ, V, TQ_i, and TQ_r are all ensembles, where N represents the realization number.

identifying this system is the same as described in Section 3.4 for the time-invariant case. The time-varying correlation identification technique is used to generate the initial estimate of the linear subsystem. The algorithm then iterates between estimating the polynomial representing the non-linearity at each time, and estimating the parameters of the time-varying linear subsystem, such that each iteration minimizes the sum of squared errors (SSE) between the predicted and observed outputs. The iteration stops once the SSE fails to decrease.

3.6.4. The Time-Varying, Parallel-Cascade algorithm

The time-invariant, parallel-cascade algorithm has been used extensively to study ankle stiffness under static conditions [5-8]. These studies revealed that ankle stiffness varies with position and the level of torque [5]. Therefore, when either position or torque change, stiffness will also change and may be treated as time-varying (TV). Furthermore, while a movement is executed both intrinsic and reflex stiffness may vary independently and therefore, must be identified concurrently. Mackenzie Baker extended the existing parallel-cascade algorithm for the time-varying case [13] as the topic of her thesis [70]. Figure 3-5 shows the time-varying, parallel-cascade (TVPC) model of ankle stiffness. The same iterative procedure is used with the TV identification as with the time-invariant, parallel-cascade algorithm. However, intrinsic stiffness and reflex stiffness are TV and therefore, must be identified using the linear and non-linear TV ensemble identification methods described in Sections 3.6.2 and 3.6.3, respectively. This requires input and output data ensembles, as with all ensemble methods.

Improvements to the algorithm's implementation and initial experimental validation were the topic of Heidi Giesbrecht's thesis [80]. The following section describes further improvements made to the implementation of the TVPC algorithm, as part of this thesis work.

3.7. TVPC Algorithm Improvements

Previous studies were done to validate the TVPC algorithm [70, 80] and although the simulation results were encouraging, the algorithm had little success when applied experimentally. The simulation studies of the TVPC algorithm generated the data ensem-

bles by TV convolution. TV IRF ensembles were created and convolved with a simulated input to generate the output. The simulated input and output ensemble were then used to validate the TVPC algorithm. This method did not uncover the problems that occurred with experimental data; likely due to the simulated model having the same form as the system estimates produced by the identification algorithm. As part of this thesis work, a different simulation method was devised; ankle stiffness was modeled in Simulink (The MathWorks Inc.). The Simulink model included time-varying parameters and did not explicitly perform time-varying convolution to generate the output. The results were likely more representative of experimental data. Exploration of the algorithm with this new simulation method uncovered some previously undocumented problems. This section describes the steps taken to further improve the algorithm.

The TVPC algorithm was tested extensively by simulating various experimental conditions. Under certain conditions, a small number of reflex IRFs had a larger amplitude than the others, and the associated non-linearities had a negative offset. These 'glitches' occurred at seemingly random time points. Considerable time was spent determining that the problem stemmed from the iterative nature of the reflex identification. Recall that reflex stiffness is modeled as a Hammerstein system. Under certain conditions, the initial estimate of the linear subsystem of the Hammerstein system had a small positive offset, which would translate into output signals with a non-zero mean. However, since the mean of the output signal was removed prior to identification, the output was required to have a zero mean overall. Therefore, to produce an overall zero offset, a negative offset was added to the non-linearity to compensate for the positive offset on the IRF. The negative offset on the non-linearity cancelled the positive offset on the IRF to produce a zero mean signal. The offset was small at the beginning of the iteration, but increased with continued iteration. This offset gave the IRF the appearance of being larger than the others. Once the root of the problem was determined, it was easily corrected by removing the mean of the post-non-linearity signal prior to identifying the linear system. Using the zero mean signal forced the identified IRF to have zero offset.

After this problem was fixed, there were still some problems with both the intrinsic and reflex IRFs for the last time points. This was due to the type of anti-aliasing filter used

prior to decimating the signals for identification. The filter caused large end-point transients, which affected the identification. This filter was replaced by a two-pass filtering method that first filtered the signals in the forward direction, followed by the backwards direction. This minimized the end-points transients and eliminated the problem with the last IRFs.

Despite the problems with decimation, it is a necessary process that eliminates much of the high-frequency noise. Previous studies decimated the input and output ensembles from 1000 Hz down to 100 Hz [80] prior to applying the TVPC algorithm. This gave very clean results but the intrinsic stiffness estimates were always slightly off, producing parameter estimates lower than those simulated. This is because a 100 Hz signal does not contain enough frequency information to identify intrinsic stiffness, which is high-pass in nature. Changing the decimation to 200 Hz, improved the intrinsic stiffness estimates and produced more accurate parameter estimates, even though more high frequency noise was allowed for the identification.

These changes to the TVPC algorithm implementation greatly improved the accuracy and reliability of the identification. The rest of this thesis explores the performance limits of the algorithm via simulation and applies it experimentally to study ankle stiffness during a simple torque-matching task.

4. Performance Evaluation of an Algorithm for the Time-Varying Identification of Intrinsic and Reflex Stiffness: A Simulation Study

4.1. Introduction

As discussed in Chapter 2, ankle stiffness parameters change with position and the level of voluntary torque [5]. To study situations in which one or both of these conditions are time-varying (TV), the time-varying, parallel-cascade (TVPC) system identification algorithm is required (refer to Chapter 3). This algorithm has the ability to identify time-varying, intrinsic and reflex stiffness concurrently.

The goal of this chapter is to investigate the performance of the TVPC algorithm in various conditions. Simulation is used so that conditions can be controlled directly. This also permits the accuracy of the identification to be quantified by comparing the results of the identification to the simulated systems and torques. The first test evaluates the TVPC algorithm's ability to accurately track rapid, TV changes in joint stiffness, by simulating ankle stiffness with step and ramp changes in the system parameters. The second test is designed to evaluate the algorithm's noise performance. This test not only investigates the effect of changing the signal-to-noise ratio (SNR) on the quality of the identification; it also evaluates the effect of changing the relative contributions of the reflex and intrinsic pathways to the total output torque, and studies the effect of changing the number of realizations in the input and output data ensembles.

4.2. Methods

4.2.1. Analysis algorithm

Previous studies showed that ankle stiffness is described well by the model shown in Figure 4-1 [4]**.** Intrinsic stiffness, PTQ, relates position, P, to torque, TQ_i, through the following transfer function:

$$PTQ(s) = \frac{TQ_i(s)}{P(s)} = Is^2 + Bs + K,$$

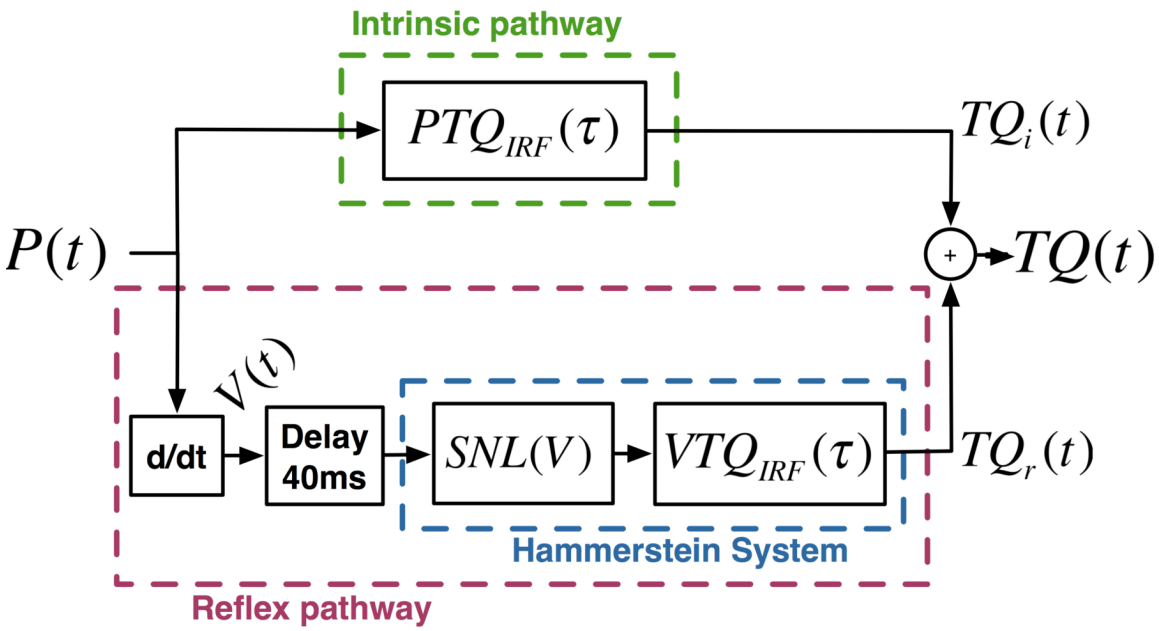

Figure 4-1. Block diagram of the time-invariant, parallel-cascade model of ankle stiffness. The torques generated by the intrinsic and reflex pathways add linearly to produce the total torque.

Legend:
$P(t)$ = ankle angular position.
$V(t)$ = ankle velocity.
$TQ(t)$ = total output torque.
$TQ_i(t)$, $TQ_r(t)$ = intrinsic and reflex torque.

$PTQ(\tau)$ = intrinsic stiffness
$SNL(V)$ = static, non-linearity of reflex stiffness Hammerstein system
$VTQ(\tau)$ = linear subsystem of reflex stiffness Hammerstein system
PTQ and VTQ are a function of the IRF lags, τ.
SNL modifies the velocity, V.

where I, B, and K are the inertial, viscous and elastic parameters, respectively. Reflex stiffness relates joint velocity, V, to torque, TQ_r, via a delay and a Hammerstein system, consisting of SNL, modeled as a half-wave rectifier, followed by VTQ, a 2nd-order low pass filter with the following transfer function:

$$VTQ(s) = \frac{TQ_r(s)}{V(s)} = \frac{G\omega_n^2}{s^2 + 2\xi\omega_n s + \omega_n^2}$$

where G, ξ, and ω_n are the gain, damping and natural frequency, respectively. The two pathways work in parallel and their individual output torques combine additively to produce the total output torque. With time-varying joint stiffness, all intrinsic and reflex stiffness parameters may change with time.

Joint stiffness becomes time-varying with changes in either the joint position or the torque acting about it. For time-invariant systems, each output point provides more information about the system to be identified. This is not the case with time-varying systems, where each output point is the result of different system dynamics. That is why ensemble methods are used. Ensemble methods use sets of input-output pairs exhibiting the same TV behavior, and perform the identification across the ensemble. An example input-output data ensemble is shown in Figure 4-2. For a fixed time, *i*, all the output points across the ensemble are a result of the same instantaneous system dynamics. A separate impulse response function (IRF) is identified for every sample time, which is dependent on time, *t*, and lags, τ. The TVPC algorithm makes use of ensemble methods and iteration to separate and identify the TV intrinsic and reflex pathways, as described in Chapter 3.

4.2.2. Simulation models

The performance of the TVPC algorithm was tested by simulating the model of ankle stiffness shown in Figure 4-1. An ensemble of position inputs were generated, using pseudo random binary sequences (PRBS) because they are used experimentally. These position inputs were applied to the joint stiffness model to generate the resulting output

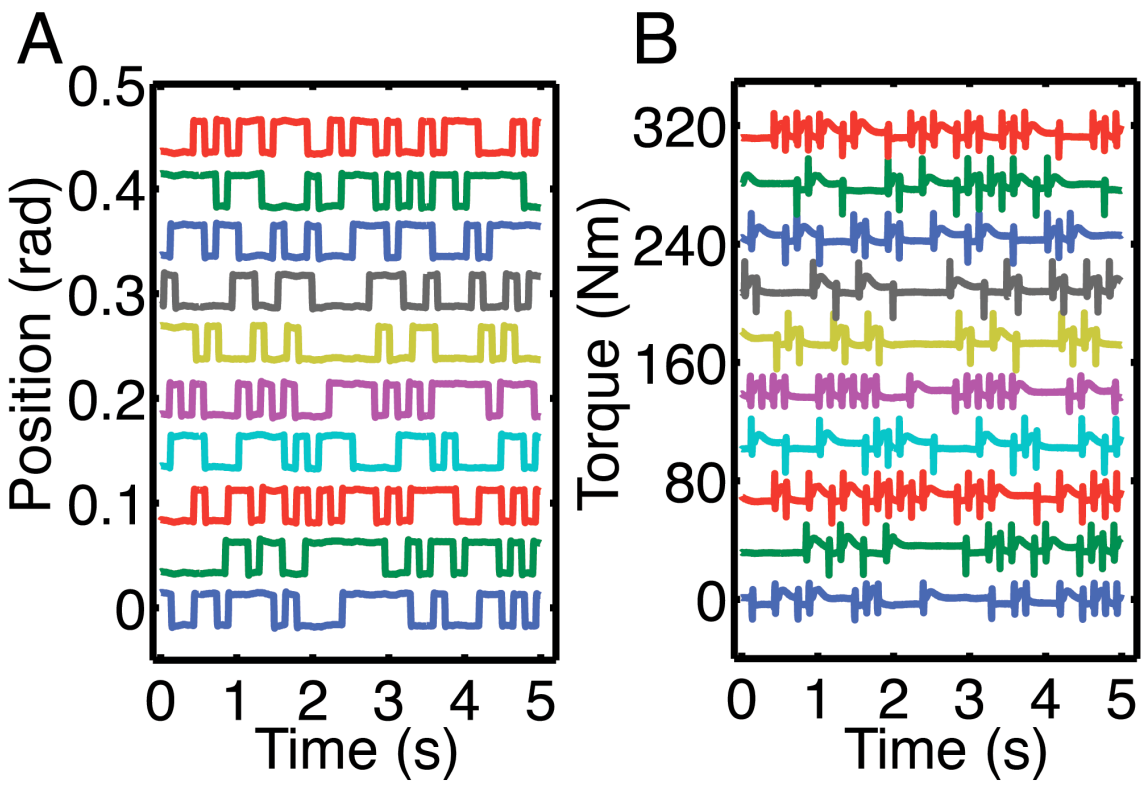

Figure 4-2. An example of (A) an input position ensemble and (B) an output torque ensemble. An arbitrary offset was added so that each realization could be clearly seen.

torque ensemble. The input position and output torque were then used in the TVPC algorithm to identify the simulated system. Ankle stiffness was modeled in Simulink (The Mathworks Inc.). A simplified block diagram of the simulation model is shown in Figure 4-3; the full Simulink model is found in Appendix A.

The simulated position input was a 0.03 rad PRBS with a 150ms switching rate. To simulate the bandwidth limitations of our experimental apparatus, the input was filtered with a 2nd-order, lowpass Butterworth filter with a 50Hz cutoff. Gaussian white noise was added to the total output torque to investigate its effect on the quality of the identification.

Time-varying behavior was achieved by changing *G*, *B*, and *K* with time. All other parameters were held constant. The data ensembles were generated by running the simulation multiple times with different realizations of the input and noise signals but the same TV behavior. Note that the term set will be used to describe the group of simula-

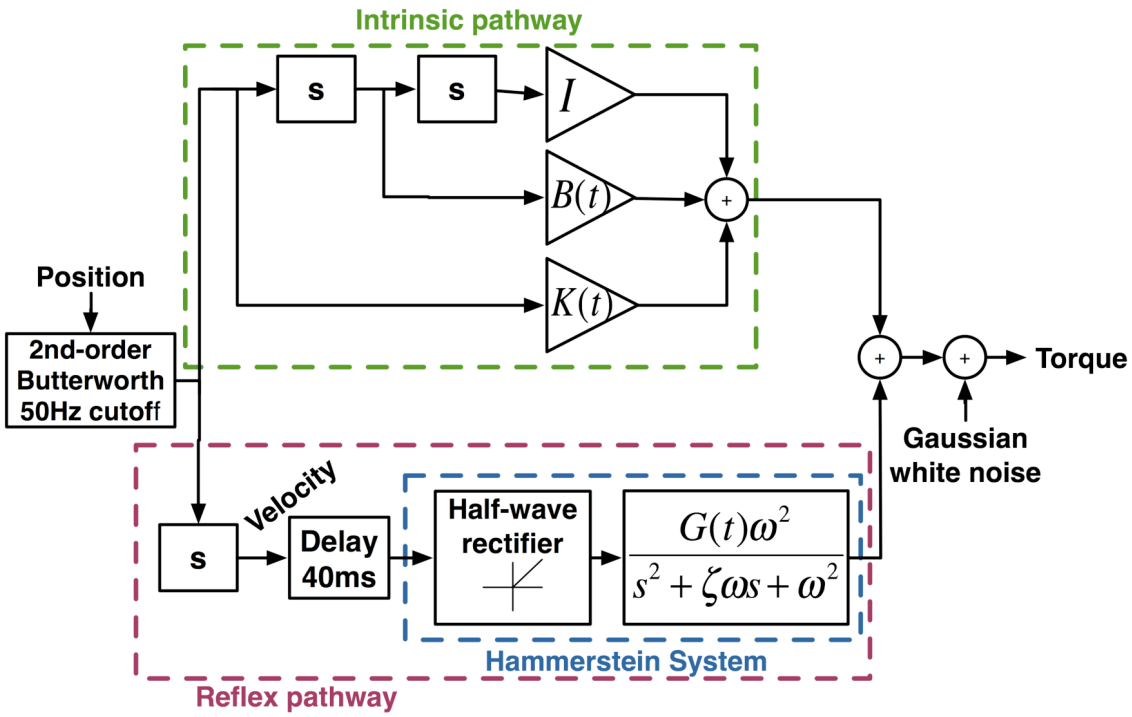

Figure 4-3. Simulation model of joint stiffness. The intrinsic viscosity, *B*, and elasticity, *K*, parameters, and reflex gain, *G*, varied with time. All other parameters were held constant.

tions used to generate the ensembles of input-output pairs, while single input-output pairs will be referred to as realizations.

The simulations were run at a 1 KHz sampling rate and were subsequently decimated to 200 Hz prior to analysis. Only the input position, P, and the total output torque, TQ, can be measured experimentally. However, with simulations we will be able to determine exactly how well the intrinsic torque, TQ_i, and the reflex torque, TQ_r, are predicted. The quality of the identification is determined by calculating the percent variance accounted for (%VAF) between the observed signal, X, and its estimate, $\hat{X}$, as follows:

$$\%VAF(X,\hat{X}) = 100\left(1 - \frac{\mathrm{var}(X-\hat{X})}{\mathrm{var}(X)}\right)$$

The intrinsic torque estimates were generated by convolving the TV intrinsic stiffness estimates with simulated position. The reflex torque was predicted by applying the TV non-

linearity to the velocity signal, and convolving the result with the TV reflex IRFs. The predicted total torque was the sum of the intrinsic and reflex torque estimates.

4.3. Results

4.3.1. Identification of rapid, TV changes

The goal of the first simulation study was to evaluate the algorithm's ability to identify rapid, TV changes in system dynamics. This was tested by simulating the model shown in Figure 4-3 with rapid changes in G, K, and B, while all other parameters were fixed. The data ensembles were composed of 600 realizations and there was no added noise. Table 4-1 lists the parameters used in the simulated model.

G, K, and B were changed according to the time-course shown in Figure 4-4. First, G underwent 3 steps changes, followed by ramp changes in both K, and B. This pattern was chosen for its fast changes (steps) and to show that changes could be detected in the parameters known to vary under different stationary conditions. Also, by varying the parameters independently, cross-talk between parameters could be detected. Otherwise, the pattern was not chosen to resemble that of a particular movement, since that remains unknown.

Intrinsic stiffness parameters		**Reflex stiffness parameters**	
K(t)	see Figure 4-4B	G(t)	see Figure 4-4A
B(t)	see Figure 4-4C	ζ	0.075
I	0.02 Nm/rad/s^2	ω	20 rad/s

Table 4-1. Parameters used in the simulation model shown in Figure 4-3 to study the TVPC algorithm's ability to track system dynamics that change rapidly in time. *K*, *B*, and *G* are time-varying, while all other parameters are fixed.

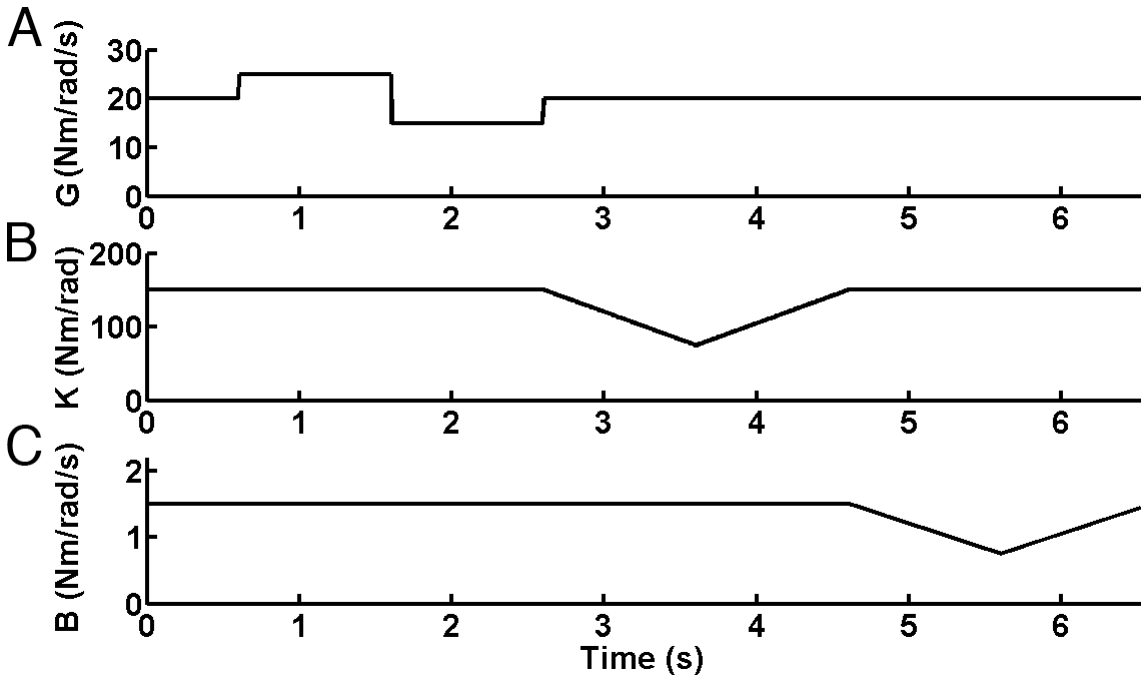

Figure 4-4. Time-course of (A) reflex gain, *G,* (B) elasticity, *K,* and (C) viscosity, *B*.

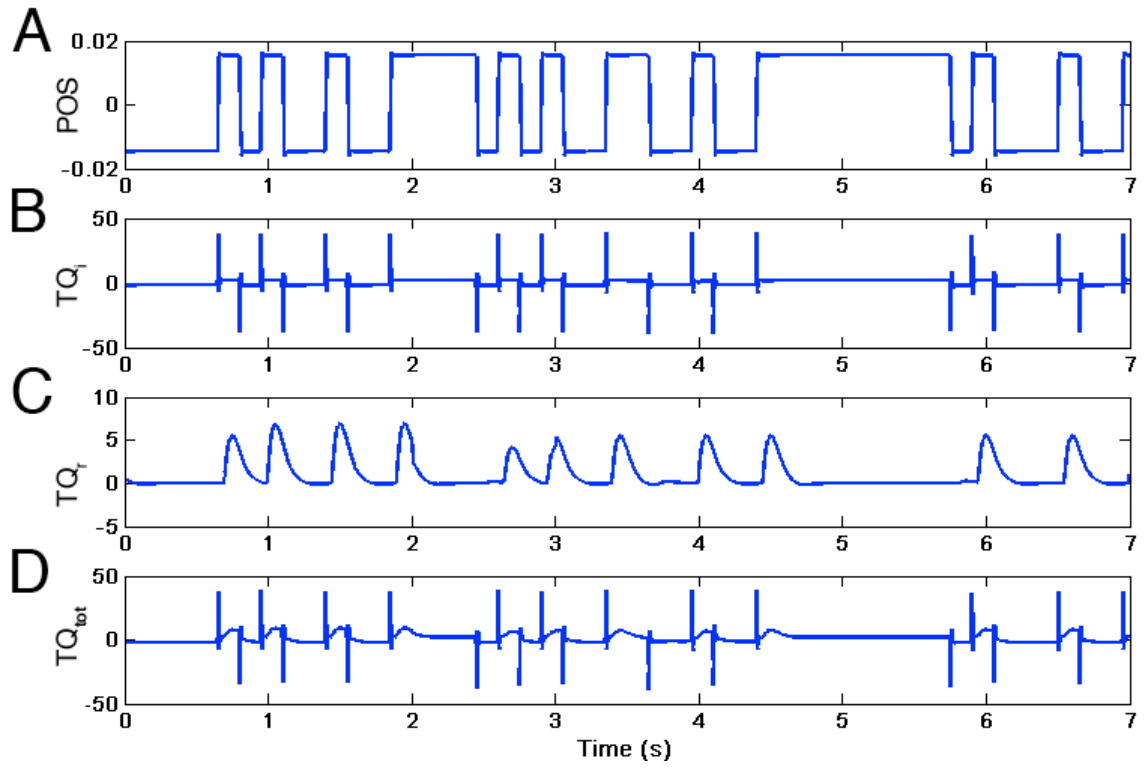

Figure 4-5. Single realization of (A) position (rad), (B) intrinsic torque (Nm), (C) reflex torque (Nm), and (D) total torque (Nm).

Figure 4-5 shows a single realization of simulated position, intrinsic torque, reflex torque, and total torque. The effect of changing *G* can be seen in the simulated reflex torque (Figure 4-5C) as the amplitude of the reflex response changes with the steps in gain. The TV behavior of the intrinsic stiffness is not apparent in the intrinsic torque trace (Figure 4-5B).

Figure 4-6(A-D) shows the theoretical stiffness and compliance ensembles corresponding to the simulated systems. Figure 4-6A shows the intrinsic stiffness IRFs as they change through time. The effect of the ramp change in *K* decreases the IRF amplitude and looks like a notch in the stiffness ensemble. The effect of changing *B* is less apparent. Figure 4-6B shows the intrinsic compliance IRF ensemble. Intrinsic stiffness is usually converted to compliance following the identification procedure because it is causal and is more readily interpreted. For instance, not only is the effect of changing *K* apparent, but the effect of changing *B* is also visible. There are two peaks in the compliance ensembles, corresponding to the changes in *K* and *B*, which were difficult see in the stiffness IRFs. The compliance IRFs are also less affected by the identification noise. This is clear in the identification results, discussed later. Figure 4-6C shows the reflex non-linearity ensemble, which is a half-wave rectifier with no time-varying behavior, and a gain of 1 (i.e. a slope of 1). Finally, Figure 4-6D shows the reflex stiffness IRF ensemble. The three step changes in gain are clearly visible.

The simulated data was analyzed using the TVPC algorithm. Figure 4-6(E-H) shows the resulting estimates of the stiffness and compliance IRF ensembles. TV behavior is not visible in the intrinsic stiffness IRF ensemble (Figure 4-6E). It does not share any of the same visual features as the theoretical ensemble and has an increased amplitude due to noise, and yet, when converted to compliance (Figure 4-6F) the TV behavior is clear. This is due to its sensitivity to identification noise, mentioned above. A small amount of high frequency noise distorts the stiffness IRFs, but when it is converted to a low-pass compliance IRFs the high frequency noise has less effect. The estimated compliance IRF ensemble shows all the same gain and shape changes as the theoretical ensemble, though slightly noisier. The estimated reflex stiffness IRF ensemble (Figure 4-6H) shows the three step changes in *G*, but has a smaller gain. This is because some of its gain was

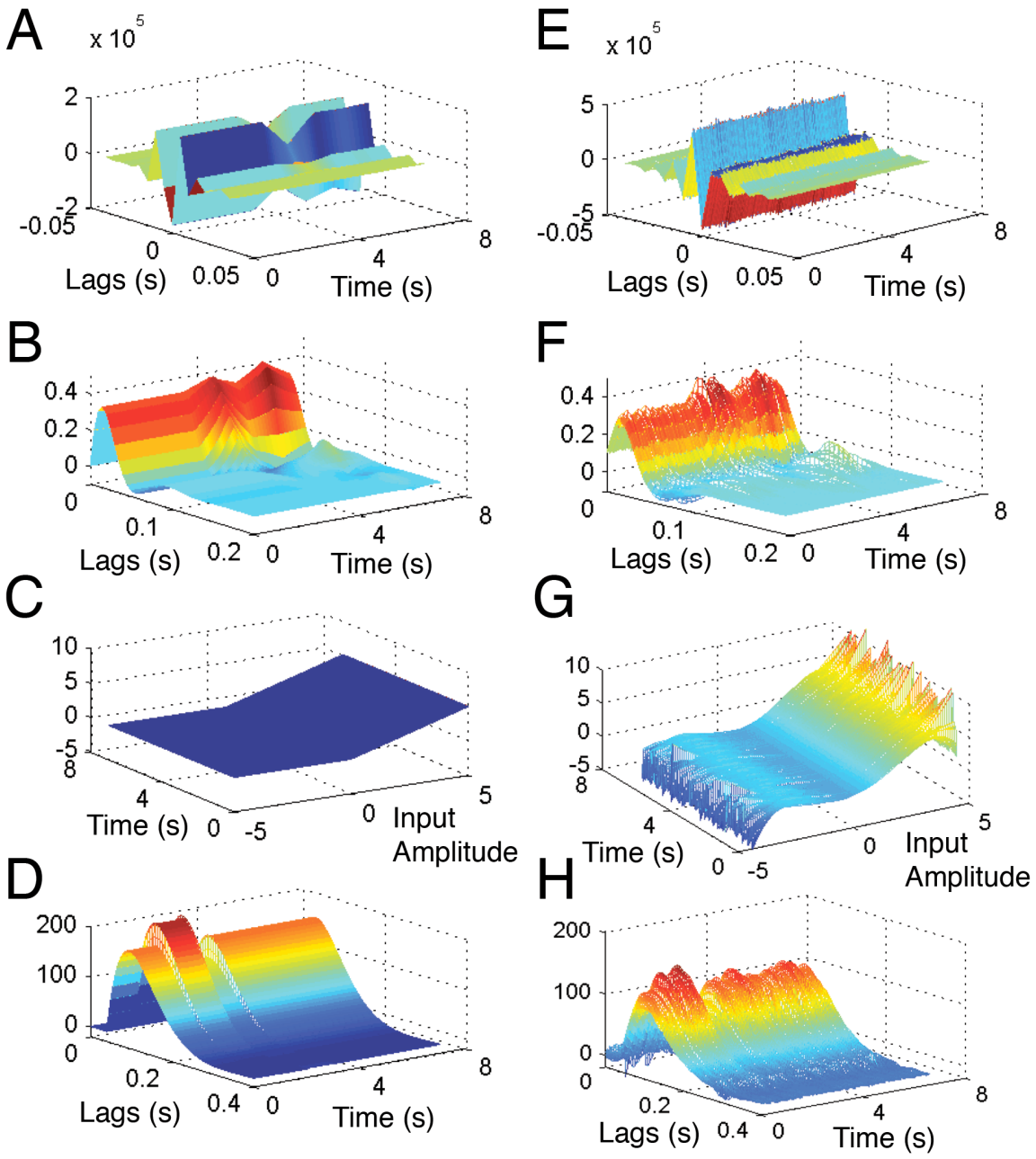

Figure 4-6.
Theoretical TV systems:
(A) Intrinsic stiffness IRF ensemble
(B) Intrinsic compliance IRF ensemble
(C) Reflex non-linearity ensemble
(D) Reflex linear IRF ensemble

System estimates generated by the TVPC algorithm:
(E) Estimated intrinsic stiffness IRF ensemble
(F) Estimated intrinsic compliance IRF ensemble
(G) Estimated reflex non-linearity ensemble
(H) Estimated reflex linear IRF ensemble

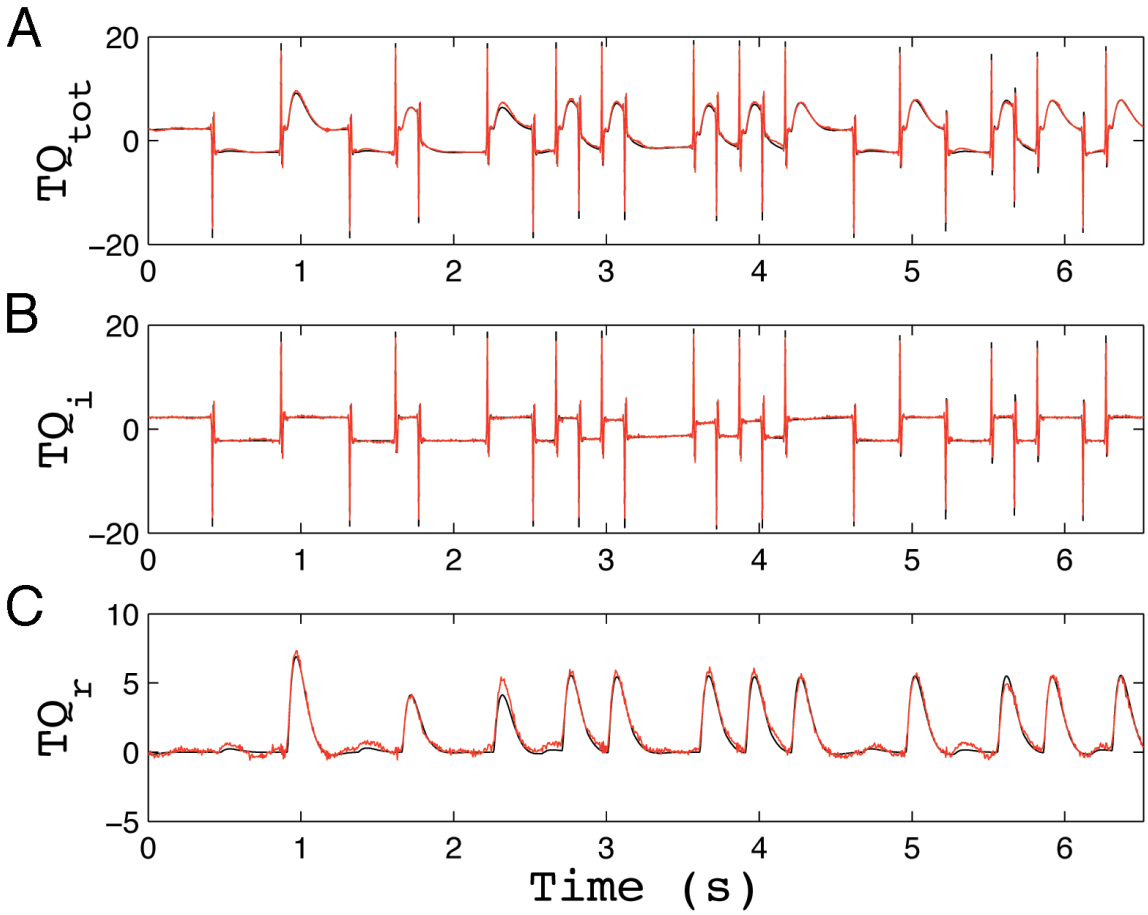

Figure 4-7. Predicted torque (red) superimposed on the simulated torque (black) for (A) total torque, (B) intrinsic torque, and (C) reflex torque. The predicted torques closely match those simulated.

transferred to the non-linearity (Figure 4-6G), which does not have a gain of 1, as was simulated. This is not a problem, because the reflex stiffness is in a series arrangement. With this structure, the overall gain of the reflex pathway can be distributed arbitrarily between the non-linearity and the low-pass filter [53]. Whether the gain is all on one or the other of the Hammerstein component, or distributed over both, gives the same results, as long as product of the gains remains the same. The total reflex gain, *G*, is a combination of the gain of the linear element, and the gain of the non-linearity. Therefore, that some of the gain was associated with the estimated reflex non-linearity, instead of all on the reflex IRFs, was not an error.

The estimated systems were used to predict the output torques, which estimated the simulated torques well. Figure 4-7 shows a single realizations of predicted torques (red)

superimposed on simulated torques (black). There is very close agreement between the simulated and predicted torques; the black trace of the simulated torques is barely visible behind the red trace of the predicted torques. Figure 4-8 shows the %VAF calculated across the ensemble at each time. The total and intrinsic torque were estimated well consistently (see Figure 4-8(A-B), with an average %VAF of 98.5% and 98.3%, respectively. The reflex torque was also predicted well (see Figure 4-8C), with an average %VAF of 96.8%. This is not as high as for the intrinsic torque, the reason for this is explored in the following section.

To further confirm that the simulated systems were correctly modeled, the parametric models used to simulate them were fit to the estimated TV systems, providing an estimate of the simulated parameters, such as *G*, *B*, and *K*. Fitting was accomplished

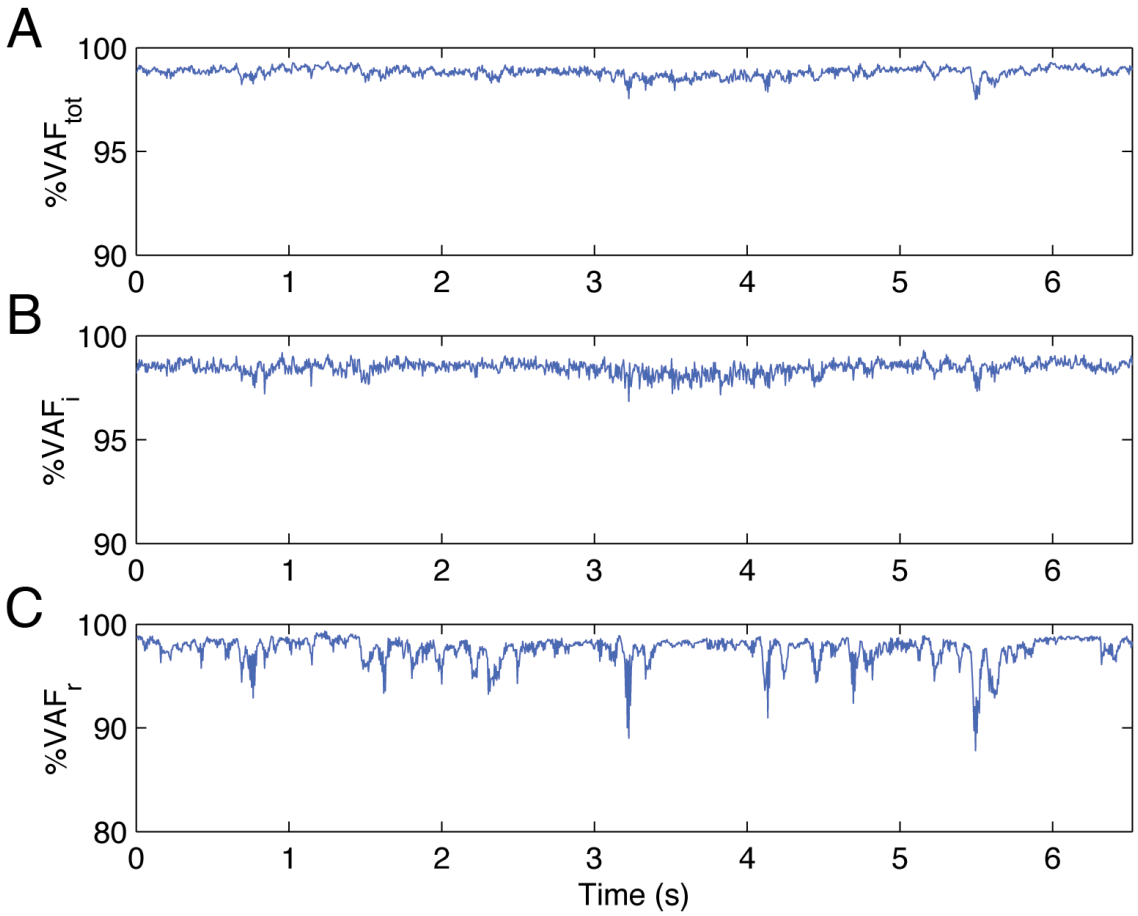

Figure 4-8. %VAF calculated across the ensemble at each time point. The %VAF is very good for the total torque (A), and intrinsic torque (B). The % VAF for the reflex torque (C) is lower, although still good.

using the Levenberg-Marquardt non-linear, least-square fit algorithm. Intrinsic compliance was parameterized using a 2nd-order, lowpass system relating torque to position. The linear subsystem of reflex stiffness was parameterized using a second order, lowpass system relating half-wave rectified velocity to torque. A parametric fit was calculated for the intrinsic and reflex IRFs at every time point. The parametric models fit the IRFs quite well. The quality of the parametric fit was assessed by calculating the %VAF between the parametric fits and their corresponding non-parametric IRF. The average %VAF between the non-parametric intrinsic and reflex IRF estimates and their parametric fit was 96.1% and 99.7%, respectively.

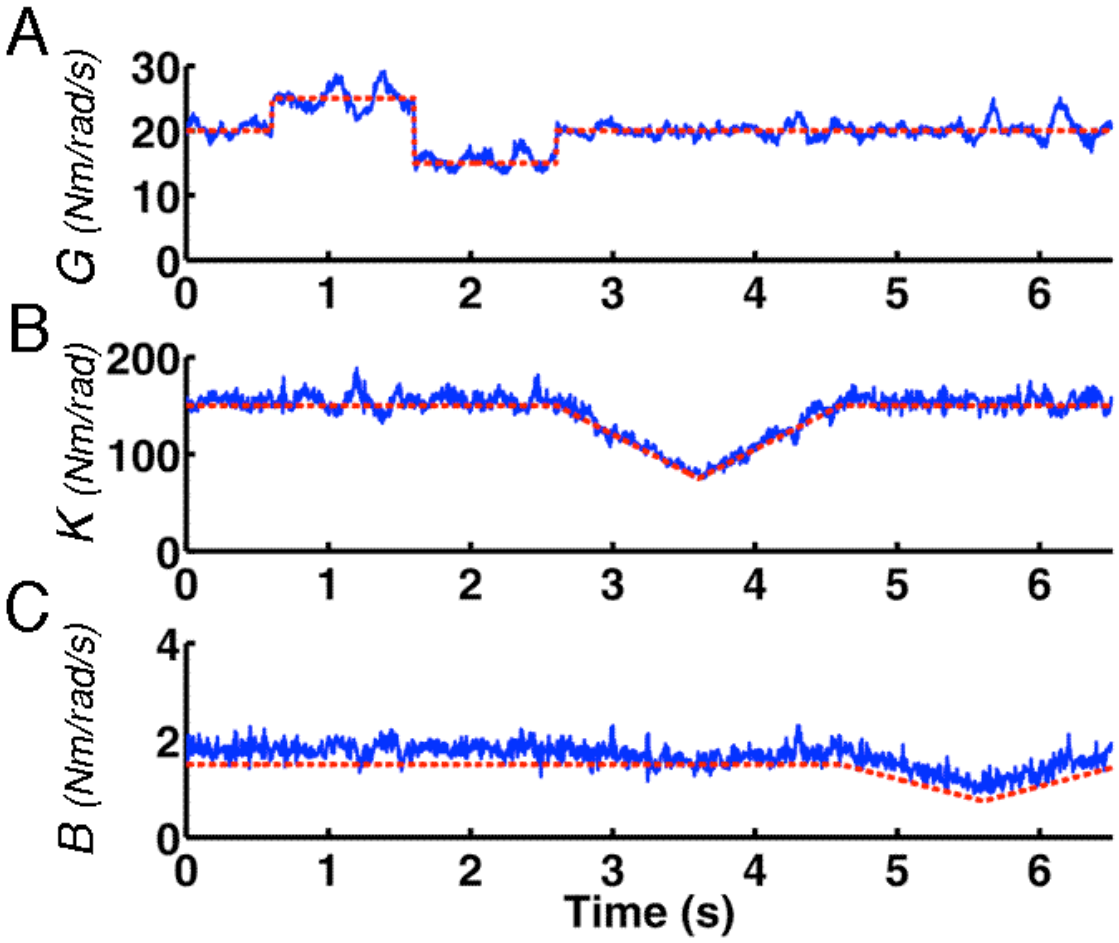

Figure 4-9. Parametric fit results for parameters (A) reflex gain, *G*, (B) elasticity, *K*, and (C) viscosity, *B*. The values obtained by the parametric fits are in blue (solid). These are compared to the values of parameters used in the simulations, in red (dotted). The simulation parameters are estimated well.

The parametric fits provided values for *K*, *B*, and the reflex IRF gain. Recall that the total reflex gain is the product of the gain on the non-linear and linear subsystems. Therefore, the gain of the non-linearity must also be determined in order to have the equivalent of the simulated parameter, *G*. The gain of a polynomial is difficult to define. Recall that the gain of a half-wave rectifier is determined by the slope of the line above zero. By applying the knowledge that the polynomial is approximating a half-wave rectifier, a straight line that starts at the origin, can be used to approximate the positive portion of the polynomial; the slope of that line is an estimate of the gain of the non-linearity. The total reflex gain, *G*, is calculated by multiplying the gain of the non-linearity with the gain of the parametric fit of the reflex IRF.

Figure 4-9 shows the value of the parameters estimated for G, K, and B. The estimated parameters closely follow the time-course of those simulated. Even the step changes in *G* are predicted precisely (see Figure 4-9A). The ramp changes in *K* and *B* are also predicted well (see Figure 4-9(B-C)). This demonstrates that the TVPC algorithm is able to track rapid changes in system dynamics with no *a priori* information about the time-course of the TV behavior.

4.3.2. Noise performance

The second goal of the simulation study was to evaluate the robustness of the TVPC algorithm in the presence of noise. Specifically, we wanted to study the effect of the signal-to-noise ratio (SNR) on the quality of the identification and determine the conditions needed for successful identification. Time-invariant system dynamics were simulated to isolate the exact system conditions affecting the algorithm's performance. With a constant noise level, varying the stiffness gain over a realization would change the signal-to-noise ratio; time-invariant simulations allow for a constant SNR to be maintained. Furthermore, the relative gain of the intrinsic and reflex pathways in the parallel-cascade structure, may affect the algorithm's performance. This can be controlled with time-invariant simulations.

The same TV procedure was used to simulate and identify the time-invariant systems. The input and output were organized into ensembles of 500 realizations and the system

Parameters	Value(s)
I (same for all sets)	0.02 Nm/rad/s^2
B (same for all sets)	1.5 Nm/rad/s
K (same for all sets)	150 Nm/rad
ζ (same for all sets)	0.75
ω (same for all sets)	20 rad/s
G	10, 20, 30 Nm/rad/s
SNR	0, 5, 10, 15, 20, 25, 30, 35 dB
# of realizations (same for all sets)	500

Table 4-2. Value of the parameters used to evaluate the TVPC algorithm's performance with various noise levels (SNR) and reflex gain (G).

was identified using the TVPC algorithm. Table 4-2 shows the values of the simulated parameters. All system parameters were held constant for each set and the reflex gain and SNR were varied between sets. The reflex gain, *G*, took on three values, representing low, medium, and high gain, to explore the effect of changing the relative strength of the reflex pathway on the quality of the identification. For each reflex gain, SNRs from 0 dB to 35dB, in 5 dB increments, were simulated. There were a total of 24 simulated sets; each with a different combination of reflex gain and SNR. The quality of the identification was assessed by the %VAF between the simulated, noise-free torques and the estimated torques.

Figure 4-10 shows the %VAF between the simulated and predicted total torque (A), intrinsic torque (B), and reflex torque (C) for the various SNRs and reflex gain combinations. Each point represents the results of the identification of a single set. The identification was considered to have failed if the %VAF fell below zero; the %VAF was set to zero for those points.

Figure 4-10(A-B) shows that the total and intrinsic torque were estimated consistently well. The %VAFs are above 80% for all SNRs and reflex gains; dropping only slightly as the SNR decreases. This, however, was not the case with the reflex torque. The size of the

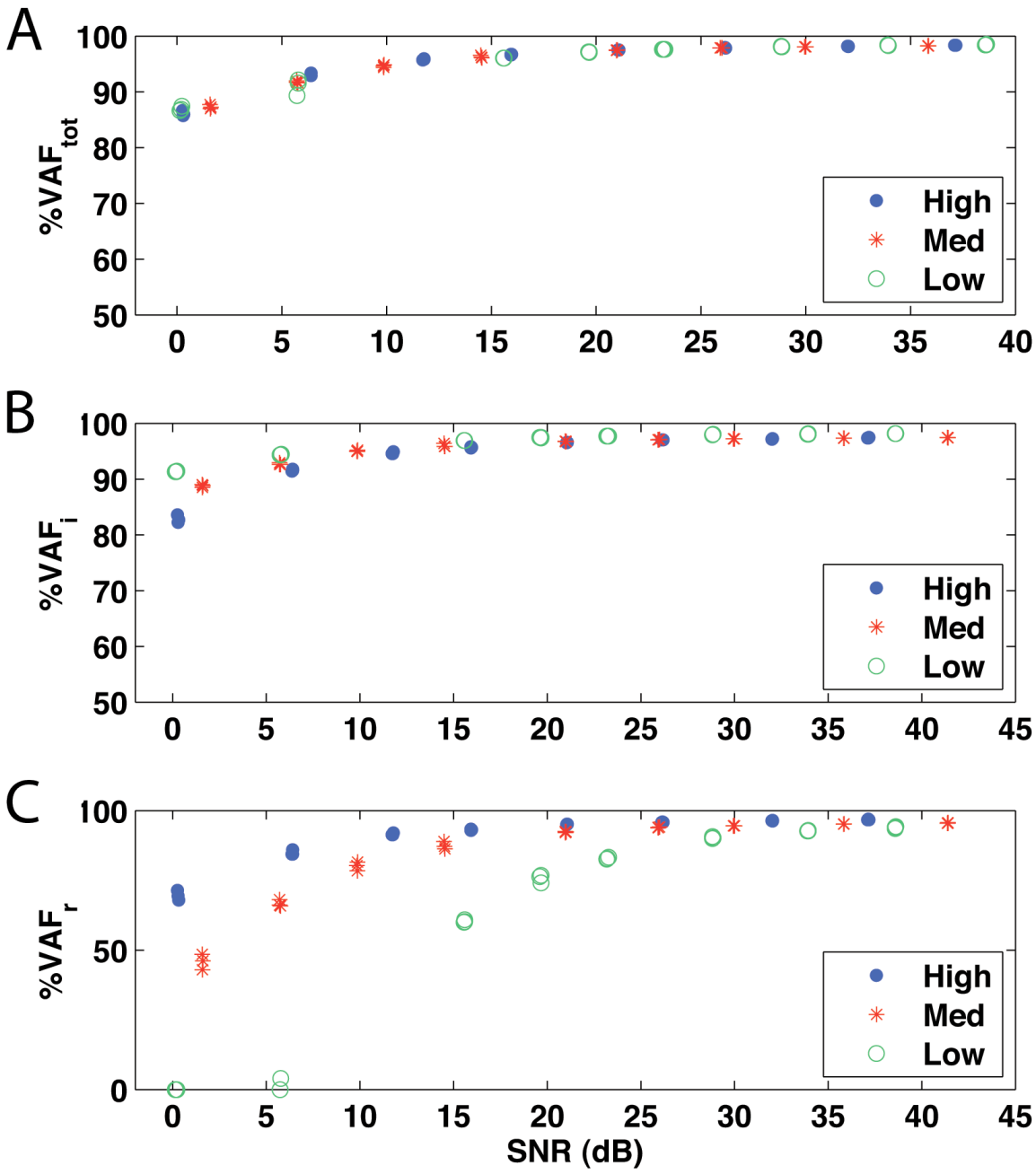

Figure 4-10. Percent VAF between simulated and predicted (A) total, (B) intrinsic, and (C) reflex torque as a function of SNR for high, medium, and low reflex gains. The reflex identification is more sensitive to higher noise levels than the intrinsic identification.

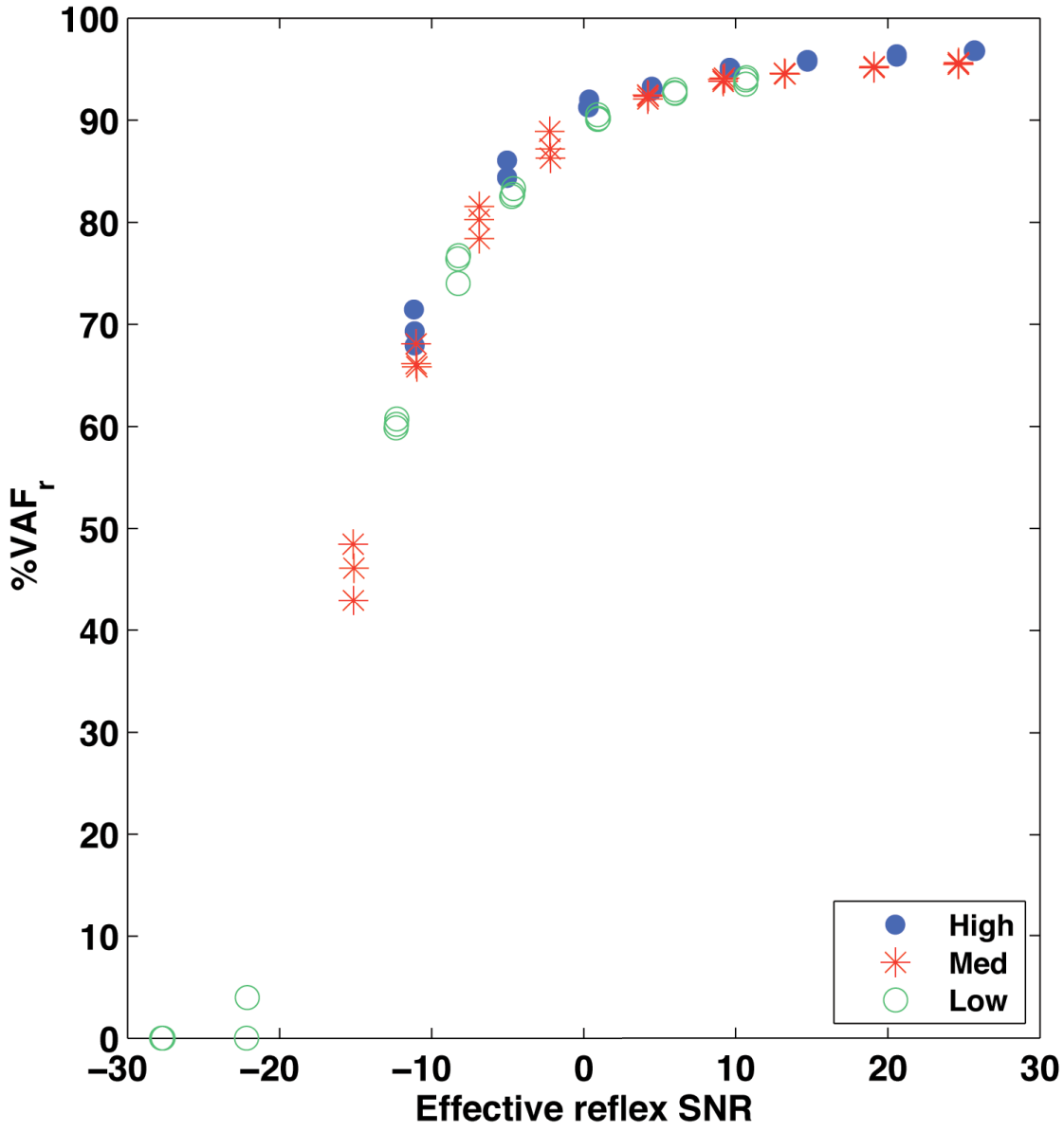

Figure 4-11. Percent VAF between simulated and predicted reflex torque as a function of effective reflex SNR for low, medium, and high reflex gains. The quality of the reflex identification shows the same degradation behavior for all reflex gains when plotted against the effective reflex SNR.

reflex gain had a large effect on the amount of noise that could be tolerated during reflex identification. This is most clearly illustrated by the points corresponding to low reflex gain (see Figure 4-10C), where the identification failed for SNRs less than 10 dB. The quality of the reflex identification degraded at higher SNRs for lower reflex gains.

In light of the above result, a new metric was calculated: the effective reflex SNR, defined as the ratio of reflex torque power to noise power. Figure 4-11 plots the %VAF between simulated and predicted reflex torque against effective reflex SNR. Using this new metric, the reflex identification showed the same degradation behavior for all reflex gains. The %VAF was above 80% for effective reflex SNRs above 0 dB, and fell off rapidly below that.

4.3.3. Number of realizations

In TV ensemble identification methods, the quality of the identification is not improved by using longer realizations to generate the estimates, as it is with time-invariant identification. This is because noise averaging is not performed in time but across the ensemble. Consequently, the quality of the identification should improve as more realizations are added to the data ensembles. Similarly, more realizations should be required as the SNR

Parameters	Value(s)
I (same for all sets)	0.02 Nm/rad/s^2
B (same for all sets)	1.5 Nm/rad/s
K (same for all sets)	150 Nm/rad
ζ (same for all sets)	0.75
ω (same for all sets)	20 rad/s
G (same for all sets)	20 Nm/rad/s
SNR (same for all sets)	10 dB
# of realizations	400, 450, 500, 550, 600, 650, 700, 750, 800, 900

Table 4-3. Parameter values used to investigate the effect of increasing the number of realizations in the data ensembles. All parameters were fixed except the number of realizations.

decreases. To test these hypotheses, we first studied the effect of increasing of the number of realizations on the quality of the torque estimates. Table 4-3 shows the values of the simulated system parameters. The SNR was fixed at 10 dB and a medium reflex gain was chosen because these conditions were observed in a previous study that used the time-invariant, parallel-cascade algorithm to evaluate ankle stiffness [5].

Figure 4-12A shows the %VAF between the simulated total, intrinsic and reflex torques and their estimates versus the number of realizations included in the data ensembles. The total and intrinsic torques were modeled consistently well; maintaining a %VAF between simulated and predicted torques above 90%. Increasing the number of realizations in the ensembles only slightly improved the estimates. A more drastic improvement was seen in the reflex identification; the %VAF increased from approximately 60% with 400 realizations, to 90% with 900 realizations. The previous results showed that with a medium reflex gain, the identification of the reflex pathway was more sensitive to the SNR than that of the intrinsic pathway (refer to Figure 4-10(B-C)). Therefore, it was expected that increasing the number of realizations, which increases the noise averaging, would more significantly improve the reflex torque estimates.

The second part of the study varied both the number of realizations and the SNR in order to determine the minimum number of realizations required to reliably identify the system under various noise conditions. Reliability was determined by simulating 5 sets with the same SNR and number of realizations but different realizations of the input and noise signals. If the identification of all 5 sets was successful, the identification was considered reliable. If, however, one or more identifications failed, determined by a %VAF below zero for either the total, intrinsic or reflex torque, the identification was considered unreliable. Failure results from limiting the amount of noise averaging by reducing the number of realizations. When approaching the minimum number of realizations required for identification, certain combinations of the input, output and noise may result in a successful identification, while others may fail. The minimum number of realizations required for reliable estimation for a particular SNR was determined by decreasing the number of realizations in the ensembles by 25 until at least one identification failed. The

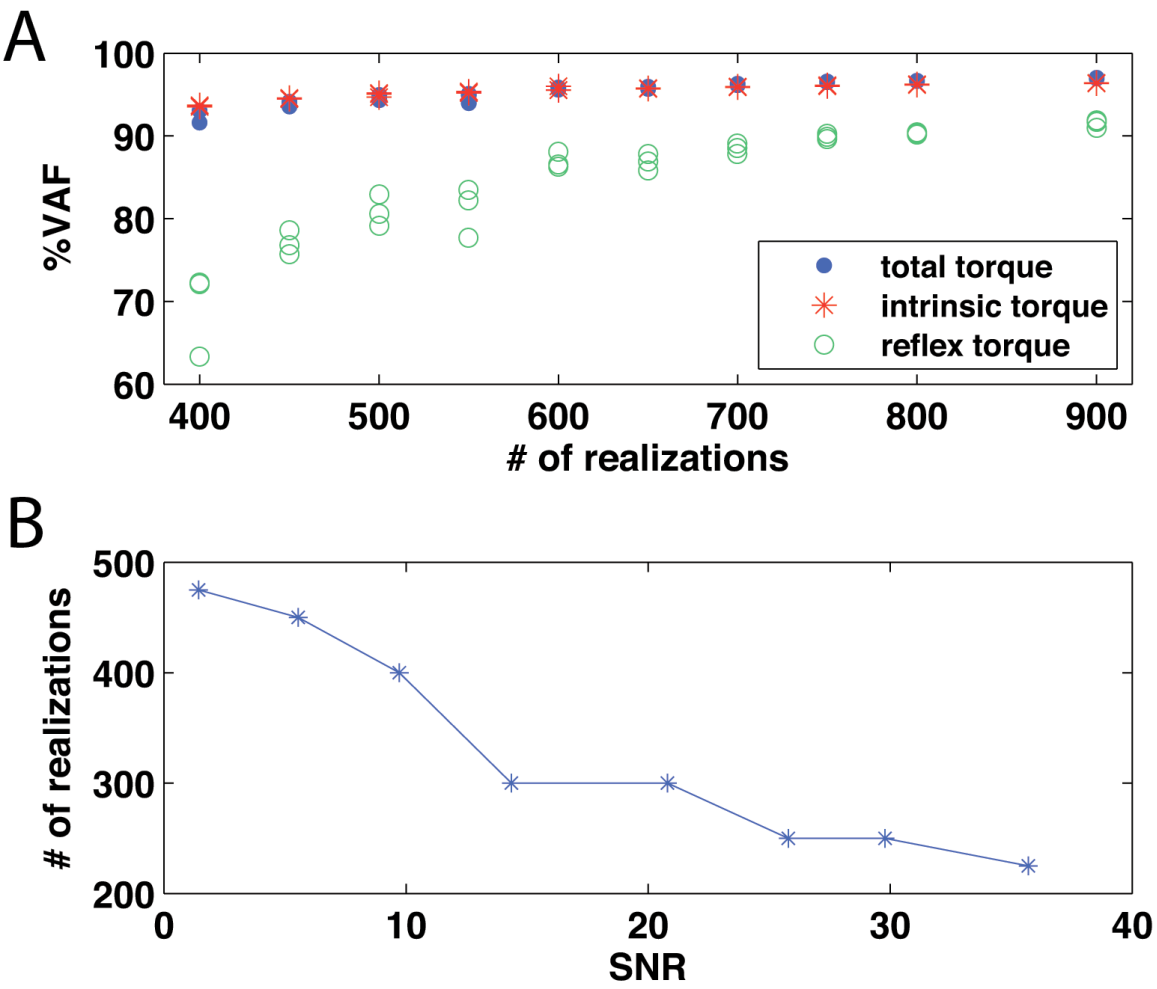

Figure 4-12. (A) %VAF between the simulated and estimated total, intrinsic and reflex torques vs. the number of realizations used in the data ensembles. Increasing the number of realizations improves the %VAF of the identification. The reflex identification shows the most improvement. (B) The minimum number of realizations required for reliable identification vs. SNR. Less realizations are required for reliable identification as the SNR increases.

minimum allowable ensemble size was determined to be that of the last successful identifications of a group of 5 sets. A medium reflex gain was used.

Figure 4-12B shows the minimum number of realizations required for successful identification as a function of SNR. As expected, the minimum number of realizations required for reliable identification decreased in a non-linear manner as the SNR increased. Even for a SNR close to 0 dB less than 500 realizations were required, and as few as 225 realizations were required for SNRs above 35 dB. Note that although few realizations were

required to achieve an identification, increasing the number of realizations in the ensemble would improve the estimates.

4.4. Discussion and Conclusions

The results of this simulation study demonstrate several important properties of the TVPC algorithm. First, the TVPC algorithm is capable of estimating system dynamics that change rapidly with time. In fact, it was even able to accurately track step changes, which were nearly instantaneous. Therefore, there are no limitations on the speed of the dynamics that may be studied using this method. Secondly, the TVPC algorithm is limited by the relative contribution of the reflex pathway, which is unlikely to be constant during movement. As the reflex gain decreases, the algorithm's ability to adequately identify the reflex pathway diminishes. Consequently, more realizations will be needed to maintain a high %VAF as the reflex gain decreases, and the SNR and effective reflex SNR decrease.

That the reflex identification cannot tolerate as much noise when the intrinsic component dominates the output is unsurprising because of the iterative nature of the algorithm. Consider the following: the intrinsic stiffness is estimated first and its contribution is removed from the total output torque prior to reflex identification. This is made possible by the reflex delay, which causes the reflex torque to be uncorrelated with the input for the duration of the reflex delay, which is longer than that of the intrinsic IRF. For the same reason, the noise is also not included in the intrinsic estimates because it is uncorrelated with the input for all times. Therefore, when the intrinsic component is removed from the total torque, the reflex component and the entirety of the noise remain for the reflex identification. This means that with smaller reflex gains, the effective reflex SNR is much lower than the total SNR, which, as the results of the previous section revealed, would require more realizations to achieve a similar identification quality as the intrinsic component. A similar trend could be expected if the situation were reversed and the reflex component dominated the output. In that case the intrinsic identification would have a lower effective SNR than the reflex identification, which would likely result in a lower %VAF of the intrinsic torque. However, there is an added complication, which is

that the reflex dynamics have more free parameters that must be identified, because the reflex IRF is longer than the intrinsic IRF and the non-linearity must be identified. Therefore, reflex stiffness presents a more difficult estimation problem and will always be more challenging to identify.

The number of realizations used in the data ensembles must take into account both the predicted reflex gain and the SNR. For a fixed SNR, more realizations will be required if the reflex gain is low rather than high. The less dominant pathway will have a lower effective SNR and therefore, more noise averaging will be required. A previous study [5] that used the time-invariant, parallel-cascade identification algorithm achieved a %VAF($TQ, T\hat{Q}$) of 90% and above, which is approximately equivalent to a 9 dB SNR. The same study found the reflex stiffness to have a low to medium gain. If these conditions are assumed for future experiments, between 500 and 800 realizations would be required for reliable and accurate estimation using the TVPC algorithm. This is a large amount of data; however, if experiments are designed such that one realization of a task takes 3 seconds to complete, 800 realizations recorded consecutively would take 40 minutes. If rest periods are included, the full experiment could be completed in under an hour, which is a realistic and reasonable amount of time to expect a subject to perform a task. Carefully designed experiments will improve the likelihood of successful system identification. When possible, experiments should aim to maximize the reflex gain and the SNR, and when this cannot be controlled, more realizations will improve the results.

The next chapter describes a study in which the TVPC algorithm is used to study changes in intrinsic and reflex dynamics during an isometric contraction relaxation task.

5. ANKLE STIFFNESS DURING AN ISOMETRIC CONTRACTION/RELAXATION TASK

5.1. INTRODUCTION

Position and the level of muscle activation have been found to greatly influence joint stiffness under quasi-stationary conditions [5]. Even though stationary studies indicate that joint stiffness is a variable property, they cannot be used to predict temporal changes during movement. Stationary studies can predict the stiffness once a transition is complete, but cannot predict its pattern of change between two points. Furthermore, the amplitude of the reflex EMG response, for matched background EMG levels and joint position, changes depending on the movement being executed [9, 10]. Due to the underlying non-linear properties of ankle stiffness, changing either ankle position or torque in time affects the system dynamics. These changes in stiffness throughout a task can be treated as time-varying (TV) dynamics, which require specialized identification techniques. Since most day-to-day tasks involve changes in position or torque, TV identification techniques must be used to identify stiffness as it changes throughout a particular task.

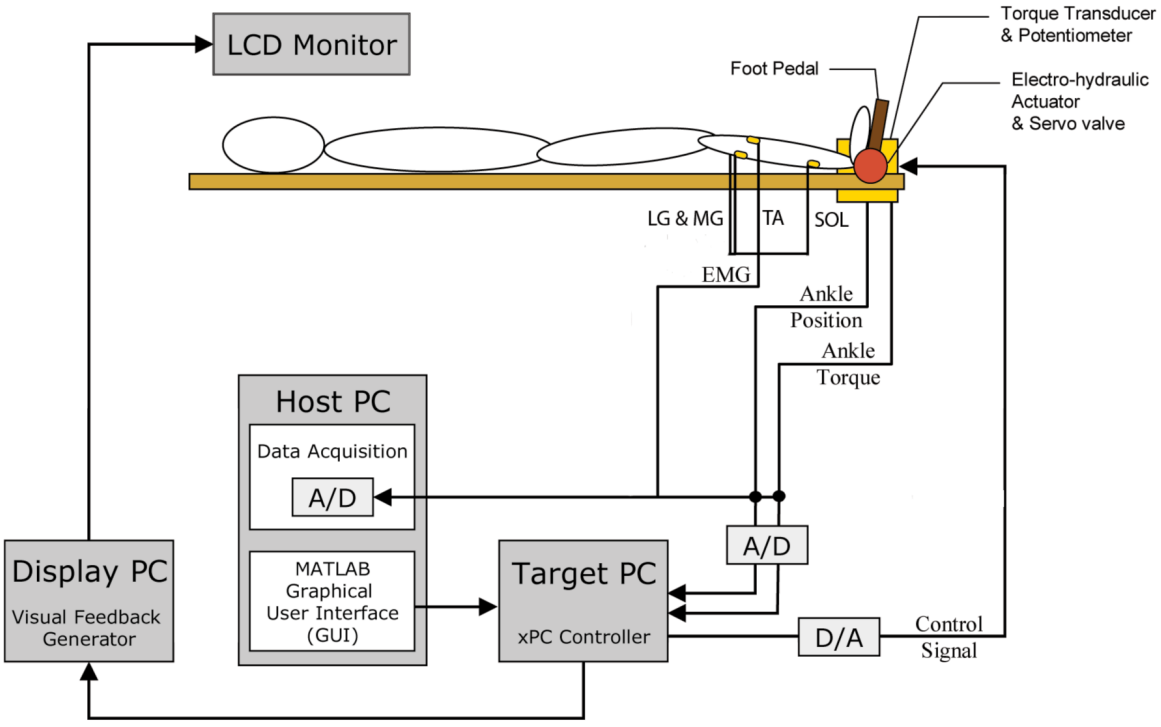

Figure 5-1. Schematic of the experimental setup

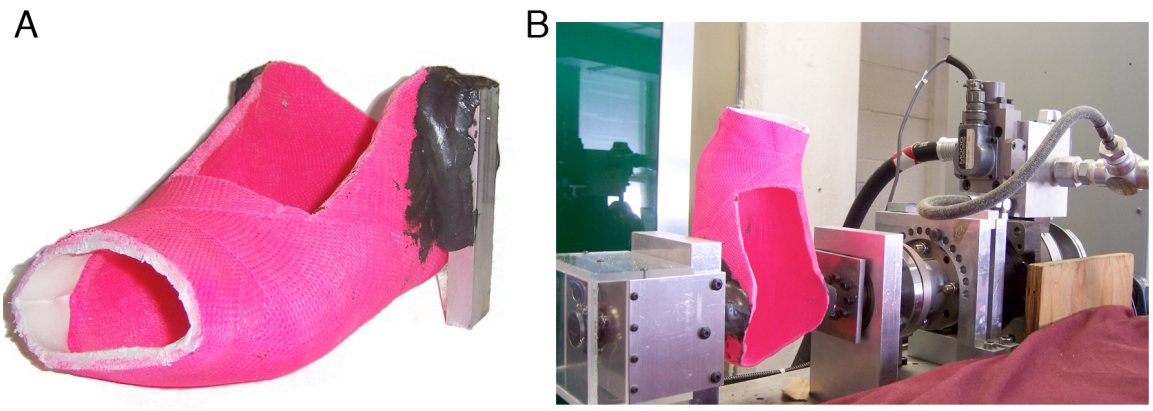

Figure 5-2. (A) Custom-made fibreglass boot (B) Boot attached to foot pedal of the hydraulic actuator

This chapter describes the use of a time-varying, parallel-cascade (TVPC) algorithm (refer to chapter 3) to examine the time-course of intrinsic and reflex stiffness modulation during a simple isometric contraction/relaxation task. The goal is to confirm that the TVPC algorithm produces reasonable results with experimental data. Subjects were required to periodically contract and relax their triceps surae (TS) while small, pseudo-random, position perturbations were applied. Kirsch et al.[58] and Kimura et al. [56] studied the reflex EMG response during similar tasks. Kirsch et al. found an increase in reflex EMG gain just prior to and during the early phase of contraction, and a gain decrease associated with relaxation. They also found that these changes closely followed the changes in background EMG, leading them to conclude that the muscle activation level and reflex gain were commonly controlled. Similarly, Kimura et al. found that the amplitude of the reflex EMG was largest during the contraction phase and smallest during the relaxation phase. The following sections provide detailed methods and results.

5.2. METHODS

5.2.1. Experimental setup

A general schematic of the experimental setup is shown in Figure 5-1. The subject lay supine with their foot attached to a hydraulic actuator by means of a custom made fibreglass boot (Figure 5-2A). The knee was held in a slightly bent position, supported by sandbags. A strap across the thigh prevented motion at the knee joint. The custom boot was attached to a foot pedal (Figure 5-2B), which produced the rotation around the an-

kle joint. Position and rotation were controlled by a proportional position servo implemented using xPC Target (The Mathworks Inc.) on the Target PC.

Six signals were recorded: position, torque, and 4 EMGs. Angular position was measured using a precision potentiometer (BI Technologies, 6273). Ankle torque was acquired using a general purpose reaction torque sensor (Lebow, 2110-5K). EMG signals were recorded from the lateral (LG) and medial gastrocnemius (MG), soleus (SOL), and tibialis anterior (TA) muscles using a 8-channel Bagnoli EMG System (Delsys Inc.). These signals were sampled at 1 kHz by a dynamic signal acquisition card (National Instruments, 4472), which also performed the anti-aliasing, and stored on the Host PC. These signals were also used by the Target PC for the position controller and subject feedback.

The subject was provided with visual feedback through an LCD monitor suspended overhead. The Display PC generated the feedback display (discussed in detail in Section 5.2.4) using signals from the Target PC.

5.2.2. Subjects and Task

Six male subjects between the ages of 24 and 42, with no prior history of neuromuscular disease, participated in this study. They were required to perform a simple torque matching task, while the ankle underwent small perturbations about the neutral position. The perturbation was a 0.03 rad pseudo random binary sequence (PRBS) with a 127 ms switching rate, assumed to be small enough not to affect system properties and dynamics. The ankle was placed in a neutral position and the target torque levels kept small to maximize the reflex contribution to the total torque output [5] and to avoid fatigue. A detailed experimental protocol follows.

5.2.3. EMG Preparation

For the EMG recordings, the subject was required to shave five small patches of hair, about 6 cm^2 each, for the placement of the electrodes. The shaved areas were cleaned with alcohol swabs. Single differential surface electrodes (DE-2.1) were attached using double sided tape. Electrodes were placed on the belly of the lateral and medial heads of

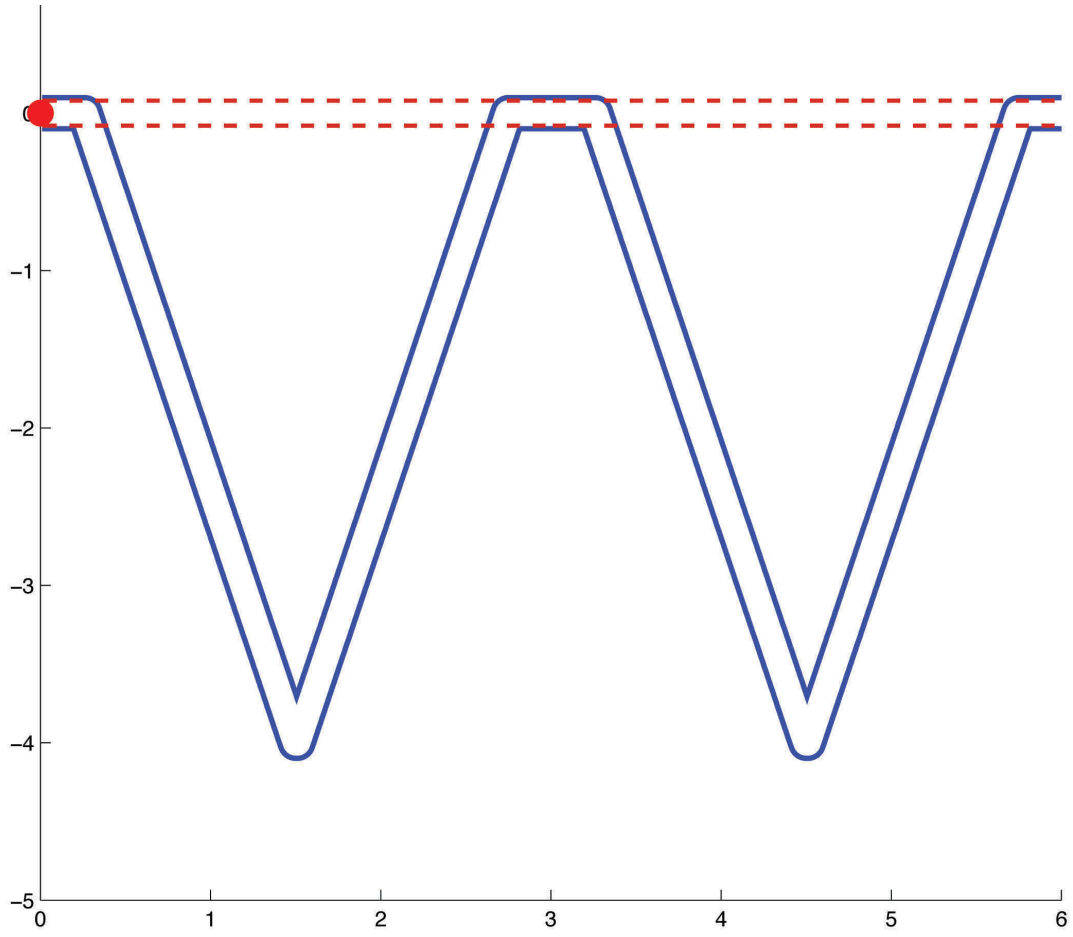

Figure 5-3. Visual torque feedback given to the subject. The red dashed lines are used for the stationary torque matching task. The blue lines are used for the time-varying, isometric contraction/relaxation task. The red ball provides feedback about the torque generated by the subject. When the subject pushes on the foot pedal (plantarflexion) the ball moves down on the screen. It moves up when the subject pulls back (dorsiflexion).

the gastrocnemius, on the soleus just below the gastrocnemius, and on the belly of the tibialis anterior. A large ground electrode was placed on the knee.

5.2.4. Visual Feedback

Visual feedback was provided to the subject by means of the LCD screen suspended overhead. The feedback display is shown in Figure 5-3. The red dashed lines were used for stationary torque matching tasks, while the blue lines were used for the time-varying, isometric contraction/relaxation task. The red ball responded to changes in torque. It moved across the screen in time; taking six seconds to cross the screen and then looping back to the beginning. The subject's filtered torque controlled the vertical ball position. Plantarflexing torques moved the ball down and dorsiflexing torques moved the ball up

on the screen. The recorded torque was filtered with a 2nd-order Bessel filter with 0.5 Hz cutoff. This cutoff removed most of the torque response to the perturbation, leaving only the slowly changing voluntary torque. Before every recording, the passive torque (i.e. the torque recorded while the subject was relaxed) was recorded and removed from the feedback torque so that the torque seen by the subject was only the voluntary torque.

5.2.5. Experimental Protocol

The subject lay supine with their foot in the custom boot attached to the actuator. The hydraulic fluid was warmed prior to the start of the experiment to avoid any change in behavior during the experiment. The subject was required to perform the following tasks:

5.2.5.1. Preliminary recordings

1. *Zero-levels*: The subject was asked to relax and the base level signals were recorded for reference.

2. *Maximum Voluntary Contraction (MVC)*: The subject was asked to push (plantarflexion) and pull (dorsiflexion) as hard as they could. According to the lab convention, a plantarflexing torque is negative, while a dorsiflexing torque is positive. The value obtained in the plantarflexing direction was used to set the torque levels in the torque matching task. It was also used to assess muscle fatigue at the end of the experiment.

5.2.5.2. Training

To obtain good results in a TV experiment, it is important that there be as little inter-trial variability as possible. In a torque matching task, many different combinations of TS and TA activations can produce the same torque output. The visual feedback only provides the subject with the total output torque and does not provide them with any information about how they are performing the task. Initial pilot experiments revealed that subjects had a tendency to use their TA to perform the task, even though instructed to only contract and relax the TS; the TA should not have been involved. They varied their use of TA and TS throughout the experiment, which meant the task was not being performed

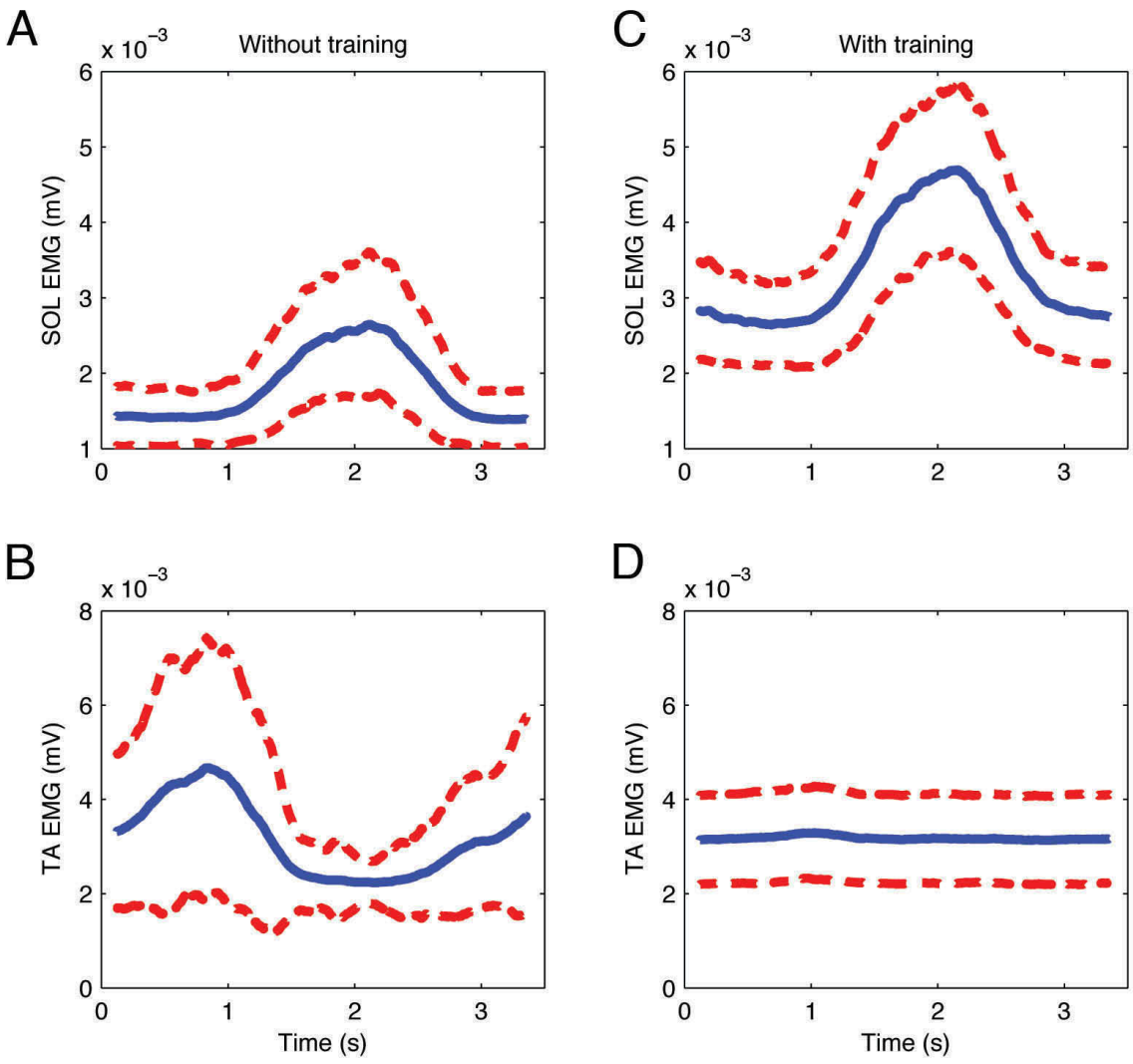

Figure 5-4. The solid blue lines are the ensemble average of the median filtered EMG. The dotted red lines indicate the standard deviation. (A) and (B) show the subject's EMG prior to training. (C) and (D) are after training. (A) SOL EMG without training (B) TA EMG without training (C) SOL EMG with training (D) TA EMG with training.

consistently. Furthermore, there could be no guarantee that all subjects performed the task in the same manner, making it difficult to compare results. For this reason, a strict training procedure was added to the experimental protocol.

The subject was given time to practice matching the torque trace both with and without perturbations. TA EMG was monitored during the practice. If the TA EMG exceeded baseline levels, indicating contraction, the subject was told to relax their TA. After 5 to 10 minutes of training, the subjects were generally able to perform the task without use of the TA. Figure 5-4 shows a subject's mean baseline EMG with standard deviation before

and after training. It is evident that there was TA EMG modulation without training and that it was no longer present after training. Furthermore, when the subject no longer used their TA, the TS modulation was larger and clearer. One subject was not able to perform the task without using the TA. Training was done in the same session as the rest of the experiment for all but one subject.

The EMG shown in Figure 5-4 is the ensemble average of median filtered traces. The individual EMG traces, with a 1 kHz sampling frequency, were filtered with a 250 point median filter. This was done to remove peaks due to the reflex response and isolate the background activity.

5.2.5.3. TV torque matching task

This task involved the isometric contraction/relaxation of the triceps surae (TS) between 1% and 5% MVC. Low torque levels were used to avoid muscle fatigue. To ensure consistent task performance, the subject was instructed to keep the red ball between the blue lines in the visual feedback (see Figure 5-3). The red ball went through two periods, three seconds each, of the task before looping back to the beginning. The subject was given approximately 5 minutes to practice matching the torque trace without perturbations. This was then recorded for 3 minutes, and could be used to assess the quality of the task performance.

The subject was then trained to perform the same task while the ankle was perturbed. The training procedure was explained in Section 5.2.5.2. The subject was required to complete 10 sets of 100 repetitions. Each set took approximately 5 minutes to complete, and the subject was given a 2 minute rest between each. A longer break was given at the half way point. A total of 1000 repetitions (realizations) of the task were acquired. The MVC was reassessed following the 10 sets.

5.2.6. Fatigue

This experiment took just over two hours to complete from start to finish, so muscle fatigue was a concern. Fatigue can change intrinsic and reflex dynamics and cause intrinsic gain to decrease and reflex gain to increase [81]. Time-varying ensemble methods rely on

the system being the same across the entire ensemble; fatigue would change the system and thus the identification would provide unreliable results. To avoid fatigue, a very low level contraction was used (5% MVC) and the subjects were given frequent rest periods. Fatigue was assessed by comparing the subject's MVC before and after the experiment. All subjects achieved or surpassed their original MVC, indicating that muscle fatigue was not a problem.

5.2.7. Data Preparation

The TV trials were collected continuously in 10 sets of 100 cycles. These long records were segmented into individual realizations and aligned to form the data ensembles (as Figure 5-5 illustrates). There were several challenges involved in this process.

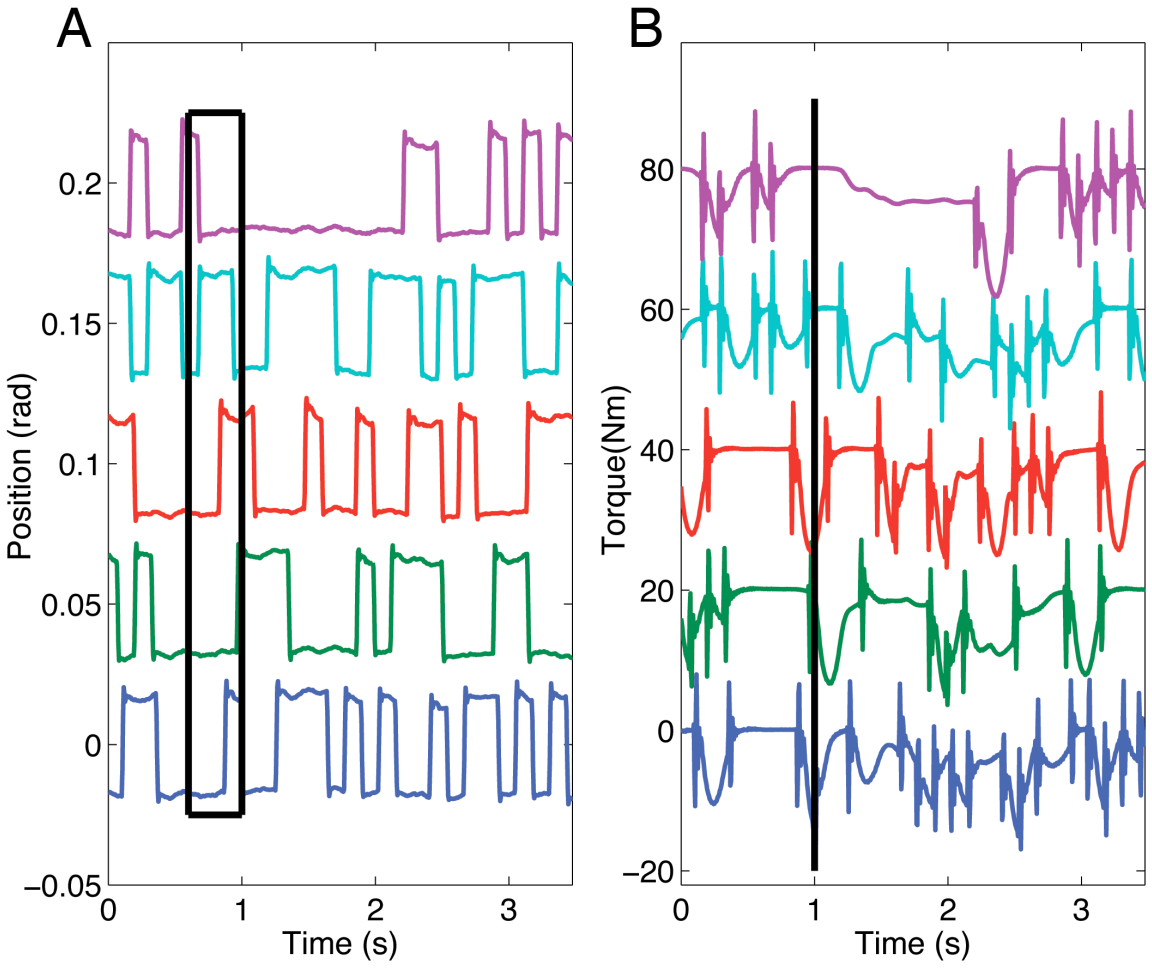

Figure 5-5. (A) Example input ensemble (B) Related output torque ensemble. The points denoted by the black box in A are convolved with the IRF at time = 1 to generate the output at the black line in B (time =1).

First the trials had to be segmented and aligned in a consistent way for all 10 data sets. The trials would, ideally, be aligned according to the underlying voluntary torque. This cannot be done directly because the torque recording includes the reflex response. Xu and Hollerbach [78] suggested that the underlying voluntary movement could be approximated by applying a filter with a cutoff frequency equal to the movement frequency. This idea was adapted by filtering the torque with a 2nd-order Butterworth filter with a 0.5 Hz cutoff to approximate the underlying voluntary torque. This filtered torque was used to align the trials and choose the most similar. The following is the alignment and selection algorithm used to generate the data sets used for system identification:

1. *Initial segmentation:* The filtered torque was first segmented according to the 3-second modulus of a clock signal. This clock signal controlled the movement of the red ball across the screen of the feedback display. A modulus value of zero indicated the

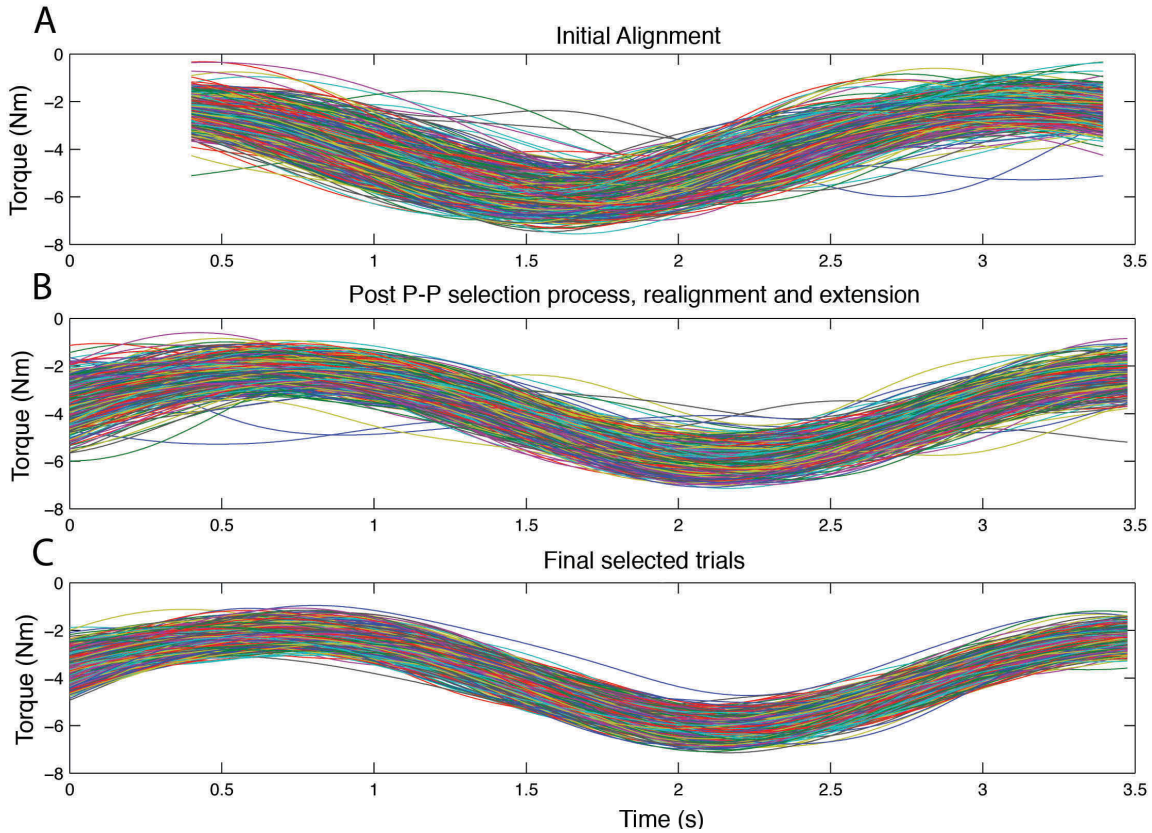

Figure 5-6. Filtered torque traces after (A) initial alignment, (B) P-P selection process, realignment and extension, (C) Final selection

beginning of each repetition. The clock signal ran continuously throughout the entire experiment and therefore could be used to align data in the ten different sets.

The point at which the clock signal crossed zero for the first time in each set was used as the starting point. Beginning at the reference point for each set, the signals were broken into 3-second segments and reorganized into an ensemble. Figure 5-6A shows the result of this initial segmentation.

This first alignment, although consistent with the command trace given to the subjects, does not represent the ideal alignment because it does not account for variability in the subject's response. The subject may have started or ended their contraction at different times in each cycle. Further alignment was necessary for optimal results.

2. *Removal of trials with abnormal peak-to-peak (P-P) amplitude:* Following the initial segmentation, filtered torque traces with abnormally small or large amplitudes were removed from the ensemble. To accomplish this, the first step was to calculate the ensemble mean filtered torque trace and its P-P amplitude. Next, the P-P amplitude of the mean was subtracted from the individual P-P values, and the standard deviation of these differences was calculated. Trials were sorted according to their P-P amplitudes and those with P-P amplitudes that differed from the mean value by more than 2 standard deviations were removed from the ensemble.

3. *Realignment according to cross-covariance values:* The ensemble mean filtered torque trace was recalculated for the remaining realizations. The remaining trials were shifted to a point of maximum correlation with the ensemble mean torque. This was determined by calculating the unbiased cross-covariance between the ensemble mean torque and the individual realizations. Each trial was then shifted to the point determined to produce the maximum correlation. The newly shifted segments were retrieved from the original continuous traces and reorganized into an ensemble. At this point, each realization was extended to include additional points at the beginning and end of the period; thus allowing an entire period of ankle stiffness to be identified. The ensemble following realignment and extension is shown in Figure 5-6B; notice the closer alignment and tighter grouping of the trials.

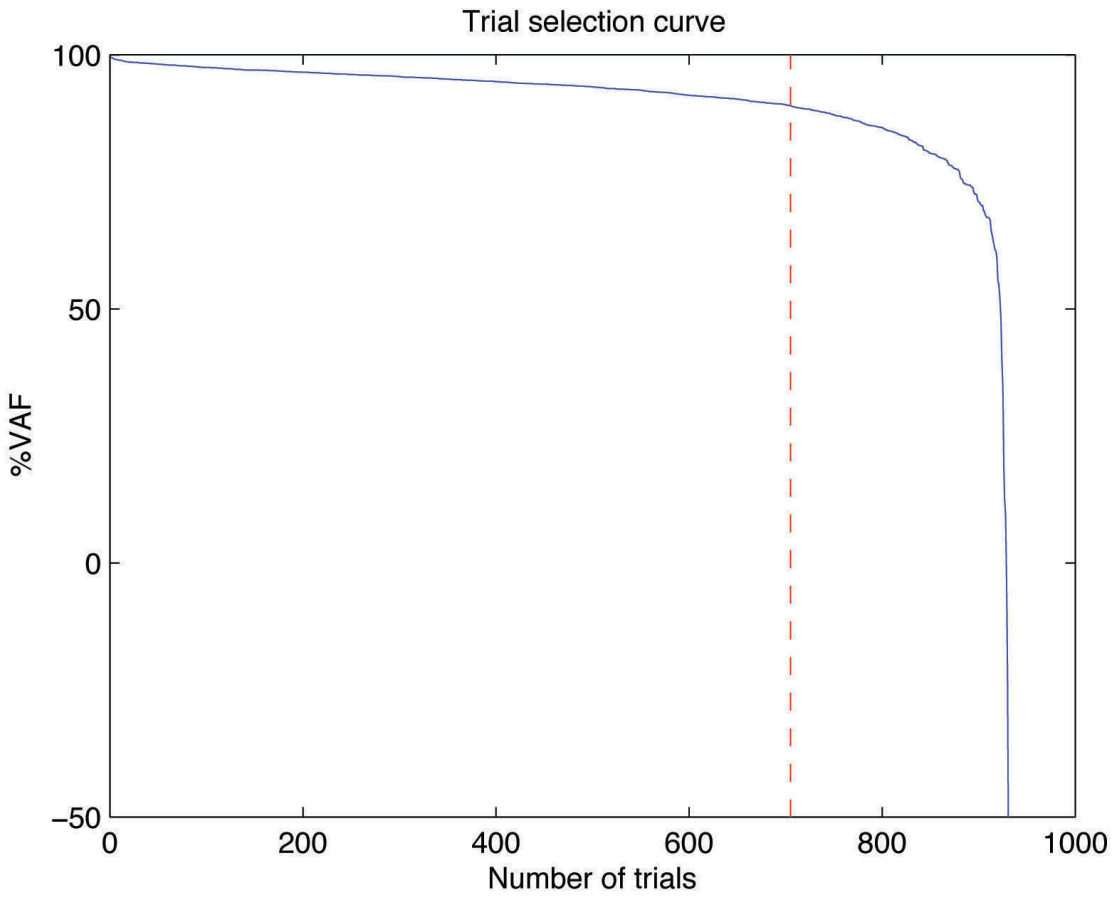

Figure 5-7. Trial Selection curve. The blue curve is the sorted %VAF. The red dashed line marks the 90% cutoff point.

4. *Selection of most similar realizations according to %VAF:* Once the realizations were optimally aligned, the most similar trials were selected. The mean ensemble filtered torque trace was recalculated. The match between it and the individual traces was assessed in terms of percent variance accounted for (%VAF). The %VAF between two signals, X and, $\hat{X}$, is calculated as follows:

$$\%VAF(X,\hat{X}) = 100\left(1 - \frac{\mathrm{var}(X - \hat{X})}{\mathrm{var}(X)}\right)$$

The %VAFs were sorted in descending order and plotted against the realization number (see Figure 5-7). This selection curve was used to determine how many realiza-

tions should be kept. The goal was to keep only the realizations with a %VAF greater than 90%; typically, between 600 and 750 realizations were kept. A minimum of 600 were retained if the 90% mark could not be achieved. The final selected trials completed the data ensemble used for identification. Figure 5-6C shows an example the data ensemble after the final selection process. Notice that the dissimilar traces were removed and there is a tight grouping of trials.

5.2.8. Data Analysis

The TVPC algorithm (see Chapter 3) was used to identify TV joint stiffness. The algorithm generated intrinsic and reflex stiffness estimates at each time. Intrinsic stiffness was converted to compliance for ease of interpretation. The resulting system estimates were used to predict the output torque. The predicted intrinsic torque was calculated by convolving the position with the estimated time-varying intrinsic stiffness dynamics. The predicted reflex torque was the result of applying the estimated TV Hammerstein system to the velocity signal. Predicted total torque was calculated as the sum of the predicted intrinsic and reflex torques. The quality of the predictions was assessed in terms of %VAF. The quality of the total torque prediction is denoted as $\%VAF_{TOT}$. Intrinsic and reflex torque were not directly observed, consequently, a direct measure of the quality of their estimates is impossible. The %VAF between the total observed torque and the intrinsic and reflex torque estimates, denoted $\%VAF_I$ and $\%VAF_R$ respectively, was used to quantify the relative contributions of each pathway to the total output torque.

The physical significance of non-parametric models is difficult to interpret because the parameters have no physical meaning. For this reason, parametric fits of the intrinsic compliance and reflex stiffness were calculated. Parameterization was accomplished using the Levenberg-Marquardt non-linear, least-squares fit algorithm. Intrinsic compliance was parameterized using a 2nd-order, low-pass filter, with the following equation:

$$\frac{1}{Is^2 + Bs + K}$$

where I , B , and K are the inertial, viscous and elastic parameters, respectively. This transfer function has been shown to describe intrinsic stiffness well [3]. K is typically used to describe the overall gain of the intrinsic pathway.

The linear component of reflex stiffness was parameterized using a delayed, 2nd-order, low-pass filter, with the following equation:

$$\frac{G\omega^2}{s^2 + \zeta\omega s + \omega^2}$$

where G, ζ, and ω are the reflex gain, damping and and natural frequency, respectively. The delay was fixed at 40 ms and overall reflex gain was calculated as the product of the gain of the non-linearity and *G.*

5.3. RESULTS

5.3.1. General behavior

Figure 5-8 shows single trial responses for position, torque, and GL, GM, SOL and TA EMGs for one subject. Figures 5-9 to 5-14 show results from this same subject. These results are a good representation of the trend seen in all subjects, except where otherwise noted. Figure 5-8A shows the 0.03 rad PRBS used as the position input. The rising edge of the position perturbation stretched the TS, and a clear reflex response can be seen in the torque and TS EMG. In Figure 5-8B**,** the underlying voluntary torque change is seen by the drop in the mean of the signal at around 2 s. The TA EMG (Figure 5-8C), shown on a different scale than the other EMG responses, shows small peaks. These peaks are likely due to crosstalk with LG and not due to a stretch because they are very small and occur during TS stretching and not TA stretching. The TS EMG reflex response (refer to Figure 5-8(D-F)) shows some time-varying behavior; the amplitude of the response changes over the length of the trial. The response is clearly non-linear, since there is no response to the falling edge of the position perturbation. This non-linear reflex behavior has been previously documented **[25, 53]**.

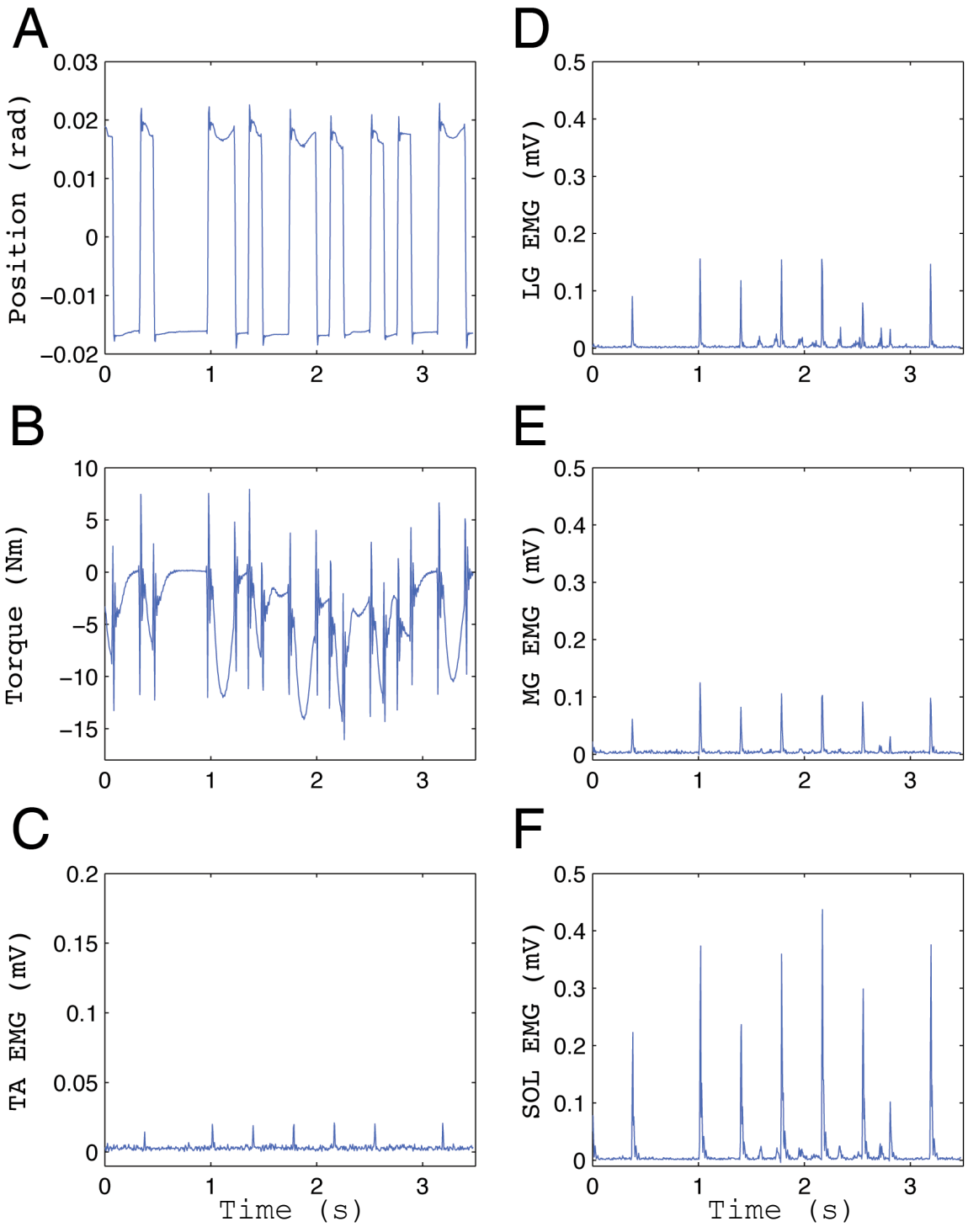

Figure 5-8. Single trials of (A) position, (B) torque, (C) TA EMG, (D) LG EMG, (E) MG EMG, and (F) SOL EMG.

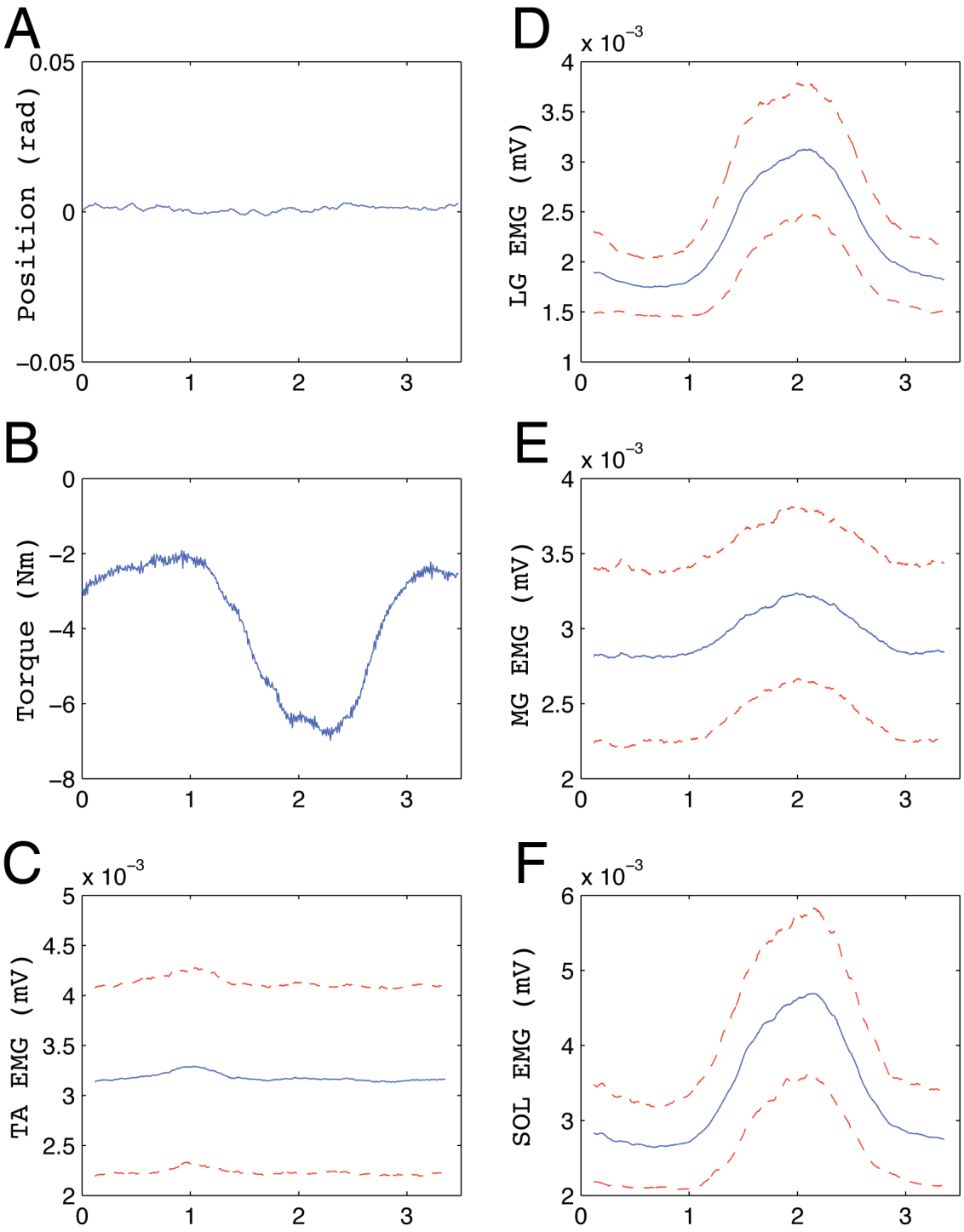

Figure 5-9. Ensemble average of (A) position, (B) torque, (C) TA EMG, (D) LG EMG, (E) MG EMG, and (F) SOL EMG.

Figure 5-9 shows the ensemble mean of position, torque and EMGs for one subject. The position (Figure 5-9A) averages to zero, which is what was desired. The mean torque (Figure 5-9B) and TS EMG (Figure 5-9(D-F)) show the desired TV behavior, gradual contraction-relaxation of the TS. The TA EMG is flat, indicating that the TA was not used, as the subject was trained to avoid. All subjects showed similar behavior, except subject 4 who was unable to use only his TS muscles to perform the task. His identification results, which are discussed later, show similar trends to subjects 1-3 and were included for support.

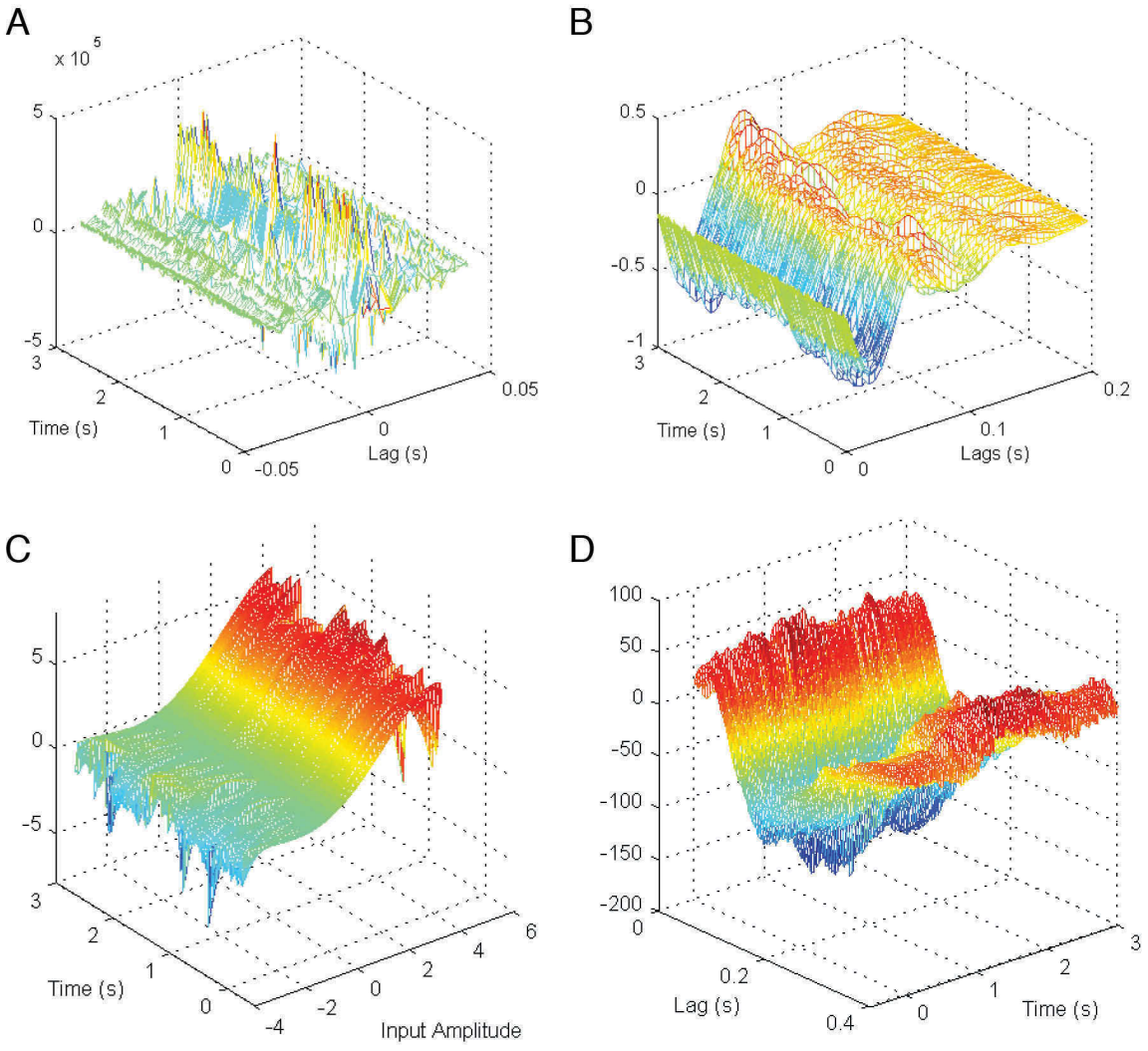

Figure 5-10. Results of TVPC algorithm. (A) Intrinsic stiffness, (B) Intrinsic compliance, (C) Reflex nonlinearity, and (D) Reflex linear subsystem.

5.3.2. Identification results

5.3.2.1. System estimates

Figure 5-10 shows the estimated intrinsic stiffness, intrinsic compliance, and reflex stiffness at each time. The intrinsic stiffness estimates (Figure 5-10A) were quite noisy, which made it difficult to see time-varying behavior. However, when converted to compliance (Figure 10B) time-varying behavior was apparent; the amplitude of the large negative peak and the second positive peak of the compliance IRFs change over time. The nonlinearity ensemble (Figure 5-10C) did not show any clear time-varying behavior. The negative peaks of the reflex IRF ensemble (Figure 5-10D) show some time-varying changes. Clearly, there was time-varying behavior, as the IRFs were not identical through time.

5.3.2.2. Goodness of Fit

Figure 5-11 shows a sample of five observed position-torque pairs**.** The predicted torque (red) is superimposed on the observed torque (blue). The observed torque was not perfectly predicted, but an examination of the frequency content of the residuals indicated that the majority of the power was below 5 Hz. The reflex component has been shown to dominate at 5-10 Hz, while the intrinsic component dominates at higher frequencies **[4]**. The frequency of the residuals fell below the range of reflex and intrinsic components, indicating the discrepancy was likely due to inconsistencies in the low frequency voluntary torque. The ensemble mean torque was subtracted from each realization prior to identification. However, since the voluntary torque was not modulated exactly the same way each trial, the voluntary torque that differed from the ensemble mean remained in the data.

Despite this, the identification yielded good predictions. Figure 5-12 shows $\%VAF_{TOT}$, $\%VAF_{I}$, and $\%VAF_{R}$ for one subject calculated across the ensemble throughout a period of the task; the ensemble mean torque is also shown for comparison. Notice that the contribution of each pathway changes throughout the task. Figure 5-12B shows that the contribution of the intrinsic pathway drops near the beginning and end of the contraction. The drop in the intrinsic contribution is also reflected in $\%VAF_{TOT}$ (see Figure 5-12A).

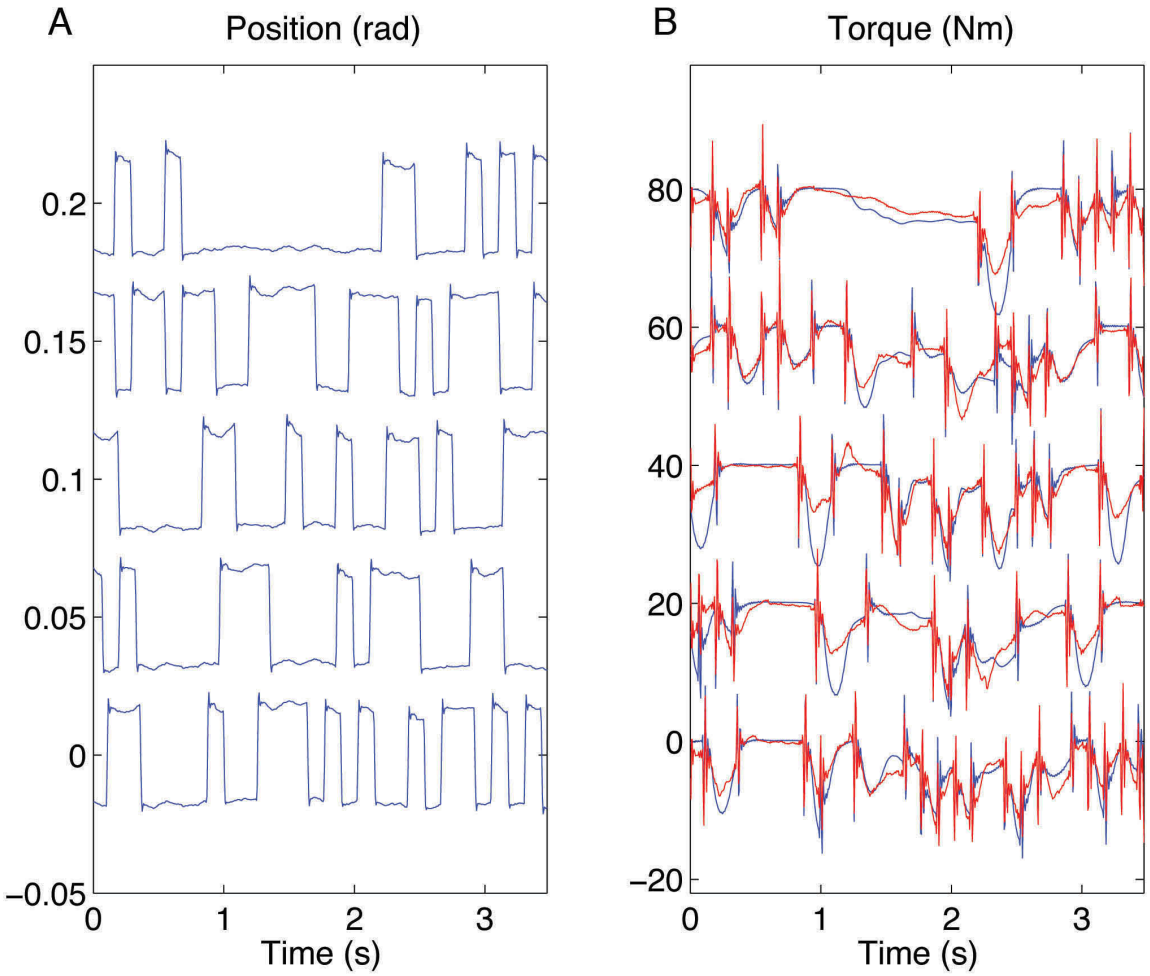

Figure 5-11. (A) Five observed position trials. (B) Corresponding observed torque (blue) and predicted torque (red). The offsets were added for clarity and do not reflect the mean of the signals.

	$\%VAF_{TOT}$	$\%VAF_{I}$	$\%VAF_{R}$
Subject 1	77.8	38.3	39.2
Subject 2	83.0	59.3	23.5
Subject 3	77.7	35.9	44.9
Subject 4	78.1	45.2	32.2
Subject 5	72.3	21.4	45.6

Table 5-1. Average $\%VAF_{TOT}$, $\%VAF_{I}$, and $\%VAF_{R}$ for one cycle, for all subjects.

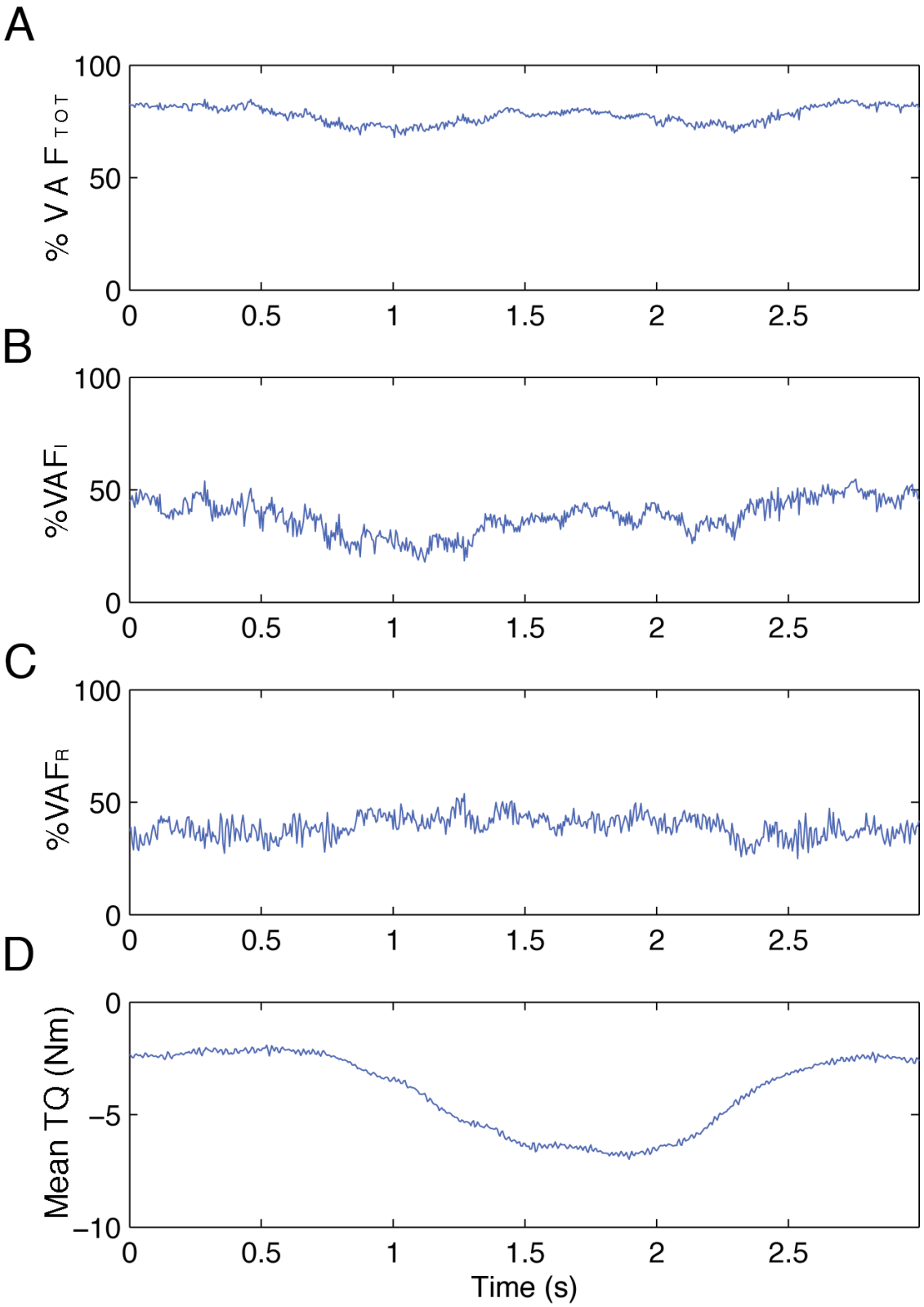

Figure 5-12. %VAF between the observed total torque and (A) predicted total torque, (B) predicted intrinsic torque, and (C) predicted reflex torque. (D) Mean torque.

Figure 5-12C shows that, for this subject, the reflex contribution stayed relatively constant; some subjects showed some slight change. We'd expect to see change in $\%VAF_R$ and $\%VAF_I$ as the gain of each pathway changed. If the intrinsic stiffness was constant, an increase in reflex gain would increase the torque contributed by the reflex pathway to the output, thereby increasing the $\%VAF_R$. However, if the intrinsic gain increased in the same way as the reflex gain, there will be no change in the relative contribution of the reflex pathway to the output.

The average $\%VAF_{TOT}$ for one cycle was between 72.3% and 83.0% for all subjects. Table 5-1 lists the average $\%VAF_{TOT}$, $\%VAF_I$, and $\%VAF_R$ over one cycle, for all subjects. Note that the reflex pathway contributed more than the intrinsic pathway for three of the five subjects.

5.3.2.3. Parametric fits

The intrinsic compliance IRFs, the reflex stiffness IRFs, and the reflex non-linearities were fit parametrically, as described in Section 5.2.8. Figure 5-13 shows an example of parametric fits superimposed on their associated intrinsic IRF, reflex non-linearity, and reflex IRF for one time point; clearly, they are closely matched. The parametric fits were generally quite good. All the parameters of the fits for both intrinsic compliance and reflex stiffness for one subject are shown in Figure 5-14. The red dashed lines indicate the beginning and end of the contraction, and the green dashed line indicates the middle. The intrinsic parameters were much noisier than the reflex parameters and the %VAF of the fits were not as consistently high. Despite the noise, it is apparent that B, and I change very little, while K follows the same pattern as the mean torque. It increased with the contraction and decreased with relaxation. The reflex gain, G, shows a completely different pattern. The reflex gain had two peaks; the first began just prior to the start of the contraction and the second just prior to the relaxation. Neither ω or ζ showed any significant changes.

The time-course of the intrinsic and reflex gain changes, for all subjects, is shown in Figure 5-15. Subject 1-4 show similar trends in both intrinsic and reflex gain. Their results showed that the intrinsic gain followed the same pattern as the voluntary torque, in

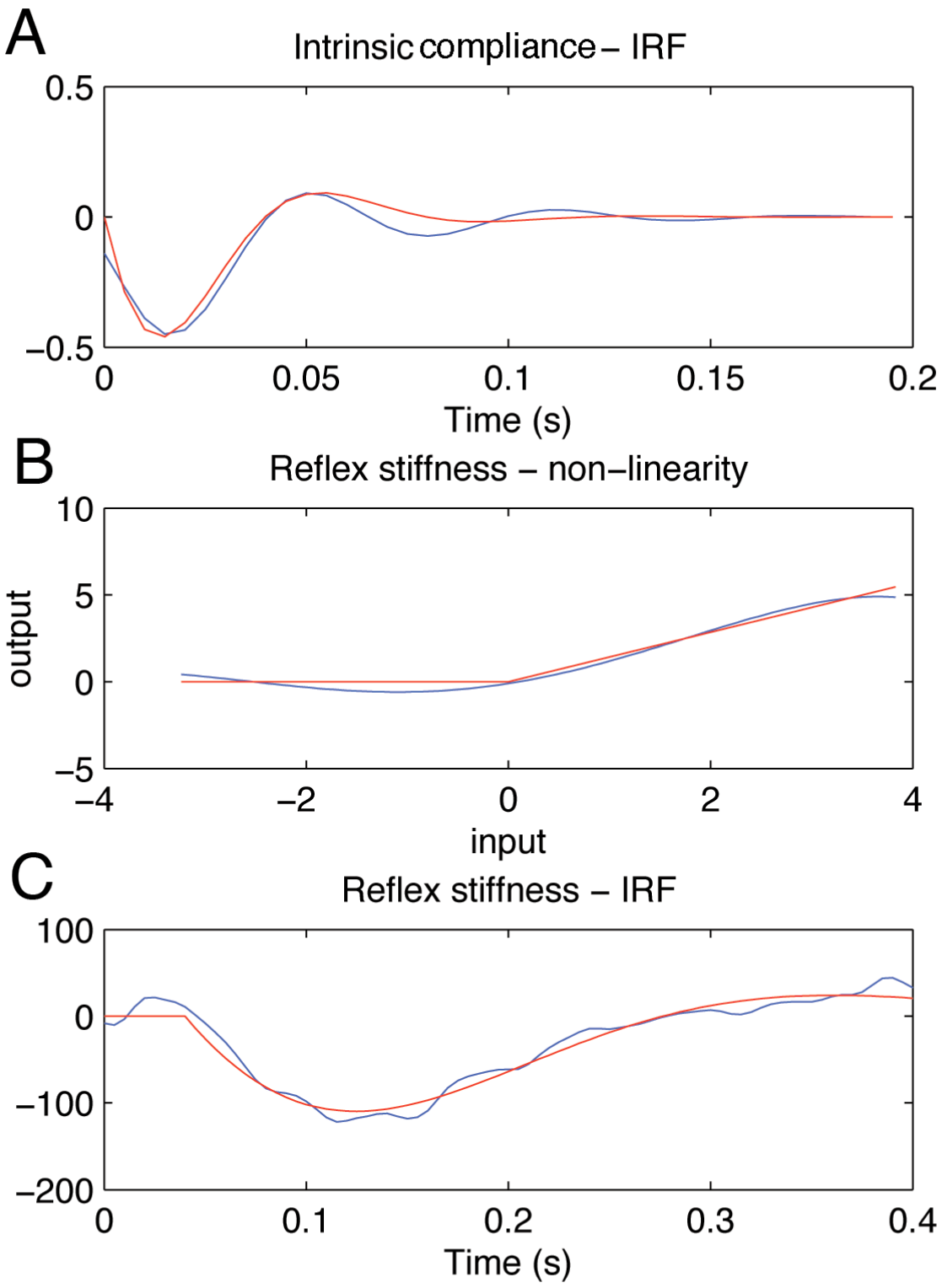

Figure 5-13. Example of identified systems (blue) and their parametric fits (red) for one time point. (A) Intrinsic compliance (B) Reflex non-linearity (C) Reflex IRF. The fits approximate the identified system dynamics well.

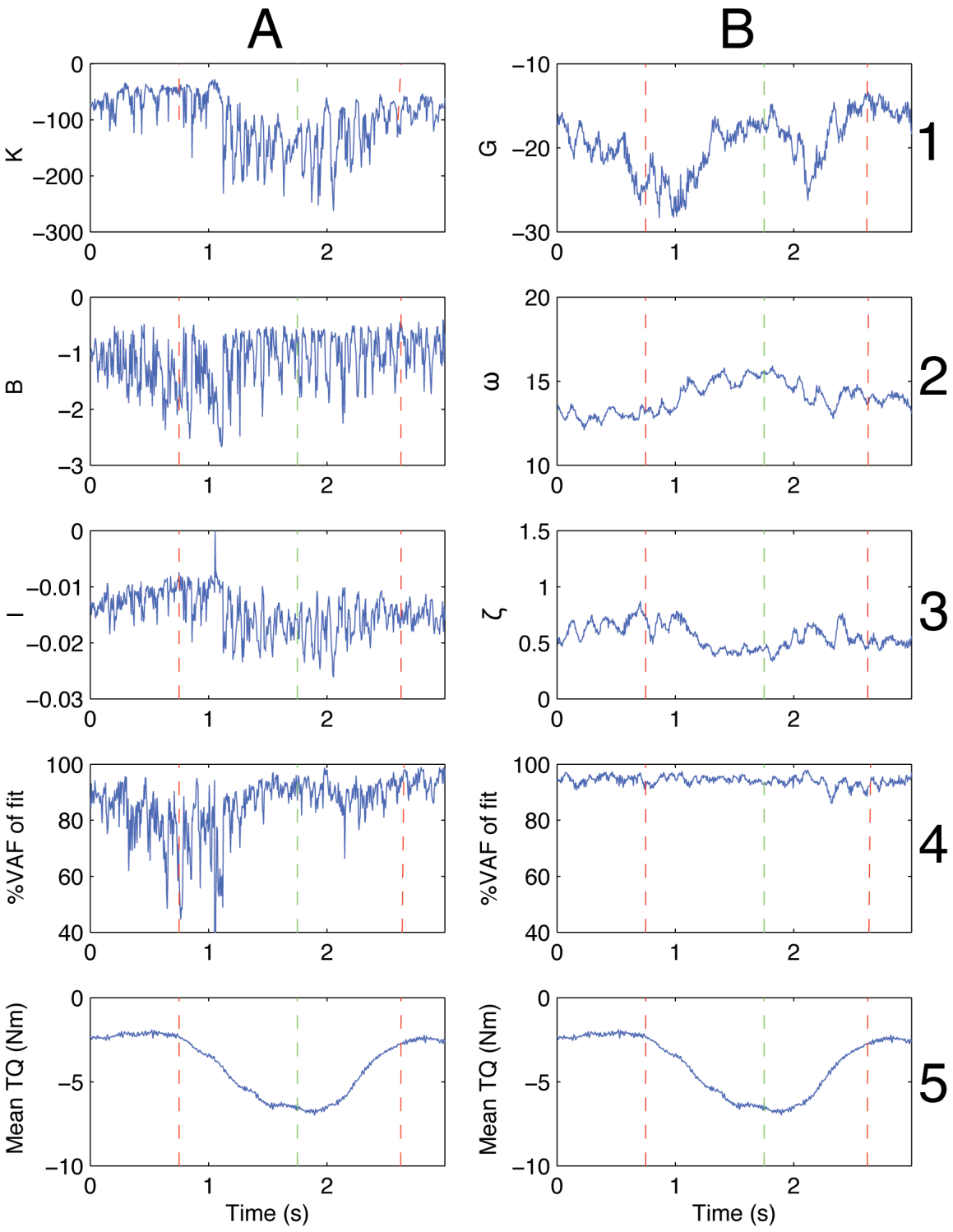

Figure 5-14. Parametric fit parameters for both intrinsic compliance (column A) and reflex stiffness (column B) for one subject. The red dashed lines mark the approximate beginning and end of the contraction. The green dashed line marks the mid point of the contraction. (A1) Elasticity, K. (A2) Viscosity, B. (A3) Inertia, I. (A4) %VAF of intrinsic IRF fit. (A5 and B5) Mean ensemble torque. (B1) Gain, G. (B2) Natural frequency, ω. (B3) Damping, ζ. (B4) %VAF of reflex IRF fit.

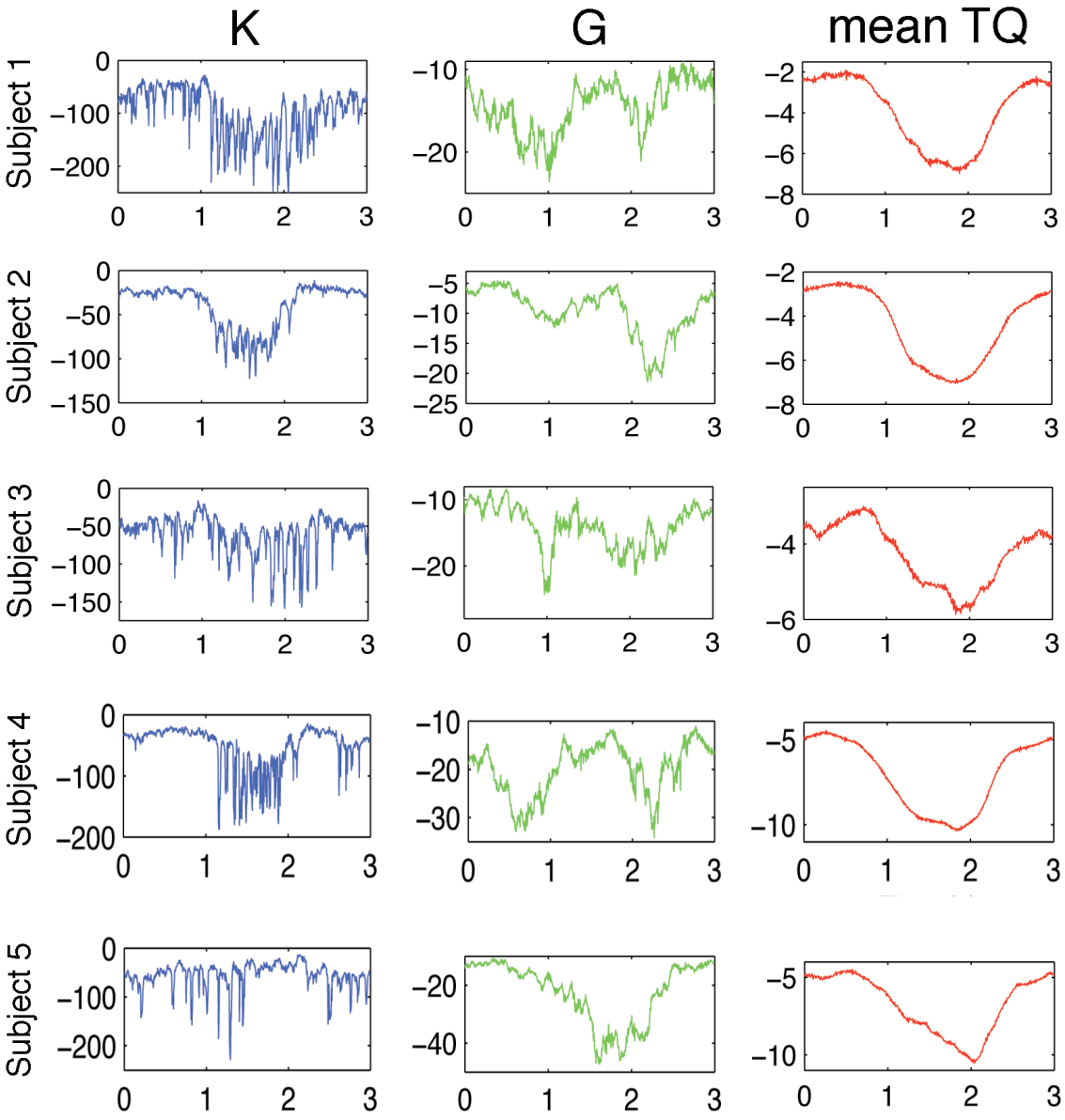

Figure 5-15. Time-course of intrinsic gain, *K*, in blue, and reflex gain, *G*, in green, for all subjects. The mean torque (red) is included for comparison. Notice that, for subjects 1-4, the intrinsic gain follows the change in the mean torque, while the reflex gain has one peak near the beginning of the contraction, and another near the beginning of the relaxation. Subject 5 shows different behavior; the intrinsic gain shows little change, while the reflex gain follows same pattern as the mean torque.

agreement with previous time-invariant studies that have shown that it increases with increasing voluntary contraction [3, 5]. The reflex gains, for subjects 1-4, all had two peaks; one near the beginning of the contraction and one near the beginning of the relaxation. There was variability in the amplitude and width of the peaks between subjects but they occurred at similar points in the task.

Subject 5 showed entirely different behavior; the intrinsic gain was small and remained relatively constant throughout the contraction and the reflex gain had only one peak, which coincided with the peak contraction level. The background EMG showed no abnormalities; it followed the same pattern as the mean ensemble torque, as with all subjects.

5.4. Discussion

We used a time-varying, parallel-cascade system identification method to examine temporal changes in ankle joint stiffness during a torque matching task. A small position perturbation was applied around the neutral ankle position while the subject generated torque to track a command on the feedback display. The TVPC algorithm produced good results, with $\%VAFs_{TOT}$ between 72.3% and 83.0%; this shows that the method works with real data. Furthermore, this study shows that the TV behavior could not be predicted from time-invariant behavior. For 4 out of 5 subjects, there were two peaks in reflex gain; the first peak occurred near the lowest torque level, while the second occurred near the maximum torque level. Time-invariant studies would have predicted that the pattern of reflex gain modulation would have followed the mean torque. This is clearly not the case.

The intrinsic stiffness estimates were noisy, likely because of the low stiffness requirements of the task. The intrinsic stiffness gain was generally below 100 Nm/rad during this task, for all subject, while other studies have found stiffness gains as high as 500 Nm/rad [5]. Stationary studies would predict that the neutral position of the ankle and small torques levels used here would result in a small intrinsic gain [5]. When one of the parallel pathways has a small gain, it is more difficult to accurately identify it, as revealed in the simulation study (Chapter 4). In spite of the noisy estimates, the results showed that

the intrinsic stiffness gain behaved as expected. It increased with increasing torque and decreased with decreasing torque. This behavior was predicted by stationary studies [5].

Subject 5 exhibited different intrinsic and reflex gain modulation behavior. No reason was found for this discrepancy. Subject 5 performed the task in the same manner as all other subjects and did not used his TA during the experiment. The background EMG followed the pattern of the mean torque, in the same way as the other subjects. It appears that his reflex modulation strategy was simply different.

5.4.1. Methodological considerations

5.4.1.1. Inter-trial variability

Time-varying ensemble methods are based on the assumption that, for a given point in time, the underlying system is the same across the entire ensemble. This is possible to achieve with simulated systems but not with human subjects, where there will always be inter-trial variability. To minimize this, a trial selection process is necessary, which keeps only the most similar realizations. This should not bias the results, as it simply ensures that the identification algorithm requirements are met. In fact, including trials that exhibited different behavior could have resulted in erroneous system estimates.

5.4.1.2. Goodness of fit

The TVPC algorithm only models intrinsic and reflex stiffness, and therefore, does not account for voluntary torque. So the mean torque, representing the voluntary component, is removed prior to the identification. However, any voluntary torque that does not exactly match the mean will remain in the torque ensemble. As discussed above, this residual voluntary torque will act as another noise source, in addition to the general output noise. Recall, that the selection process used here is based on low-pass filtered torque, representative of the voluntary torque. Using this process, the mean filtered torque accounted for 90% or more of the variance of the realizations selected. However, this does not take into account any higher frequency variability.

A side experiment was performed on Subject 1 to determine the best possible tracking that he could do with perturbations. The subject was asked to track the command signal

of the feedback display, while the ankle was perturbed with a predictable square-wave. The subject knew when the perturbations would occur and therefore had the best chance of performing the task repeatably. After some allotted practice time, the tracking was recorded. The data was segmented and aligned to form an ensemble. The mean ensemble torque trace was calculated and compared to each individual realization. The mean ensemble torque accounted for an average of 83% of the variance of each realization. This means that the predicted total torque could not be expected to account for more than 83% of the variance of the observed torque. This places an upper limit on how much variance the TVPC algorithm could predict. The predicted torque, from the main experiment, for Subject 1 accounted for 77.8% of the total torque. This value is only slightly lower than the subject was able to obtain with predictable perturbation. Therefore, the results are very good; the total %VAF attained during the main experiment approaches that of the controlled, best-case tracking experiment. The variability in the subject's tracking was the principle source of noise, and accounted for most of the unpredicted torque.

5.4.2. Comparison with Other Results

The reflex stiffness modulation pattern found in this study does not agree with that of the reflex EMG dynamics in similar studies. Kimura et al. [56] studied the reflex EMG response during a gradual increment/decrement of isometric force. They found that the reflex gain was largest during contraction and smallest during relaxation. The pattern of reflex EMG gain did not correlate with the reflex stiffness changes in this study. However, their study confirmed that the background torque level does not predict the reflex gain. For matched background torque levels, the reflex gain was different depending on when that torque occurred during the task.

In contrast, Kirsch et al. [58] found that the reflex EMG gain during a rapid isometric contraction closely followed the background EMG. However, in their experiment, the EMG did not closely follow the torque level, in comparison to this experiment. They saw a similar burst in reflex gain just prior to the contraction, but saw a dip in gain prior to relaxation, instead of another increase. They also used a much stronger contraction (up to 25% MVC), which may explain the difference in the EMG activation pattern. In their ex-

periment, the subject was required to produce a much stronger, faster contraction in the same amount of time as our much weaker contraction. The experimental paradigm was not similar enough for a direct comparison of results.

6. CONCLUSION

The time-varying, parallel-cascade (TVPC) algorithm is a tool to study ankle stiffness during tasks in which the torque and/or position are changing. A simulation study was conducted to assess the algorithm's performance limits. Specifically, the study examined the algorithm's ability to track system dynamics that change quickly in time, and isolated the factors influencing its performance in the presence of noise. The algorithm was applied experimentally to confirm that it could produce good results with real data. The following section summarizes the key results.

6.1. SUMMARY

6.1.1. Simulation Study

The simulation study showed that the TVPC algorithm can identify rapid, time-varying changes in system dynamics; therefore, there is no theoretical limit on the speed of the movement to be identified. The study isolated three factors that impacted the algorithm's performance: the relative contribution of intrinsic and reflex stiffness, the signal-to-noise ratio (SNR), and the number of realizations in the data ensembles. Given a fixed SNR, the quality of the reflex identification degraded as its gain decreased; this is because it faced a lower effective SNR as its gain decreased. Ideally, each pathway would contribute equally to the output torque. The gain of the system and the SNR are not fully under experimental control, while the number of realizations in the data ensembles is under the investigator's control. The simulation study showed that the quality of the identification increased as the number of realizations in the data ensembles increased. Assuming conditions where the SNR and reflex gain are similar to the time-invariant studies, approximately 500-800 realizations of the time-varying behavior would be necessary to produce good results. The following section outlines how the results of the simulation helped guide the design of the experimental procedure.

6.1.2. Experimental Design

The TVPC algorithm was used to study dynamic ankle stiffness during an isometric contraction-relaxation task. The design of the experiment was critical to the successful implementation of the TVPC algorithm. The simulation study showed that, when possi-

ble, the experiment should be designed such that the intrinsic and reflex pathways contribute equally to the output, and the SNR is high. Unfortunately, these two conditions cannot both be optimized. A study of stationary ankle stiffness [5] showed that the gain of each pathway increases as the ankle is dorsiflexed, increasing the overall SNR. However, the relative contribution of the reflex pathway decreases as the ankle is dorsiflexed because its gain doesn't increase as quickly as the intrinsic gain. The largest relative reflex contribution actually occurs near the neutral ankle position with low contraction levels. Therefore, when designing the experiment, a choice had to be made between maximizing the reflex contribution or the overall SNR. We decided to maximize the reflex contribution by using a neutral ankle position and a low level of voluntary torque. Using a low torque also had the added benefit of avoiding muscle fatigue, which was a concern because of the large number of realizations the time-varying (TV) identification required. The simulation study showed that between 500 and 800 realizations should be used in the data ensemble to get good results; with more realizations providing better results. Therefore, the experiment was designed such that 1000 realizations were collected and only the most similar were used in the identification; typically, between 600 and 800 realizations were kept. The investigation of the performance limitations of the TVPC algorithm helped guide the design choices that led to good experimental results. These results are discussed in the following section.

6.1.3. Experimental results

The TVPC algorithm was successfully used to identify the progression of intrinsic and reflex stiffness during a torque matching task. The subjects were asked to slowly contract their triceps surae from 1% to 5% of their maximum voluntary contraction and then slowly relax. The TVPC algorithm yielded good results, accounting for up to 83% of the total torque output variance; confirming that the algorithm works with real data. Furthermore, the study showed that time-invariant stiffness behavior cannot be used to predict the modulation pattern of TV stiffness. The results showed peaks in reflex gain near the lowest and highest torque levels; time-invariant data would predict that they would occur at the same level of background torque.

Reflex stiffness contributed more to the output torque than intrinsic stiffness, in 3 of 5 subjects. This led to good reflex estimates but the intrinsic stiffness estimates were noisy. The experiment was designed to maximize reflex stiffness, by using a neutral position and small torques. This, consequently, minimized the intrinsic stiffness. The simulation study predicted that a small relative gain for one pathway would result in poorer estimates of it, because of the lower effective SNR. This is what was seen with the intrinsic stiffness identification. In spite of this, the TVPC algorithm produced good overall results with real data and will be a useful tool for studying the modulation pattern of joint stiffness during various tasks.

6.2. FUTURE WORK

The simulation study addressed the problem of additive noise at the output but not the problem of inconsistent TV behavior. Inter-trial variability is a common difficulty encountered in TV experiments [78]. The TVPC algorithm assumes that at a fixed point in time the system is in the same state across the entire ensemble, but this will never be the case with human subjects. Despite this, it is assumed that the system parameters will vary around a mean and be correctly estimated with averaging. This has not been confirmed via simulation and is an area that requires further investigation.

There are still many ways in which the TVPC algorithm can be used to explore ankle stiffness. This thesis addresses only the TV behavior during a relatively small, slow contraction with a fixed position. It would be informative to vary the speed or strength of the contraction to investigate their effect on the reflex stiffness gain pattern.

The TVPC algorithm could also be applied to a task where the hydraulic actuator rotates the ankle while the subject maintains a constant torque. There are added challenges to this type of experiment. It is difficult to provide the subject with feedback of their voluntary torque, because as the ankle position changes the intrinsic torque is also changing. Therefore, the torque the subjects sees is a combination of the slow changes in the intrinsic and voluntary torque. Without proper feedback, it is difficult to ensure repeatable performance of the task.

It is important to be able to study more realistic tasks; the TVPC algorithm is currently limited to task in which the subject pushes against a stiff load. This means that the torques produced by the subject do not affect the position of the ankle. However, most tasks involve moving against a compliant load, where the torques produced as a result of perturbations change the position. This situation requires closed-loop identification techniques, because the position affects the torque and the torque affects the position. The TVPC algorithm is currently not designed to handle this identification problem. Future work could involve expanding the TVPC algorithm to handle situations that require closed loop identification. This would make it possible to study ankle stiffness during any repeatable task. The ultimate goal is to study ankle stiffness during every day tasks, such as walking, to gain a better understanding of the reflex modulation patterns in normal function.

REFERENCES

1. Kearney, R.E. and I.W. Hunter, *System-identification of human joint dynamics.* Critical Reviews In Biomedical Engineering, 1990. **18**(1): p. 55-87.

2. Kearney, R.E. and I.W. Hunter, *Dynamics of human ankle stiffness - Variation with displacement amplitude.* Journal Of Biomechanics, 1982. **{15}**({10}): p. {753-756}.

3. Hunter, I.W. and R.E. Kearney, *Dynamics of human ankle stiffness: variation with mean ankle torque.* Journal Of Biomechanics, 1982. **15**(10): p. 747-52.

4. Kearney, R.E., R.B. Stein, and L. Parameswaran, *Identification of intrinsic and reflex contributions to human ankle stiffness dynamics.* Ieee Transactions On Biomedical Engineering, 1997. **44**(6): p. 493-504.

5. Mirbagheri, M.M., H. Barbeau, and R.E. Kearney, *Intrinsic and reflex contributions to human ankle stiffness: variation with activation level and position.* Experimental Brain Research, 2000. **135**(4): p. 423-436.

6. Mirbagheri, M.M., et al., *Intrinsic and reflex stiffness in normal and spastic, spinal cord injured subjects.* Experimental Brain Research, 2001. **141**(4): p. 446-459.

7. Galiana, L., J. Fung, and R. Kearney, *Identification of intrinsic and reflex ankle stiffness components in stroke patients.* Experimental Brain Research, 2005. **165**(4): p. 422-434.

8. Ludvig, D., I. Cathers, and R.E. Kearney, *Voluntary modulation of human stretch reflexes.* Experimental Brain Research, 2007. **183**(2): p. 201-213.

9. Capaday, C. and R.B. Stein, *Amplitude-modulation of the soleus H-reflex in the human during walking and standing.* The Journal of neuroscience : the official journal of the Society for Neuroscience, 1986. **6**(5): p. 1308-1313.

10. Capaday, C. and R.B. Stein, *Difference in the amplitude of the human soleus H-reflex during walking and running.* Journal Of Physiology-London, 1987. **392**: p. 513-522.

11. Lortie, M. and R.E. Kearney, *Identification of physiological systems: estimation of linear time-varying dynamics with non-white inputs and noisy outputs.* Medical & Biological Engineering & Computing, 2001. **39**(3): p. 381-390.

12. Lortie, M. and R.E. Kearney, *Identification of time-varying Hammerstein systems from ensemble data.* Annals Of Biomedical Engineering, 2001. **29**(7): p. 619-635.

13. Baker, M., et al., *Time-varying parallel-cascade system identification of ankle stiffness from ensemble data*, in *26th Annual International Conference of the IEEE EMBS*. 2004: San Francisco, CA, USA. p. 4688-4691.

14. Tortora, G.J. and B. Derrickson, *Principles of Anatomy and Physiology*. 11 ed. 2006, Danvers, MA: John Wiley & Sons, Inc. 1146.

15. Liu, M.Q., et al., *Muscles that support the body also modulate forward progression during walking.* Journal Of Biomechanics, 2006. **39**(14): p. 2623-2630.

16. Rao, S., C. Saltzman, and H.J. Yack, *Ankle ROM and stiffness measured at rest and during gait in individuals with and without diabetic sensory neuropathy.* Gait & Posture, 2006. **24**(3): p. 295-301.

17. Butler, A.A., et al., *Muscle weakness impairs the proprioceptive control of human standing.* Brain Research, 2008. **1242**: p. 244-251.

18. Hodson-Tole, E.F. and J.M. Wakeling, *Motor unit recruitment for dynamic tasks: current understanding and future directions.* Journal Of Comparative Physiology B-Biochemical Systemic And Environmental Physiology, 2009. **179**(1): p. 57-66.

19. Merletti, R. and P. Parker, eds. *Electromyography - Physiology, Engineering, and Noninvasive Applications*. 2004, John Wiley & Sons: Hoboken, New Jersey.

20. Genadry, W.F., R.E. Kearney, and I.W. Hunter, *Dynamic relationship between EMG and torque at the human ankle - Variation with contraction level and modulation.* Medical & Biological Engineering & Computing, 1988. **26**(5): p. 489-496.

21. Kearney, R.E., M. Lortie, and R.B. Stein, *Modulation of stretch reflexes during imposed walking movements of the human ankle.* Journal Of Neurophysiology, 1999. **81**(6): p. 2893-2902.

22. Kandel, E.R., J.H. Schwartz, and T.M. Jessell, eds. *Principles of Neural Science*. 4th ed. 2000, McGraw-Hill: New York. 1414.

23. Stein, R.B., *Nerve and Muscle: Membranes, Cells, and Systems*. 1980, New York: Plenum Press.

24. Lacquaniti, F., N.A. Borghese, and M. Carrozzo, *Transient reversal of the stretch reflex in human arm muscles.* Journal Of Neurophysiology, 1991. **66**(3): p. 939-954.

25. Kearney, R.E. and I.W. Hunter, *System-identification of human triceps surae stretch reflex dynamics.* Experimental Brain Research, 1983. **51**(1): p. 117-127.

26. Stein, R.B. and R.E. Kearney, *Nonlinear behavior of muscle reflexes at the human ankle joint.* Journal Of Neurophysiology, 1995. **73**(1): p. 65-72.

27. Feldman, A.G., *Origin and Advances of the Equilibrium-Point Hypothesis.* Progress In Motor Control: A Multidisciplinary Perspective, 2009. **629**: p. 637-643.

28. Hinder, M.R. and T.E. Milner, *The case for an internal dynamics model versus equilibrium point control in human movement.* Journal Of Physiology-London, 2003. **549**(3): p. 953-963.

29. Kistemaker, D.A., A.J. Van Soest, and M.F. Bobbert, *Equilibrium point control cannot be refuted by experimental reconstruction of equilibrium point trajectories.* Journal Of Neurophysiology, 2007. **98**(3): p. 1075-1082.

30. Ostry, D.J. and A.G. Feldman, *A critical evaluation of the force control hypothesis in motor control.* Experimental Brain Research, 2003. **153**(3): p. 275-288.

31. Wainscott, S.K., O. Donchin, and R. Shadmehr, *Internal models and contextual cues: Encoding serial order and direction of movement.* Journal Of Neurophysiology, 2005. **93**(2): p. 786-800.

32. Georgopoulos, A.P., et al., *Spatial coding of movement: a hypothesis concerning the coding of movement direction by motor cortical populations.* Exp. Brain Res. Suppl., 1983. **7**: p. 327 - 336.

33. Ashe, J. and A.P. Georgopoulos, *Movement parameters and neural activity in motor cortex and area 5.* Cereb Cortex, 1994. **4**(6): p. 590-600.

34. Georgopoulos, A.P., et al., *On the relations between the direction of two-dimensional arm movements and cell discharge in primate motor cortex.* J Neurosci, 1982. **2**(11): p. 1527-37.

35. Georgopoulos, A.P. and C.N. Stefanis, *Local shaping of function in the motor cortex: Motor contrast, directional tuning*, in *Brain Res Rev*. 2007. p. 383-389.

36. Hollerbach, J.M., *Computers, brains and the control of movement.* Trends In Neurosciences, 1982. **5**(6): p. 189-192.

37. Evarts, E., *Relation of Pyramidal Tract Activity to Force Exerted During Voluntary Movement.* J Neurophysiol, 1968. **31**: p. 14-27.

38. Sergio, L.E., C. Hamel-Pâquet, and J.F. Kalaska, *Motor cortex neural correlates of output kinematics and kinetics during isometric-force and arm-reaching tasks.* J Neurophysiol, 2005. **94**(4): p. 2353-78.

39. Zehr, E.P. and R.B. Stein, *What functions do reflexes serve during human locomotion?* Progress In Neurobiology, 1999. **58**(2): p. 185-205.

40. Gribble, P.L., et al., *Are complex control signals required for human arm movement?* Journal Of Neurophysiology, 1998. **79**(3): p. 1409-1424.

41. Latash, M.L., *Evolution of motor control: From reflexes and motor programs to the equilibrium-point hypothesis.* Journal Of Human Kinetics, 2008. **19**: p. 3-23.

42. Feldman, A.G. and M.F. Levin, *The Equilibrium-Point Hypothesis - Past, Present and Future.* Progress In Motor Control: A Multidisciplinary Perspective, 2009. **629**: p. 699-726.

43. Gomi, H. and M. Kawato, *Equilibrium-point control hypothesis examined by measured arm stiffness during multijoint movement.* Science (New York, NY), 1996. **272**(5258): p. 117-120.

44. Gomi, H. and M. Kawato, *Human arm stiffness and equilibrium-point trajectory during multi-joint movement.* Biological Cybernetics, 1997. **76**(3): p. 163-171.

45. Weiss, P.L., R.E. Kearney, and I.W. Hunter, *Position dependence of ankle joint dynamics .2. Active mechanics.* Journal Of Biomechanics, 1986. **19**(9): p. 737-751.

46. Weiss, P.L., R.E. Kearney, and I.W. Hunter, *Position dependence of ankle joint dynamics .1. Passive mechanics.* Journal Of Biomechanics, 1986. **19**(9): p. 727-735.

47. Sinkjaer, T., et al., *Muscle-stiffness in human ankle dorsiflexors - Intrinsic and reflex components.* Journal Of Neurophysiology, 1988. **60**(3): p. 1110-1121.

48. Toft, E., et al., *Mechanical and electromyographic responses to stretch of the human ankle extensors.* Journal Of Neurophysiology, 1991. **65**(6): p. 1402-1410.

49. Carter, R.R., P.E. Crago, and M.W. Keith, *Stiffness regulation by reflex action in the normal human hand.* Journal Of Neurophysiology, 1990. **64**(1): p. 105-118.

50. Lehmann, J.F., et al., *Spasticity: quantitative measurements as a basis for assessing effectiveness of therapeutic intervention.* Archives of physical medicine and rehabilitation, 1989. **70**(1): p. 6-15.

51. Hoffer, J.A. and S. Andreassen, *Regulation of soleus muscle-stiffness in premammillary cats - Intrinsic and reflex components.* Journal Of Neurophysiology, 1981. **45**(2): p. 267-285.

52. Nichols, T.R. and J.C. Houk, *Improvement in linearity and regulation of stiffness that results from actions of stretch reflex.* Journal Of Neurophysiology, 1976. **39**(1): p. 119-142.

53. Kearney, R.E. and I.W. Hunter, *Nonlinear identification of stretch reflex dynamics.* Annals Of Biomedical Engineering, 1988. **16**(1): p. 79-94.

54. Meinders, M., et al., *The stretch reflex response in the normal and spastic ankle: Effect of ankle position.* Archives of physical medicine and rehabilitation, 1996. **77**(5): p. 487-492.

55. Grey, M.J., et al., *Soleus stretch reflex during cycling.* Motor Control, 2001. **5**(1): p. 36-49.

56. Kimura, T., et al., *Gradual increment/decrement of isometric force modulates soleus stretch reflex response in humans.* Neuroscience Letters, 2003. **347**(1): p. 25-28.

57. Stein, R.B. and C. Capaday, *The modulation of human reflexes during functional motor-tasks.* Trends In Neurosciences, 1988. **11**(7): p. 328-332.

58. Kirsch, R.F., R.E. Kearney, and J.B. Macneil, *Identification of time-varying dynamics of the human triceps surae stretch reflex .1. Rapid isometric contraction.* Experimental Brain Research, 1993. **97**(1): p. 115-127.

59. Kirsch, R.F. and R.E. Kearney, *Identification of time-varying dynamics of the human triceps surae stretch reflex .2. Rapid imposed movement.* Experimental Brain Research, 1993. **97**(1): p. 128-138.

60. Sinkjaer, T., J.B. Andersen, and J.F. Nielsen, *Impaired stretch reflex and joint torque modulation during spastic gait in multiple sclerosis patients.* Journal Of Neurology, 1996. **243**(8): p. 566-574.

61. Sinkjaer, T., et al., *Nonreflex and reflex mediated ankle joint stiffness in multiple-sclerosis patients with spasticity.* Muscle & Nerve, 1993. **16**(1): p. 69-76.

62. Macneil, J.B., R.E. Kearney, and I.W. Hunter, *Identification of time-varying biological-systems from ensemble data.* Ieee Transactions On Biomedical Engineering, 1992. **39**(12): p. 1213-1225.

63. Kirsch, R.F. and R.E. Kearney, *Identification of time varying stiffness dynamics of the human ankle joint during an imposed movement.* Experimental Brain Research, 1997. **114**(1): p. 71-85.

64. Hunter, I.W. and M.J. Korenberg, *The identification of nonlinear biological systems - Wiener and Hammerstein cascade models.* Biological Cybernetics, 1986. **55**(2-3): p. 135-144.

65. Korenberg, M.J. and I.W. Hunter, *The identification of nonlinear biological systems - LNL cascade models.* Biological Cybernetics, 1986. **55**(2-3): p. 125-134.

66. Hunter, I. and R. Kearney, *Two-sided linear filter identification.* Medical and Biological Engineering and Computing, 1983. **21**(2): p. 203-209.

67. Westwick, D.T. and R.E. Kearney, *Generalized eigenvector algorithm for nonlinear system identification with non-white inputs.* Annals Of Biomedical Engineering, 1997. **25**(5): p. 802-814.

68. Westwick, D.T. and R.E. Kearney, *Identification of physiological systems: A robust method for non-parametric impulse response estimation.* Medical & Biological Engineering & Computing, 1997. **35**(2): p. 83-90.

69. Bussgang, J.J., *Crosscorrelation functions of amplitude-distorted gaussian signals*, in *Technical report no. 216*. 1952, Massachusetts Institute of Technology. Research Laboratory of Electronics: Boston.

70. Baker, M., "Identification of time-varying Ankle Stiffness", Masters of Engineering, McGill University, Montreal, Quebec, 2005

71. Niedzwiecki, M. and P. Kaczmarek, *Identification of quasi-periodically varying systems using the combined nonparametric/parametric approach.* Ieee Transactions On Signal Processing, 2005. **53**(12): p. 4588-4598.

72. Shi, Z.Y., S.S. Law, and H.N. Li, *Subspace-based identification of linear time-varying system.* Aiaa Journal, 2007. **45**(8): p. 2042-2050.

73. Kameyama, K. and A. Ohsumi, *Subspace-based prediction of linear time-varying stochastic systems.* Automatica, 2007. **43**(12): p. 2009-2021.

74. Chen, S., H. Lai, and K. Ho, *Identification of linear time varying systems by Haar wavelet.* International Journal Of Systems Science, 2006. **37**(9): p. 619-628.

75. Pillonetto, G., *Identification of Time-Varying Systems in Reproducing Kernel Hilbert Spaces.* Ieee Transactions On Automatic Control, 2008. **53**(9): p. 2202-2209.

76. Bennett, D.J., et al., *Time-varying stiffness of human elbow joint during cyclic voluntary movement.* Experimental Brain Research, 1992. **88**(2): p. 433-442.

77. Soechting, J.F., J.R. Dufresne, and F. Lacquaniti, *Time-varying properties of myotatic response in man during some simple motor-tasks.* Journal Of Neurophysiology, 1981. **46**(6): p. 1226-1243.

78. Xu, Y.M. and J.M. Hollerbach, *A robust ensemble data method for identification of human joint mechanical properties during movement.* Ieee Transactions On Biomedical Engineering, 1999. **46**(4): p. 409-419.

79. Verhaegen, M. and X.O. Yu, *A class of subspace model identification algorithms to identify periodically and arbitrarily time-varying systems.* Automatica, 1995. **31**(2): p. 201-216.

80. Giesbrecht, H., "Time-varying identification of intrinsic and reflex joint stiffness", McGill University, Montreal, Quebec, 2007

81. Qita, W.A. and R. Kearney, Engineering in Medicine and Biology Society, 2000. Proceedings of the 22nd Annual International Conference of the IEEE, 2000. **1**: p. 335-338 vol.1.

82. Guyton, A.C. and J.E. Hall, *Textbook of Medical Physiology*. 11th ed. 2006, Philadelphia, Pennsylvania: Elseviers Saunders. 1116.

APPENDIX A: Simulink simulation model used in Chapter 4

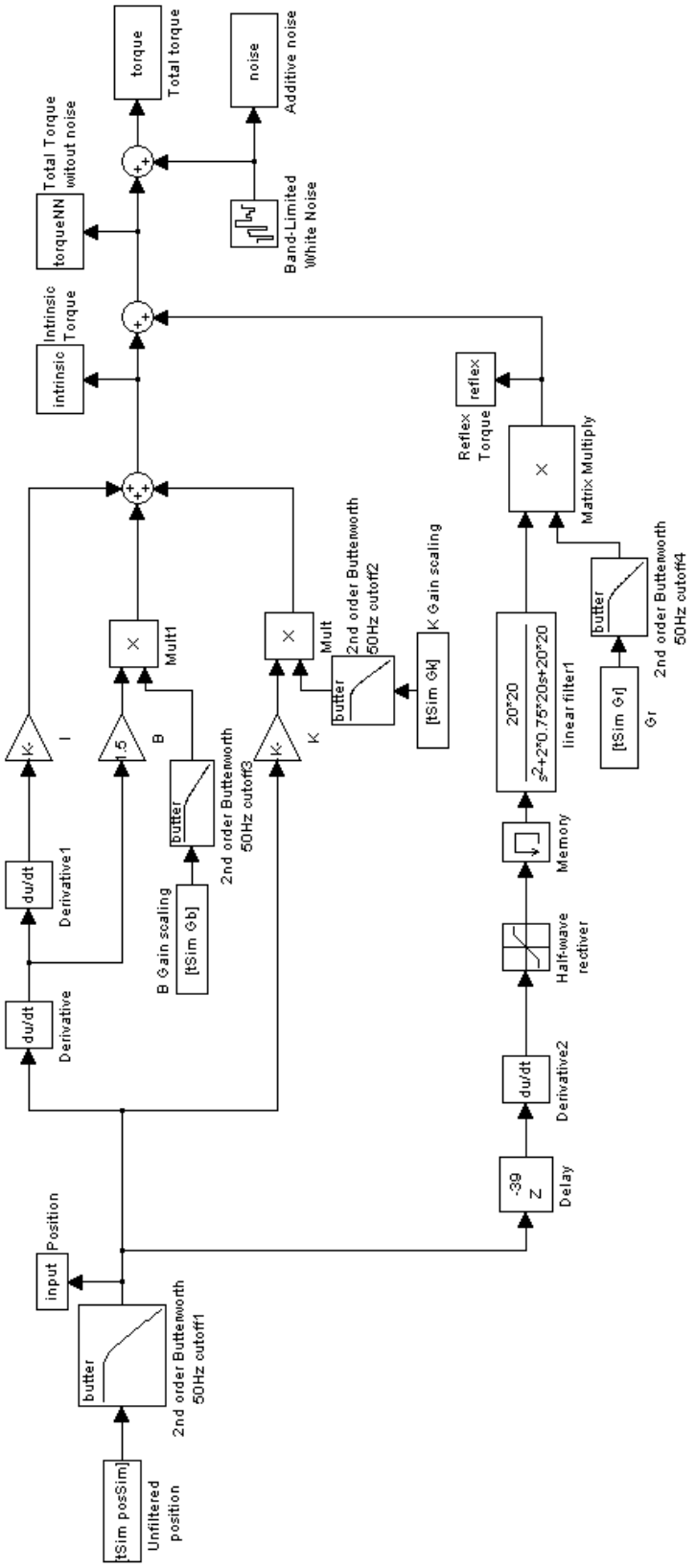

APPENDIX B: Research Ethics Certificate

Attached is our Ethics Certificate, approved by the McGill Institutional Review Board. The certificate is dated May 11th, 2009 and is valid until April 12th, 2010.